The 12th Symposium on Polar Science
15 – 18 November 2021

National Institute of Polar Research
Research Organization of Information and Systems

Session OM
Polar Meteorology and Glaciology

Program and Abstracts

Convener : Jun Inoue (NIPR)

【OM】Polar Meteorology and Glaciology

Scopes

This session covers research topics from the fields of atmospheric science, meteorology, glaciology, sea ice, oceanography, and paleoclimatology.

Convener : **Jun Inoue (NIPR)**

Real-time Oral presentations (09:30 – 12:15, 13:30 – 16:20)

Date: Wed. 17 November

Chair: Ikumi Oyabu (NIPR)				
OMo01	09:30 - 09:50	Simulating the evolution of the Antarctic ice sheet until the year 2300 with a climate–index method	*Ralf Greve(Hokkaido University), Christopher Chambers(Hokkaido University), Takashi Obase(University of Tokyo), Fuyuki Saito(Japan Agency for Marine-Earth Science and Technology) ,Wing-Le Chan(University of Tokyo), Ayako Abe-Ouchi(University of Tokyo)	OMo01_Greve_00145_01.pdf
OMo02	09:50 - 10:10	Continuous flow analysis of black carbon in Dome Fuji deep ice core over Termination I using a wide–range single–particle soot photometer	*Kumiko Goto-Azuma(NIPR), Nobuhiro Moteki(The University of Tokyo), Kaori Fukuda(NIPR), Jun Ogata(NIPR), Tatsuhiro Mori(The University of Tokyo), Sho Ohata(Nagoya University), Yutaka Kondo(NIPR), Makoto Koike(The University of Tokyo), Motohiro Hirabayashi(NIPR), Kyotaro Kitamura(NIPR), Ayaka Yonekura(SOKENDAI), Shuji Fujita(NIPR), Fumio Nakazawa(NIPR), Yoshimi Ogawa-Tsukagawa(NIPR), Kenji Kawamura(NIPR)	OMo02_Goto–azuma_00104_01.pdf
OMo03	10:10 - 10:30	Reconstruction of methane concentration variations during the penultimate glacial period from a Continuous Flow Analysis of the Dome Fuji ice core	*Ayaka Yonekura(The Graduate University for Advanced Studies, SOKENDAI), Kenji Kawamura(SOKENDAI, NIPR, JAMSTEC), Ikumi Oyabu(NIPR), Kyotaro Kitamura(NIPR), Jun Ogata(NIPR), Motohiro Hirabayashi(NIPR), Kaori Fukuda(NIPR), Yoshimi Tsukagawa(NIPR), Tomotaka Saruya(NIPR), Fumio Nakazawa(SOKENDAI,NIPR),Shuji Fujita(SOKENDAI,NIPR), Kumiko Goto-Azuma(SOKENDAI,NIPR), Hideaki Motoyama(SOKENDAI,NIPR)	OMo03_Yonekura_00113_01.pdf
	10:30 - 10:40	Break		
Chair: Naoko Nagatsuka (NIPR)				
OMo04	10:40 - 11:00	Cause of fluctuation in crystal orientation fabric in the Dome Fuji ice core inferred from comparison of dielectric anisotropy with physicochemical properties	*Tomotaka Saruya(NIPR,SOKENDAI), Shuji Fujita(NIPR,SOKENDAI), Yoshinori Iizuka(Institute of Low Temperature Science, Hokkaido University), Atsushi Miyamoto (Institute for the Advancement of Higher Education, Hokkaido University), Hiroshi Ohno(Kitami Institute of Technology), Akira Hori(Kitami Institute of Technology), Shigeyama Wataru(SOKENDAI), Motohiro Hirabayashi(NIPR), Kumiko Goto-Azuma(NIPR / SOKENDAI),	OMo04_Saruya_00209_01.pdf
OMo05	11:00 - 11:20	High–resolution subglacial topography around Dome Fuji, Antarctica, based on ground–based radar surveys conducted over 30 years	Shun Tsutaki(NIPR), *Shuji Fujita(NIPR), Kenji Kawamura(NIPR), Ayako Abe-Ouchi(Atmosphere and Ocean Research Institute, The University of Tokyo), Kotaro Fukui(Tateyama Caldera Sabo Museum), Hideaki Motoyama(NIPR), Yu Hoshina(Graduate School of Environmental Studies, Nagoya University), Fumio Nakazawa(NIPR), Takashi Obase(Atmosphere and Ocean Research Institute, The University of Tokyo), Hiroshi Ohno(Kitami Institute of Technology), Ikumi Oyabu(NIPR),Fuyuki Saito(JAMSTEC), Konosuke Sugiura (Faculty of Sustainable Design, University of Toyama), Toshitaka Suzuki(Faculty of Science, Yamagata University)	OMo05_Fujita_00251_01.pdf
OMo06	11:20 - 11:40	Surface temperature changes at Dome Fuji region during the past four decades	Shohei Morino(Graduate School of Environmental Studies, Nagoya University), *Naoyuki Kurita(Institute of Space-Earth Environmental Research, Nagoya University), Takao Kameda(Snow and Ice Research Laboratory, Kitami Institute of Technology), Naohiko Hirasawa(NIPR) , Hideaki Motoyama(NIPR)	OMo06_Kurita_00161_01.pdf

Chair: Jun Inoue (NIPR)				
	11:40 - 12:15	1-min poster presentation (31 lightning talks from OMp01 to OMp31)		
Lunch				
Chair: Atsushi Yoshida (NIPR)				
OMo07	13:30 - 13:50	Atmospheric responses to the sea surface temperature in the Chukchi and Bering Seas	*Yoshimi Kawai(Japan Agency for Marine-Earth Science and Technology)	OMo07_Kawai_00500_01.pdf
OMo08	13:50 - 14:10	Year-round measurements of ice nucleating particles in Svalbard during MOSAiC 2019/20	*Yutaka Tobo(NIPR), Hitoshi Matsui(Nagoya Univ.), Kei Kawai(Nagoya Univ.), Sho Ohata(Nagoya Univ.), Yutaka Kondo(NIPR), Ove Hermansen(NILU), Jun Inoue(NIPR), Makoto Koike(Univ. Tokyo)	OMo08_Tobo_00428_01.pdf
OMo09	14:10 - 14:30	Marine ice-nucleating particles and its effect on ice cloud formation: A result from the Arctic research cruise during a cold-air outbreak in early winter	*Jun Inoue(NIPR), Yutaka Tobo(NIPR), Fumikazu Taketani(Japan Agency for Marine-Earth Science and Technology), Kazutoshi Sato(Kitami Institute of Technology)	OMo09_Inoue_00043_01.pdf
OMo10	14:30 - 14:50	Seasonal change in satellite-retrieved ice cloud fraction in the lower troposphere over the Southern Ocean	*Kazutoshi Sato(Kitami Institute of Technology), Jun Inoue(NIPR)	OMo10_Sato_00088_01.pdf
	14:50 - 15:00	Break		
Chair: Daisuke Hirano (NIPR)				
OMo11	15:00-15:20	Diffusive CDW flux in the East Antarctic margin	*Kaihe Yamazaki(Hokkaido University), Kohei Mizobata(Tokyo University of Marine Science and Technology), Shigeru Aoki(Hokkaido University)	OMo11_Yamazaki_00592_01.pdf
OMo12	15:20 - 15:40	Investigation on the interactions between the downslope flow of Antarctic Bottom water and upslope flow of modified Circumpolar Deep Water using a high-resolution model.	*Vigan Mensah(Hokkaido University, Institute of Low Temperature Science), Yoshihiro Nakayama(Hokkaido University, Institute of Low Temperature Science), Masakazu Fujii(NIPR), Yoshifumi Nogi(NIPR), Kay I Ohshima(Hokkaido University, Institute of Low Temperature Science)	OMo12_Mensah_00533_01.pdf
OMo13	15:40 - 16:00	Spatiotemporal high-resolution mapping of biological production in the Southern Ocean	*Xiangxing Lai(Hokkaido university. Graduate of Env.Science), Xianliang Pan(Hokkaido university. Graduate of Env.Science), Bofeng Li(Hokkaido university. Graduate of Env.Science), Ryosuke Makabe(NIPR), Daisuke Hirano(NIPR), Yutaka Watanabe(Hokkaido university. Graduate of Env.Science)	OMo13_Lai_00544_01.pdf
OMo14	16:00 - 16:20	Excess silicate removal over the Southern Ocean	*Xianliang Pan(Hokkaido University Graduate School of Env.Science), Xiangxing Lai(Hokkaido University Graduate School of Env.Science), Bofeng Li(Hokkaido University Faculty of Env.Earth Science), Yutaka Watanabe(Hokkaido University Faculty of Env.Earth Science)	OMo14_Pan_00065_01.pdf

Poster presentations (1 November - 18 November)

OMp01	Antarctic Peninsula warm winters influenced by Tasman Sea temperatures	*Sato Kazutoshi(Kitami Institute of Technology), Jun Inoue(NIPR), Ian Simmonds(The University of Melbourne), Irina Rudeva(Australian Bureau of Meteorology)	OMp01_Sato_00088_02.pdf
OMp02	Seasonal and daily variation in Be-7 concentration of surface air at Syowa Station, Antarctica	*Naohiko Hirasawa(NIPR), Taku Nakamura(Department of physics, Gifu University), Miyoko Miwa(Life Science Research Center, Gifu University), Mutsuo Inoue(Low level radioactivity laboratory, Kanazawa University), Sakae Shirayama(NIPR), Haruhito Yasuda(Department of physics, Gifu University), Shigeki Tasaka(Department of physics, Gifu University)	OMp02_Hirasawa_00301_01.pdf
OMp03	Fractionation of O2/N2 and Ar/N2 in the Antarctic ice sheet from precise gas measurements of the Dome Fuji ice core – Constraining permeabilities of O2, N2 and Ar in the ice sheet with a simple diffusion model–	*Ikumi Oyabu(NIPR), Kenji Kawamura(NIPR), Tsutomu Uchida(Hokkaido Univ.), Shuji Fujita(NIPR), Kyotaro Kitamura(NIPR), Motohiro Hirabayashi(NIPR), Shuji Aoki(Tohoku Univ.), Shinji Morimoto(Tohoku Univ.), Takakiyo Nakazawa(Tohoku Univ.), Jeffrey Severinghaus (SIO), Jacob Morgan(SIO)	OMp03_Oyabu_00040_01.pdf
OMp04	On-shelf warm water circulation toward Totten Ice Shelf, East Antarctica	*Daisuke Hirano(NIPR), Takeshi Tamura(NIPR), Kazuya Kusahara(Japan Agency for Marine-Earth Science and Technology), Masakazu Fujii(NIPR), Kaihe Yamazaki(Institute of Low Temperature Science, Hokkaido University), Yoshihiro Nakayama(Institute of Low Temperature Science, Hokkaido University), Kazuya Ono(Institute of Low Temperature Science, Hokkaido University), Takuya Itaki(National Institute of Advanced Industrial Science and Technology), Yuichi Aoyama(NIPR), Daisuke Simizu(NIPR), Kohei Mizobata(Tokyo University of Marine Science and Technology), Kay I. Ohshima(Institute of Low Temperature Science, Hokkaido University), Yoshifumi Nogi(NIPR), Shigeru Aoki(Institute of Low Temperature Science, Hokkaido University)	OMp04_Hirano_00488_01.pdf
OMp05	Effects of snow and remineralization processes on nutrients distributions in the multi-year land-fast Antarctic sea ice	*Reishi Sahashi(Faculty of Fisheries Sciences, Hokkaido University), Daiki Nomura(Field Science Center for Northern Biosphere, Hokkaido University), Takenobu Toyota(Institute of Low Temperature Science, Hokkaido University), Masato Ito(NIPR), Manami Tozawa(Faculty of Fisheries Sciences, Hokkaido University), Pat Wongpan(Institute for Marine and Antarctic Studies, University of Tasmania), Kazuya Ono(Institute of Low Temperature Science, Hokkaido University), Daisuke Shimizu(NIPR), Kazuhiro Naoki(Research and Information Center, Tokai University), Takeshi Tamura(NIPR), Shigeru Aoki(Institute of Low Temperature Science, Hokkaido University), Shuki Ushio(NIPR)	OMp05_Sahashi_00498_01.pdf
OMp06	Distribution and seasonal evolution of supraglacial lakes around Lützow-Holm Bay, East Antarctica	*Haruka Itagaki(Yokohama National University), Masahiro Ishikawa(Yokohama National University)	OMp06_Itagaki_00599_01.pdf
OMp07	Winter lake snow/ice observation with the IoT time lapse camera and satellite remote sensing	*Tatsuru Sato(National Institute of Technology, Ichinoseki Collage)	OMp07_Sato_00201_01.pdf
OMp08	The 19-year (2002-20) time series of annual sea-ice production in all Antarctic coastal polynyas based on AMSR-E/2 satellite observations	*Sohey Nihashi(National Institute of Technology (KOSEN) Tomakomai College), Takeshi Tamura(NIPR), Kay I. Ohshima(Institute of Low Temperature Science, Hokkaido University)	OMp08_Nihashi_00253_01.pdf
OMp09	Coupled model for simulating the interaction of waves and ice particles	*Zijing Jin(The University of Tokyo)	OMp09_Jin_00581_01.pdf
OMp10	Near-inertial internal wave generation by mixed layer cooling in the Indian sector of the Southern Ocean	*Matheus Azevedo(Tokyo University of Marine Science and Technology), Yujiro Kitade(Tokyo University of Marine Science and Technology)	OMp10_Azevedo_00224_01.pdf

OMp11	Changes in Antarctic Bottom Water formation, deduced from oxygen and CFC-12 in the Indian Ocean sector of the Southern Ocean between 1987 and 2020	*Narimi Baba(Tokyo University of Marine Science and Technology, Japan), Yoshihiko Ohashi(Tokyo University of Marine Science and Technology, Japan), Kenichi Sasaki(Japan Agency for Marine-Earth Science and Technology, Japan), Michiyo Yamamoto-Kawai(Tokyo University of Marine Science and Technology, Japan)	OMp11_Baba_00603_01.pdf
OMp12	Silica concentrations of seawater and sea- ice in the coastal regions of the Southern Ocean	*Natsumi Nojiro(Tokyo university of Marine Science and Technology), Michiyo Yamamoto-Kawai(Tokyo university of Marine Science and Technology), Ryosuke Makabe(Tokyo university of Marine Science and Technology, NIPR, The Graduate University for Adovanced Studies (SOKENDAI)), Keigo Takahashi(The Graduate University for Adovanced Studies (SOKENDAI))	OMp12_Nojiro_00598_02.pdf
OMp13	Difference of the xCO2 over two decades (1996 and 2019) in the eastern Indian sector of the Southern Ocean	*Manami Tozawa(Hokkaido University), Daiki Nomura(Hokkaido University), Shin-ichiro Nakaoka(National Institute for Environmental Studies), Masaaki Kiuchi(Hokkaido University), Daisuke Hirano(NIPR), Kaihe Yamazaki(Hokkaido University), Shigeru Aoki(Hokkaido University), Hiroko Sasaki(Japan Fisheries Research and Education Agency), Hiroto Murase(Tokyo University of Marine Science and Technology)	OMp13_Tamura_00002_02.pdf
OMp14	Variations of partial pressure of CO2 in the surface seawater and air-sea CO2 fluxes along 110° E in the Southern Ocean	*Takayuki Matsuura(Tohoku University), Shinji Morimoto(Tohoku University), Gen Hashida(NIPR), Tomomi Takamura(NIPR), Shin-ichiro Nakaoka(NIES), Shuji Aoki(Tohoku University)	OMp14_Matsuura_00520_01.pdf
OMp15	Processing of sea ice monitoring videos recorded by surveillance cameras on Icebreaker Shirase	*Takeshi Terui(NIPR), Keiko Iino(NIPR), Motomu Oyama(NIPR), Daisuke Simizu(NIPR), Shuki Ushio(NIPR)	OMp15_Terui_00265_01.pdf
OMp16	Characteristics of cloud base height from ceilometer observation onboard R/V Shirase	Makoto Kuji(Nara Women's University),* Mana Takada(Nara Women's University), Yumi Shimode(Nara Women's University), Sara Hirose(Nara Women's University), Naohiko Hirasawa(NIPR)	OMp16_Takada_00511_01.pdf
OMp17	Characteristics of cloud fraction from whole-sky camera observation onboard R/V Shirase from 2013 to 2020	*Sara Hirose(Nara Women's University), Makoto Kuji(Nara Women's University), Mana Takada(Nara Women's University), Masahiro Hori(University of Toyama)	OMp17_Hirose_00019_01.pdf
OMp18	Characteristics of cloud fraction and shortwave downward radiation at Ny-Alesund and Syowa station	Makoto Kuji(Nara Women's University), *Yumi Shimode(Nara Women's University), Mana Takada(Nara Women's University), Sara Hirose(Nara Women's University), Masanori Yabuki(Kyoto University)	OMp18_Shimode_00516_01.pdf
OMp19	Dating and solid particle analysis of a shallow ice core obtained from EGRIP, Greenland	*Yuki Komuro(NIPR), Fumio Nakazawa(NIPR), Kumiko Goto-Azuma(NIPR), Naoko Nagatsuka(NIPR), Motohiro Hirabayashi(NIPR), Jun Ogata(NIPR), Kaori Fukuda(NIPR), Naoyuki Kurita(Nagoya University), Kyotaro Kitamura(NIPR), Ayaka Yonekura(The Graduate University for Advanced Studies, SOKENDAI), Trevor J. Popp(University of Copenhagen), Dorthe Dahl-Jensen(University of Copenhagen)	OMp19_Komuro_00242_01.pdf
OMp20	Variations in mineralogy of dust in ice cores obtained from Greenland over the past 100 years	*Naoko Nagatsuka(NIPR), Kumiko Goto-Azuma(NIPR, SOKENDAI), Akane Tsushima(Chiba University), Koji Fujita(Nagoya University), Sumito Matoba(Hokkaido University), Yukihiko Onuma(University of Tokyo), Remi Dallmayr(AWI), Motohiro Hirabayashi(NIPR), Jun Ogata(NIPR), Yoshimi Ogawa-Tsukagawa(NIPR), Kyotaro Kitamura(NIPR), Masahiro Minowa(Hokkaido University), Yuki Komuro(NIPR), Hideaki Motoyama(NIPR, SOKENDAI), Teruo Aoki(NIPR, SOKENDAI), Fumio Nakazawa(NIPR), Trevor James Popp(University of Copenhagen), Dorthe Dahl-	OMp20_Nagatsuka_00522_01.pdf

OMp21	Effects of the glacial meltwater supply on carbonate chemistry in Bowdoin Fjord, northwestern Greenland	*Takahito Horikawa(Faculty of Fisheries Sciences, Hokkaido University), Daiki Nomura(Faculty of Fisheries Sciences, Hokkaido University, Field Science Center for Northern Biosphere, Hokkaido University, Arctic Research Center, Hokkaido University), Shin Sugiyama(Arctic Research Center, Hokkaido University, Institute of Low Temperature Science, Hokkaido University), Yasushi Fukamachi(Arctic Research Center, Hokkaido University), Naoya Kanna(Atmosphere and Ocean Research Institute, The University of Tokyo)	OMp21_Horikawa_00542_01.pdf
OMp22	Development of an ice-sheet model IcIES-1 and IcIES-2: benchmark simulation on idealized and realistic ice-sheet configuration	*Fuyuki SAITO(JAMSTEC), Ayako ABE-OUCHI(AORI), Takashi OBASE(AORI), Ryouta O'ISHI(AORI)	OMp22_Saito_00079_01.pdf
OMp23	Greenhouse gases flux through the land surface at the terminus of Glaciers in Alaskan Range	*Keiko Konya(JAMSTEC), Tetsuo Sueyoshi(NIPR), Iwahana Go(UAF), Tomoaki Motishita(FFPRI), Jun Uetake(Hokkaido univ.)	OMp23_Konya_00440_01.pdf
OMp24	Extreme Wildland Fire in Sakha in 2021	*Hiroshi Hayasaka(Arctic Research Center, Hokkaido University)	OMp24_Hayasaka_00195_01.pdf
OMp25	Forecasting sea-ice distribution during the summer season in the arctic with statistical method	*Motomu Oyama(NIPR), Hajime Yamaguchi(NIPR), Noriaki Kimura(AORI)	OMp25_Oyama_00621_01.pdf
OMp26	Validation of AMSR2 sea ice motion vector product	*Eri Yoshizawa(JAXA), Rigen Shimada(JAXA), Misako Kachi(JAXA), Noriaki Kimura(The University of Tokyo), Koji Shimada(Tokyo University of Marine Science and Technology)	OMp26_Yoshizawa_00573_01.pdf
OMp27	Experimental study on the ice-wave interaction in the small ice floes and regular wave – Relationship between ice concentration and ice vertical motion –	*Junji Sawamura(Osaka University)	OMp27_Sawamura_00608_01.pdf
OMp28	Observation of Total Ice Thickness Using UAV-SfM in the Saroma-ko Lagoon	*Kohei Sato(Graduate School of Engineering, Kitami Institute of Technology), Kazutaka Tateyama(School of Earth, and Environmental Engineering Kitami Institute of Technology), Tatsuya Watanabe(School of Earth, and Environmental Engineering Kitami Institute of Technology), Tomonori Tanikawa(Meteorological Research Institute, Japan Meteorological Agency)	OMp28_Sato_00171_01.pdf
OMp29	Seasonal cycle and inter-annual variation of atmospheric freshwater input into the Sea of Okhotsk and associated large-scale atmospheric circulation	*Kazuhiro Oshima(Aomori University), Yoshihiro Tachibana(Mie University), Kensuke Komatsu(The University of Tokyo)	OMp29_Oshima_00068_01.pdf
OMp30	Interannual variation of Warm Arctic-Cold Eurasia pattern investigated by using large ensemble experiment	*Zhou Xiling(Graduate School of Environmental Science, Hokkaido University), Tomonori Sato(Faculty of Environmental Earth Science, Hokkaido University), Tetsu Nakamura(Faculty of Environmental Earth Science, Hokkaido University), Shixue Li(Graduate School of Environmental Science, Hokkaido	OMp30_Zhou_00497_01.pdf
OMp31	An assessment of dominant patterns of lower tropospheric temperature advection contributing to the Arctic Amplication using a large-scale ensemble model experiment.	*Masatake Hori(Atmosphere and Ocean Research Institute, The University of Tokyo), Masakazu Yoshimori(Atmosphere and Ocean Research Institute, The University of Tokyo)	OMp31_Hori_00329_01.pdf

Simulating the evolution of the Antarctic ice sheet until the year 2300 with a climate-index method

Ralf Greve[1,2], Christopher Chambers[1], Takashi Obase[3], Fuyuki Saito[4], Wing-Le Chan[3], Ayako Abe-Ouchi[3]
[1]*Institute of Low Temperature Science, Hokkaido University, Sapporo, Japan*
[2]*Arctic Research Center, Hokkaido University, Sapporo, Japan*
[3]*Atmosphere and Ocean Research Institute, University of Tokyo, Kashiwa, Japan,*
[4]*Japan Agency for Marine-Earth Science and Technology, Yokohama, Japan*

As part of the Coupled Model Intercomparison Project Phase 6 (CMIP6), the Ice Sheet Model Intercomparison Project for CMIP6 (ISMIP6) was devised to assess the likely sea-level-rise contribution from the Antarctic and Greenland ice sheets until the year 2100. ISMIP6 used future climate scenarios as forcings for ice-sheet models developed by several international groups (Nowicki et al., 2020). Results obtained for the Antarctic ice sheet are described by Seroussi et al. (2020) and Payne et al. (2021). Recently, Chambers et al. (2021, preprint) extended the ISMIP6-Antarctica simulations with SICOPOLIS until the year 3000, using the original ISMIP6 climate forcings until 2100, while assuming a sustained late-21st-century climate without any further trend beyond that.

Here, we construct an ensemble of climate forcings for the Antarctic ice sheet until the year 2300, using results from a MIROC4m RCP8.5 simulation. In the first step, we derive a set of atmospheric and oceanic climate indices from this simulation such that 1995–2014 averages are mapped to zero and 2091–2100 averages to unity. In the second step, we use the climate indices to extrapolate the ensemble of ISMIP6 forcings (anomalies relative to 1995–2014, for 2015–2100) to the period 2101–2300. Together with the original ISMIP6 forcings, this method provides smooth climate forcings for the entire period 2015–2300. We use these forcings to run simulations for the Antarctic ice sheet with SICOPOLIS and assess its expected mass loss (contribution to sea-level rise) over this period. Figure 1 shows the results. For the unforced control run, the ice sheet remains stable. For the unabated warming pathway RCP8.5 (CMIP5) / SSP5-8.5 (CMIP6), it suffers a significant mass loss that, by 2300, amounts to ~1.5 m SLE (sea-level equivalent) for the 14-experiment mean, and ~3.3 m SLE for the most sensitive experiment. This mass loss originates mainly from the West Antarctic ice sheet, as a consequence of its partial collapse due to the marine ice sheet instability. For the reduced emissions pathway RCP2.6 (CMIP5) / SSP1-2.6 (CMIP6), the mass loss is limited to a 3-experiment mean of ~0.16 m SLE. These findings are in stark contrast to the original findings of ISMIP6-Antarctica, which covered only the 21st century and produced a much less clear picture for Antarctica (limited mean mass loss, large uncertainty, even sign unclear). A multi-century perspective is therefore crucial for assessing ice-sheet response to anthropogenic climate change and its possible impact on human society.

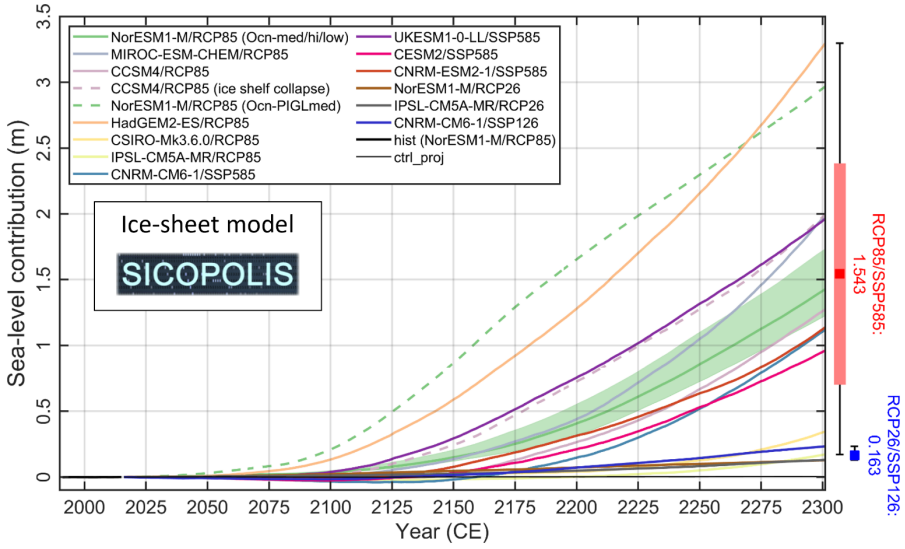

Figure 1. ISMIP6-Antarctica historical run (hist), projection control run (ctrl_proj) and future climate experiments extended until 2300: Simulated ice mass change, counted positively for loss and expressed as sea level contribution. The red and blue boxes to the right show the means for RCP8.5/SSP5-8.5 and RCP2.6/SSP1-2.6, respectively (RCP8.5/SSP5-8.5: also ± 1 sigma); the whiskers show the corresponding full ranges.

References

(1) Nowicki et al. 2020, Cryosphere 14, 2331-2368, doi: 10.5194/tc-14-2331-2020. (2) Seroussi et al. 2020, Cryosphere 14, 3033-3070, doi: 10.5194/tc-14-3033-2020. (3) Payne et al. 2021, Geophys. Res. Lett. 48, e2020GL091741, doi: 10.1029/2020GL091741. (4) Chambers et al. 2021, J. Glaciol. (submitted, preprint at EarthArXiv, doi: 10.31223/X5CP7C).

Continuous flow analysis of black carbon in Dome Fuji deep ice core over Termination I using a wide-range single-particle soot photometer

Kumiko Goto-Azuma[1,2], Nobuhiro Moteki[3], Kaori Fukuda[1], Jun Ogata[1], Tatsuhiro Mori[3], Sho Ohata[4], Yutaka Kondo[1]
Makoto Koike[3], Motohiro Hirabayashi[1], Kyotaro Kitamura[1], Ayaka Yonekura[2], Shuji Fujita[1,2], Fumio Nakazawa[1,2]
Yoshimi Ogawa-Tsukagawa[1], Kenji Kawamura[1,2]

[1]*National Institute of Polar Research, Japan*
[2]*SOKENDAI (The Graduate University for Advanced Studies), Japan*
[3] *The University of Tokyo, Japan*
[4]*Nagoya University, Japan*

Black carbon (BC) can affect Earth's radiation budget by absorbing sunlight and reducing albedo of snow and ice surfaces (e.g. Bond et al., 2013). It can also affect cloud microphysics by acting as cloud condensation nuclei or ice nucleating particles (e.g. Bond et al., 2013). Furthermore, BC emitted from large wild fires can affect air quality and ecosystems. BC can thus affect climate and environment. Climate changes can in turn change frequencies and magnitudes of wild fires and hence BC emissions. Despite numerous studies through observations and aerosol/climate models, we have only limited knowledge on impacts of BC on radiative forcing, albedo reduction, and cloud microphysics. Our knowledge on impacts of climate change on BC emissions are also limted. Ongoing global warming could impact wild fires. But predictions are hampered by limted long-term records of natural wild fires. Ice core BC data can provide us with excellent records of the past natural wild fires.

We analyzed the second Dome Fuji deep ice core drilled in East Antarctica for the depth interval between 200 and 640 m, which corresponds to the LGM to mid-Holocene period. To obtain continuous high-resolution data, we used a Continuous Flow Analysis (CFA) system developed at the National Institute of Polar Research. The CFA system enabled us to obtain high-resolution data of BC, stable isotopes of water, microparticles and 8 elements (Na, K, Mg, Ca, Fe, Al, Si and S). For BC analysis, we used a recently developed Wide-range (WR) SP2 (Single Particle Soot Photometer), which can detect BC particles in size range between 70 and 4000 nm (Mori et al., 2016). A combination of WR-SP2 and a high-efficiency nebulizer allowed us accurate measurements of BC concentrations and size distributions. Here we present the first BC record for the LGM to mid-Holocene period in East Antarctica.

Our preliminary data indicate that BC mass concentration was high at LGM, decreased over Termination I, and increased again during the early Holocene. We also find that the temporal trends in BC number concentration are different for different size ranges. The temporal trend in BC mass concentration found in Dome Fuji core is different from that found in WAIS Divide ice core. The difference could be due to spatial variability in Antarctica and/or different size ranges of BC measurements.

References

Bond, T. C. et al., Bounding the role of black carbon in the climate system: A scientific assessment, J. Geophys. Res. Atmos., 118, 5380– 5552, doi:10.1002/jgrd.50171., 2013.

Mori, T. et al., Improved technique for measuring the size distribution of black carbon particles in liquid water, Aerosol Science & Technology, 50, 3, 242-254, DOI: 10.1080/02786826.2016.1147644, 2016.

Reconstruction of methane concentration variations during the penultimate glacial period from a Continuous Flow Analysis of the Dome Fuji ice core

Ayaka Yonekura[1], Kenji Kawamura[1,2,3], Ikumi Oyabu[2], Kyotaro Kitamura[2], Jun Ogata[2], Motohiro Hirabayashi[2], Kaori Fukuda[2], Yoshimi Tsukagawa[2], Tomotaka Saruya[2], Fumio Nakazawa[1,2], Shuji Fujita[1,2], Kumiko Goto-Azuma[1,2], Hideaki Motoyama[1,2]

[1] *The Graduate University for Advanced Studies, SOKENDAI*

[2] *National Institute of Polar Research*

[3] *JAMSTEC*

Ice cores and other paleoclimate records (stalagmites and marine sediment cores) indicate that the last glacial period was characterized by the repetition of Dansgaard-Oeschger (D/O) events, which are abrupt warming events in Greenland, and associated climate changes in the Northern Hemisphere. The D/O events occur every several thousand years. The counterpart to the D/O event is seen in Antarctic temperatures, which is thought to be caused by changes in the Atlantic meridional overturning circulation (AMOC). The number and timing of D/O events are consistent among various paleoclimate records from around the world (e.g., oxygen isotope ratio of stalagmite obtained from Chinese cave) during the last glacial period. However, for periods older than the last glacial period, the number, timing, and frequency of D/O events are highly inconsistent among paleoclimate records.

The climate variabilities during the last glacial period have been reconstructed from Greenland and Antarctic ice cores drilled at high accumulation areas with a high temporal resolution, but these cores only cover the last glacial period. Therefore, the reconstruction of paleoclimate records older than the last glacial period requires analyses of Antarctic deep ice cores drilled at low accumulation areas (e.g., Dome Fuji cores). However, the reconstruction of methane concentrations before the last glacial period using deep ice cores (Vostok, EDC, Dome Fuji) have been limited to the analyses of discrete samples (a few cm samples), and its temporal resolution (about 500 years) is insufficient to reconstruct of the short-term variations like D/O events. Here, we present a continuous record of methane concentration fluctuations during the penultimate glacial period (Marine Isotope Stage 6) reconstructed from the Dome Fuji ice cores using a continuous flow analysis (CFA) system.

We analyzed the second Dome Fuji deep ice core from 1869 to 2076 m (207-m long). The ice-core samples were cut into 3.5 x 3.5 x 50 cm sticks. The ice sticks were melted on a clean metal plate heated at 15 °C, which is placed in a freezer at -20 ° C. The melt rate is about 3 cm/min, and when the remaining ice stick became 10-cm long, the next ice stick was placed above the previous one, making continuous melting of multiple ice sticks. The meltwater with air bubbles was led to a debubbler unit, where bubble-free meltwater was separated from air bubbles and led to several instruments for measuring its dust, ion, stable isotopes of water, and black carbon. For the methane measurement, the air-water mixture from the debubbler was led to a gas-permeable membrane tube to extract the bubble air and dissolved air. The extracted air was passed through a dryer (Nafion) to remove water vapor. Finally, the methane mixing ratio of the dried gas was measured by a cavity ringdown spectrometer (Picarro G2301), which was customized to operate at low cavity pressure (40 torrs). Based on the degree of signal smoothing generated by the CFA system and the melting speed, the resolution of the measurement was evaluated to be about 5 cm. Due to the incomplete extraction of gases dissolved in meltwater, the measured methane concentration is always underestimated. Therefore, a correction of about +8% was applied based on the measurement of a mixture of standard gas and ultrapure water. In addition, an additional adjustment of + 4 % was applied to the entire data set based on the comparison of the CFA data with high-precision data from discrete analyses. It would be caused by the sample measurement conditions (e.g., water temperature) not being completely copied on the calibration measurement.

We reconstructed nearly continuous methane concentrations for about 50,000 years during the penultimate glacial period (145,000-195,000 years ago) (Fig.1c). The amplitude and peak shape of the D/O-like fluctuations of several tens of ppb are agreed with the results of discrete measurements of the Dome Fuji and EDC cores (e.g., Loulergue et al., 2008), indicating the validity of the CFA results. Furthermore, the CFA data exhibit many finer-scale variations with small amplitudes (about 10 ppb) and short durations (several hundred years), which have been impossible to be detected by the discrete analyses (arrow in Fig.1c). As the CFA data revealed the detailed methane variability, it became clear that DF discrete sample data were not including outliers. During the penultimate glacial period, 26 peaks were shown using the first derivative of the methane variation as a reference (Fig.1c). The number of the D/O-like events (saw-shape with abrupt increase and gradual decrease)

during the penultimate glacial period is higher than that based on the analyses of water isotope and dust records of the DF and EDC cores (DF Project Members, 2017) as well as the discrete methane data from Dome Fuji and EDC cores (e.g., Loulergue et al., 2008). Compared to the Chinese stalagmite data (including 18peaks) (Wang et al., 2008), there is only a clear match in a few places, although the number of events is consistent during the last glacial period. The amplitudes of the D/O-like events in the penultimate glacial period are generally smaller than those in the last glacial period, and there are no events with the amplitudes exceeding 100 ppb as seen in the last glacial period (e.g., D/O8). These results suggest that the D/O-like event repeatedly occurs during the penultimate glacial period but with some differences from the last glacial period.

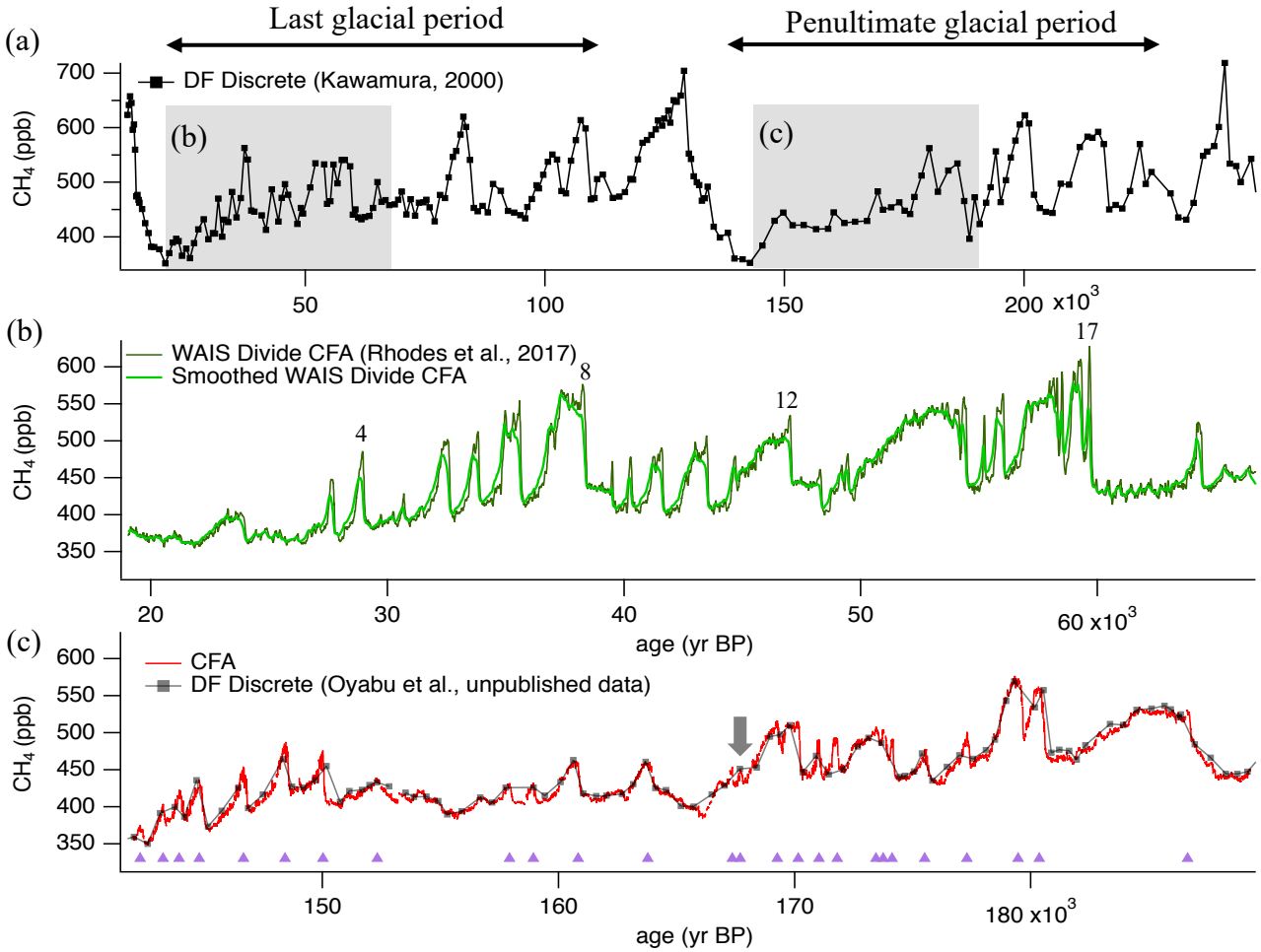

Figure 1. (a) Methane variability from the last glacial period to the penultimate glacial period. DF discrete (black).
(b) Enlarged view of shaded area during the last glacial period with the D/O event numbers. WAIS divide data measured by CFA (dark green). Smoothed WAIS divide data based on age distribution in low accumulation areas (light green).
(c) Enlarged view of shaded area during the penultimate glacial period. DF CFA data (red). Purple triangles represent peaks.

References

Dome Fuji ice core project members, State dependence of climatic instability over the past 720,000 years from Antarctic ice cores and climate modeling, Sci. Adv., 3, e1600446, 2017.

K. Kawamura, thesis, Tohoku University, Japan ,2000.

Loulergue et al., Orbital and millennial-scale features of atmospheric CH4 over the past 800,000 years, Nature, 453(15), 383-386, 2008.

Rhodes et al., Atmospheric methane variability: Centennial-scale signals in the Last Glacial Period, Global Biogeochem. Cycles, 31, 575–590, 2017.

Wang et al., Millennial- and orbital-scale changes in the East Asian monsoon over the past 224,000 years, Nature, 451(28), 1090-1093, 2008.

Cause of fluctuation in crystal orientation fabric in the Dome Fuji ice core inferred from comparison of dielectric anisotropy with physicochemical properties

Tomotaka Saruya[1], Shuji Fujita[1,2], Yoshinori Iizuka[3], Atsushi Miyamoto[4], Hiroshi Ohno[5], Akira Hori[5], Motohiro Hirabayashi[1], Kumiko Goto-Azuma[1,2]

[1]*National Institute of Polar Research*

[2]*Department of Polar Research, The Graduate University for Advanced Studies, SOKENDAI*

[3]*Institute of Low Temperature Science, Hokkaido University*

[4]*Institute for the Advancement of Higher Education, Hokkaido University*

[5]*Kitami Institute of Technology*

The crystal orientation fabric (COF) is one of the most important factors controlling the ice-sheet rheology. For a better understanding of the deformation process in ice sheet, we investigated the COF development of deep ice core obtained from Dome Fuji (DF), East Antarctica, by measuring the dielectric anisotropy of ice core samples around the vertical direction. Dielectric anisotropy is a novel indicator of the vertical clustering of COF (Saruya et al., 2021). The COF in the top 80% of DF ice core was measured with a step of every 0.02 m and with a sampling interval of 5m using bulk specimens (thickness of 38–79 mm). Compared to thin-section methods, our new data can provide information with high-resolution and largely improved statistical significance.

As a result of successive measurements, we found a large-scale increase of dielectric anisotropy with increasing depth. This trend is consistent with previous findings that c-axes concentrate toward the core axis due to the grain rotation caused by uniaxial compression. In addition, we observed small fluctuations of the degree of c-axes clustering with scales of 10–100 m. In particular, we discovered large depression in the dielectric anisotropy during three major transition periods from glacial to interglacial.

To investigate the causes of fluctuation in the COF, the data for dielectric anisotropy were compared with various physicochemical data obtained by DF ice core analyses. We found that the dielectric anisotropy was related positively with the concentration of chloride ions and inversely with the amount of dust particles at greater depth than ~1200 m. Chloride ions can increase dislocation density and promote dislocation movement, which will result in active plastic deformation and c-axis clustering. On the other hand, dust particles can impede the clustering of COF. Considering the state of chloride ions and effect on deformation, the amount of HCl that can discharge chloride ions may be more important than NaCl. Thus, we hypothesize that the COF fluctuation is mainly determined by a balance between the concentration of chloride ions and dust particles. Furthermore, our data indicate that the initial COF that is formed by metamorphism at near-surface depth is an important factor to determine the time-dependent variations of the COF cluster.

In this presentation, we discuss the causes of COF fluctuations and implications for further deformation of ice under shear and deeper englacial environment.

References

Saruya, T., S. Fujita, and R. Inoue, Dielectric anisotropy as indicator of crystal orientation fabric in Dome Fuji ice core: method and initial results, Journal of Glaciology, First view:1-12, 2021.

High-resolution subglacial topography around Dome Fuji, Antarctica, based on ground-based radar surveys conducted over 30 years

Shun Tsutaki[1,2], Shuji Fujita[1,3], Kenji Kawamura[1,3,4], Ayako Abe-Ouchi[2,1], Kotaro Fukui[5], Hideaki Motoyama[1,3], Yu Hoshina[6], Fumio Nakazawa[1,3], Takashi Obase[2], Hiroshi Ohno[7], Ikumi Oyabu[1], Fuyuki Saito[8], Konosuke Sugiura[9], Toshitaka Suzuki[10]

[1]*National Institute of Polar Research, Research Organization of Information and Systems, Tachikawa 190-8518, Japan*

[2]*Atmosphere and Ocean Research Institute, The University of Tokyo, Kashiwa 277-8564, Japan*

[3]*Department of Polar Science, The Graduate University of Advanced Studies (SOKENDAI), Tachikawa 190-8518, Japan*

[4]*Japan Agency for Marine Science and Technology (JAMSTEC), Yokosuka 237-0061, Japan*

[5]*Tateyama Caldera Sabo Museum, Toyama 930-1405, Japan*

[6]*Graduate School of Environmental Studies, Nagoya University, Nagoya 464-8601, Japan*

[7]*Kitami Institute of Technology, Kitami 090-8507, Japan*

[8]*Japan Agency for Marine Science and Technology (JAMSTEC), Yokohama 236-0001, Japan*

[9]*Faculty of Sustainable Design, University of Toyama, Toyama 930-8555, Japan*

[10]*Faculty of Science, Yamagata University, Yamagata 990-8560, Japan*

The retrieval of continuous ice core records of more than 1 Myr is an important challenge in palaeo-climatology. For identifying suitable sites for drilling such ice, the knowledge of the subglacial topography and englacial layering is crucial. For this purpose, extensive ground-based ice radar surveys were done over Dome Fuji in the East Antarctic plateau during the 2017–2018 and 2018–2019 austral summers by the Japanese Antarctic Research Expedition, on the basis of ground-based radar surveys conducted over the previous ~30 years. High-gain Yagi antennae were used to improve the antenna beam directivity and thus attain a significant decrease in hyperbolic features in the echoes from mountainous ice-bedrock interfaces. We combined the new ice thickness data with the previous ground-based data, recorded since the 1980s, to generate an accurate high-spatial-resolution (up to 0.5 km between survey lines) ice thickness map. This map revealed a complex landscape composed of networks of subglacial valleys and highlands, which sets substantial constraints for identifying possible locations for new drilling. In addition, our map was compared with a few bed maps compiled by earlier independent efforts based on airborne radar data to examine the difference in features between sets of the data.

References

Tsutaki, S., Fujita, S., Kawamura, K., Abe-Ouchi, A., Fukui, K., Motoyama, H., Hoshina, Y., Nakazawa, F., Obase, T., Ohno, H., Oyabu, I., Saito, F., Sugiura, K., and Suzuki, T.: High-resolution subglacial topography around Dome Fuji, Antarctica, based on ground-based radar surveys conducted over 30 years, The Cryosphere Discuss. [preprint], https://doi.org/10.5194/tc-2021-266, in review, 2021.

Surface temperature changes at Dome Fuji region during the past four decades

Shohei Morino[1], Naoyuki Kurita[2], Takao Kameda[3] , Naohiko Hirasawa[4] and Hideaki Motoyama[4]
[1]*Graduate School of Environmental Studies, Nagoya University*
[2]*Institute of Space-Earth Environmental Research, Nagoya University*
[3]*Research Fields in Civil and Environmental Engineering, Kitami Institute of Technology*
[4]*National Institute of Polar Research*

Inland Dronning Maud Land (DML) on East Antarctic Plateau is one of the regions in which weather observations are the shortest and sparsest in the world. Due to its remoteness and harsh environment, atmospheric weather stations (AWSs) were installed at Dome Fuji (77.32˚S, 39.70˚E, 3780m a.l.s.) and Relay station (74.01˚S, 42.98˚E, 3354m a.l.s.) in inland DML only in 1995 and there are only a few AWSs with an observation period of more than 20 years. The 20-years observations are not enough to assess climate change in association with global warming due to the influence of internally-driven decadal variability. One of the alternative tools to explore climate changes in inland DML is to use the state-of-the-art global atmospheric reanalysis data. Thanks to recent advancement of data assimilation system and model, the reanalyses reasonably capture the mean and seasonal surface air temperature cycle in the Antarctic interior. Here we present a new reconstruction of the surface air temperature (SAT) record in inland DML to explore the SAT changes in association with global warming.

It is well known that the SAT measurements over Antarctic Plateau are largely subject to warm bias due to solar radiative heating (Genthon et al. 2011). Thus, we quantified the warm bias and then removed the errors after the correction (Morino et al. under review). For missing observations before 1995, we estimated the SAT using adjusted temperature data from the European Center for Medium Range Weather Forecasts (ECMWF) ERA5 (Hersbach et al. 2020). The lack of observations leads to increased sensitivity of the reanalysis to their model dynamics and leads to increase the uncertainty of their product. Recent study reported that the ERA5 underestimate surface air temperature (SAT) during winter months over the Antarctic interior (Gossart et al. 2019). In this study, we compared the daily SAT between the ERA5 and the corrected observations and then applied the regression model to correct the winter bias of ERA5 (Fig.1a). As shown in Fig.1b, the reconstructed forty-years long SAT data at Dome Fuji does not show a clear warming trend, however we can find six record high annal-mean SATs during the twenty-first century. It is not a clear but we can think that these are early signs of the influence of global warming. In this presentation, we will discuss if these SAT peaks are localized or the are reflected the changes of large-scale atmospheric circulation.

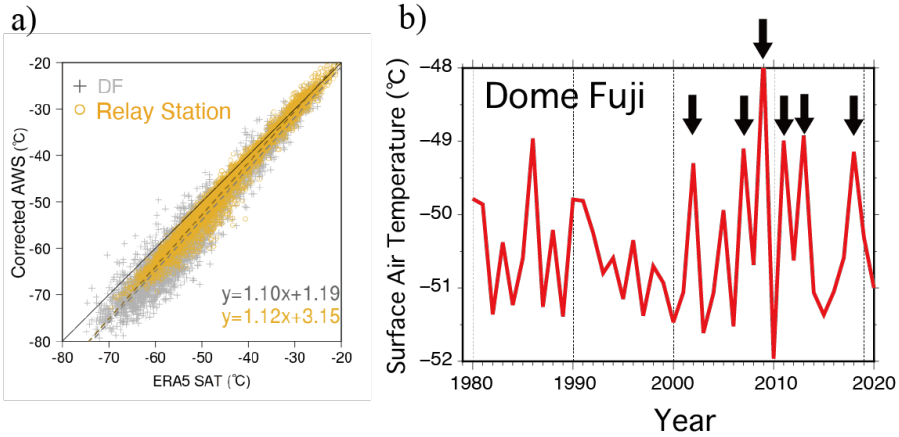

Figure1. a) Comparison of the SAT between the ERA5 and corrected AWS. b) Time series of the reconstructed annual mean SAT at Dome Fuji

References

Genthon, C., et al., Atmospheric temperature measurement biases on the Antarctic Plateau, J. Atoms. Oceanic. Technol., 28, 1598-1605, 2011.

Morino, S., et al., Comparison of ventilated and unventilated air temperature measurements in inland Dronning Maud Land on the East Antarctic Plateau, Submitted to J. Atoms. Oceanic. Technol.

Hersbach H., et al., The ERA5 global reanalysis, Q. J. R. Meteorol. Soc., 146, 1999–2049, 2020.

Gossart, A., et al, An evaluation of surface climatology in state-of-the-art reanalyses over the Antarctic ice sheet, J. Clim., 32, 6899-6915, 2019.

Atmospheric responses to the sea surface temperature in the Chukchi and Bering Seas

Yoshimi Kawai[1]
[1]*Research Institute for Global Change, Japan Agency for Marine-Earth Science and Technology*

Atmospheric responses to ocean surface temperature (ST) fronts related to western boundary currents have been extensively investigated, but at higher latitudes where sea ice exists, the responses to ST, which is defined here as the temperature of open water and sea ice, excluding land surface, has not been examined sufficiently, mainly due to the difficulties of observations. The horizontal ST gradient becomes especially large over the border between open water and sea ice, and it will affect the atmosphere. In this study, the author has analyzed 32 years of high-resolution atmospheric reanalysis data, the Climate Forecast System Reanalysis (CFSR) and Climate Forecast System version 2 (CFSv2) (Saha et al. 2010, 2014), to determine the atmospheric responses to ST fronts in the Bering Sea and Chukchi Sea. Climatological mean fields are investigated by using only the CFSR data until 2010 because diabatic heating data after 2010 are not release.

In the Chukchi Sea, ST peaks in August, but its horizontal gradient becomes largest in November. Convergence of 10-m-high wind is also large in October and November, and approximately zero or negative from February to August. On the other hand, there is a clear contrast in ST between the continental shelf and the southwestern deep basin of the Bering Sea throughout the year, which develops in winter. The ST front shifts southward as sea ice spreads over the shelf region, and the front is located immediately above the northern flank of the shelf break in March, when the marginal ice zone extends furthest south. In both the Chukchi and Bering Seas, the spatial distribution of surface wind convergence and the Laplacians of ST and sea level pressure agree well with each other, which indicates that the pressure adjustment mechanism is dominant (e.g. Minobe et al. 2008). The annual mean of 10-m-height wind convergence obviously reflects the bottom topography in the Bering Sea through the ST regulated by the seafloor depth (Fig.1).

Ascending motion and diabatic heating develop over the Chukchi Sea in October and November, corresponding to surface wind convergence; however, this response is confined to the lower troposphere (Fig.2). Diabatic heating is dominated by the vertical diffusion component. Turbulent heat fluxes at the sea surface becomes especially large in late autumn, when sea ice is increasing, resulting in the intensification of heating and low-level clouds. Ascent is also strengthened over the shelf break and a circulation pattern similar to horizontal convection appears over the shelf in the Bering Sea in late winter. Low-level clouds show a clear contrast across the shelf break in the Bering Sea, and downward solar radiation at the surface reflects the spatial pattern of the clouds. The bottom topography regulates the ST and affects clouds and incoming radiation.

During 1979–2020, the Arctic Ocean including the Chukchi Sea experienced drastic warming and retreat of sea ice in autumn, although ST exhibited no clear trends in the Bering Sea in the cold season. Over the Chukchi Sea, there was a tendency for low-level clouds to rise in October and November, which corresponded to the warming trend. This is consistent with a previous study that analyzed in situ observation data (Sato et al. 2012). The analysis of surface heat fluxes supported the indication of another previous study (Lee et al. 2017) that while downward longwave radiation was responsible for the ST increase near the Pole, the ocean warming increased turbulent heat fluxes in the northern Chukchi Sea. The results in this study have been published in Kawai (2021).

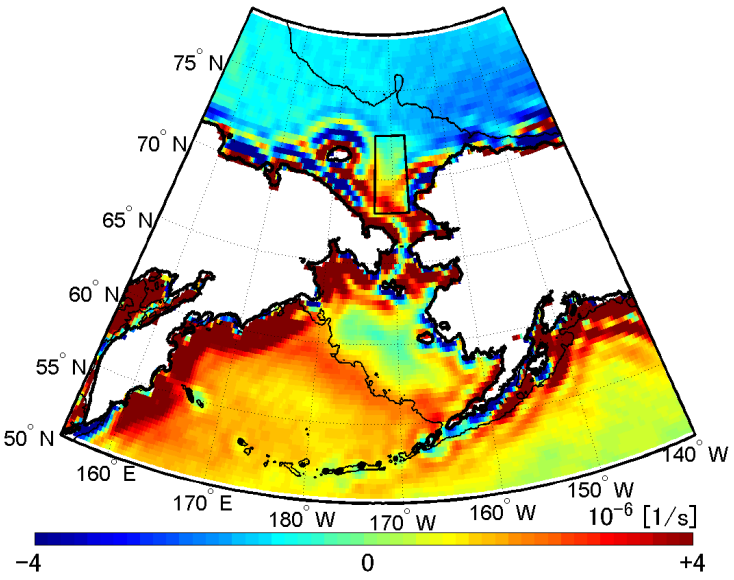

Figure 1. Annual-mean climatologies of 10-m-high wind convergence. Black solid lines are depth contours of 200 m. Black solid boxes denote analysis areas in Fig. 2.

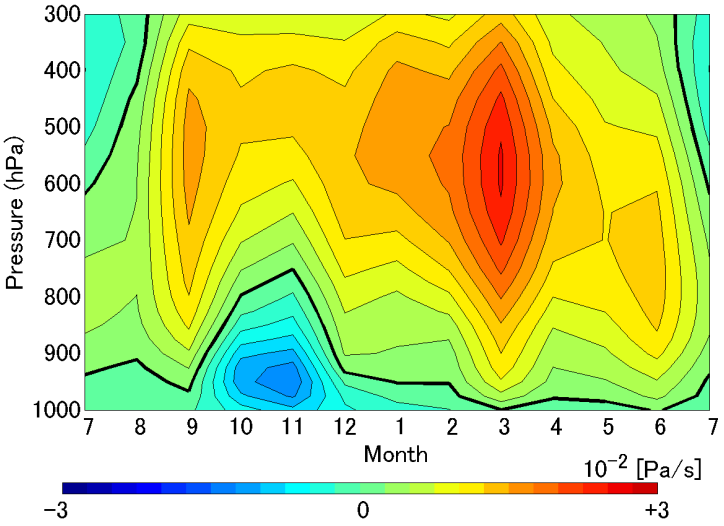

Figure 2. Seasonal variations of vertical velocity averaged over the area of 68.0–72.5°N, 167.5–173.0°W (black solid box in Fig. 1) in the Chukchi Sea. Negative values indicate ascending motion.

References

Kawai, Y. (2021). Low-level atmospheric responses to the sea surface temperature fronts in the Chukchi and Bering Seas. *Front. Mar. Sci.*, 8, doi:10.3389/fmars.2021.598981.

Lee, S., T. Gong, S. B. Feldstein, J. A. Screen, and I. Simmonds (2017). Revisiting the cause of the 1989-2009 Arctic surface warming using the surface energy budget: Downward infrared radiation dominates the surface fluxes. *Geophys. Res. Lett.* 44, 10654-10661. doi:10.1002/2017GL075375.

Minobe, S., A. Kuwano-Yoshida, N. Komori, S. –P. Xie, and R. J. Small (2008). Influence of the Gulf Stream on the troposphere. *Nature*. **452**, 206-209. doi:10.1038/nature06690.

Saha, S., and co-authors (2010). The NCEP climate forecast system reanalysis. *Bull. Amer. Meteor. Soc.* **91**, 1015-1057. doi:10.1175/2010BAMS3001.1.

Saha, S., and co-authors (2014). The NCEP climate forecast system version 2. *J. Clim*. **27**, 2185-2208. Doi:10.1175/JCLI-D-12.00823.1.

Sato, K., J. Inoue, Y. Kodama, and J. E. Overland (2012). Impact of Arctic sea-ice retreat on the recent change in cloud-base height during autumn. *Geophys. Res. Lett.* 39, L10503. doi:10.1029/2012GL051850.

Year-round measurements of ice nucleating particles in Svalbard during MOSAiC 2019/20

Yutaka Tobo[1,2], Hitoshi Matsui[3], Kei Kawai[3], Sho Ohata[3], Yutaka Kondo[1], Ove Hermansen[4], Jun Inoue[1,2] and Makoto Koike[5]
[1]*National Institute of Polar Research, Tachikawa, Tokyo, Japan*
[2]*SOKENDAI, Tachikawa, Tokyo, Japan*
[3]*Nagoya University, Nagoya, Aichi, Japan*
[4]*Norwegian Institute for Air Research, Kjeller, Norway*
[5]*University of Tokyo, Tokyo, Japan*

It is recognized that a small subset of insoluble aerosol particles called “ice nucleating particles (INPs)” can serve as nuclei for ice crystal formation in Arctic mixed-phase clouds. The existence of INPs can significantly affect the cloud properties and lifetime; however, there is no quantitative understanding of how their amount and source are characterized in the Arctic climate system. Our previous field work at various locations in the Arctic have shown that the number concentrations of INPs could be enhanced under the influence of certain local aerosols (e.g., dust and sea spray aerosols) emitted from ice-free areas in high latitudes (Tobo et al., 2019; Inoue et al., 2021). This raised the question of whether aerosol emissions from high-latitude sources could induce measurable regional and seasonal variations of INPs in the Arctic atmosphere. In this presentation, we will report on a year-round record of the number concentrations of INPs active under conditions relevant for mixed-phase clouds (i.e., temperatures of −30°C to 0°C above water saturation) measured on Mt. Zeppelin in Svalbard during the Multidisciplinary drifting Observatory for the Study of Arctic Climate (MOSAiC) project period in 2019/20 (https://mosaic-expedition.org/). We will further discuss possible factors causing the variations of INPs in the Svalbard region based on the analysis of ambient aerosols, trace gases, and meteorological conditions.

References

Tobo, Y., K. Adachi, P. J. DeMott, T. C. J. Hill, D. S. Hamilton, N. M. Mahowald, N. Nagatsuka, S. Ohata, J. Uetake, Y. Kondo and M. Koike, Glacially sourced dust as a potentially significant source of ice nucleating particles, Nature Geoscience, 12, 253-258, 2019.

Inoue, J., Y. Tobo, F. Taketani and K. Sato, Oceanic supply of ice-nucleating particles and its effect on ice cloud formation: A case study in the Arctic Ocean during a cold-air outbreak in early winter. Geophysical Research Letters, 48, e2021GL094646, 2021.

Marine ice-nucleating particles and its effect on ice cloud formation: A result from the Arctic research cruise during a cold-air outbreak in early winter

Jun Inoue[1], Yutaka Tobo[1], Fumikazu Taketani[2] and Kazutoshi Sato[3]
[1]*National Institute of Polar Research, Tachikawa, Japan*
[2]*Japan Agency for Marine-Earth Science and Technology, Yokohama, Japan*
[3]*Kitami Institute of Technology, Kitami, Japan*

The cloud representation related to the cloud phase, number concentration of ice-nucleating particles (INPs), and sea-surface conditions are vital in modeling climate systems. The Arctic sea-ice decline and intensified atmospheric forcing over the ice-free ocean induce high wave conditions, increasing dynamical geochemical oceanic mixing and sea spray supply containing organic substances. These marine aerosols could act as INPs, which promotes the formation of lower tropospheric ice-containing clouds. Here, we show that the surface ocean state regulates INP concentration and ice cloud presence in the boundary layer (Inoue et al., 2021). Data from a research cruise by RV Mirai from the marginal ice zone in the Chukchi Sea in November 2018 revealed high number concentrations of INPs active greater than -10°C. Simultaneously, ice-containing clouds under high wave conditions were observed by cloud particle sensor sondes. Chemical analysis revealed high contents of organic carbon and sea salt that coincided with the increased oceanic turbidity. The findings suggest that elevated levels of marine aerosols will modify the cloud phase from liquid droplets to ice crystals. Based on this result, we will also introduce the research plan for investigating the marine INPs over the Southern Ocean in this presentation.

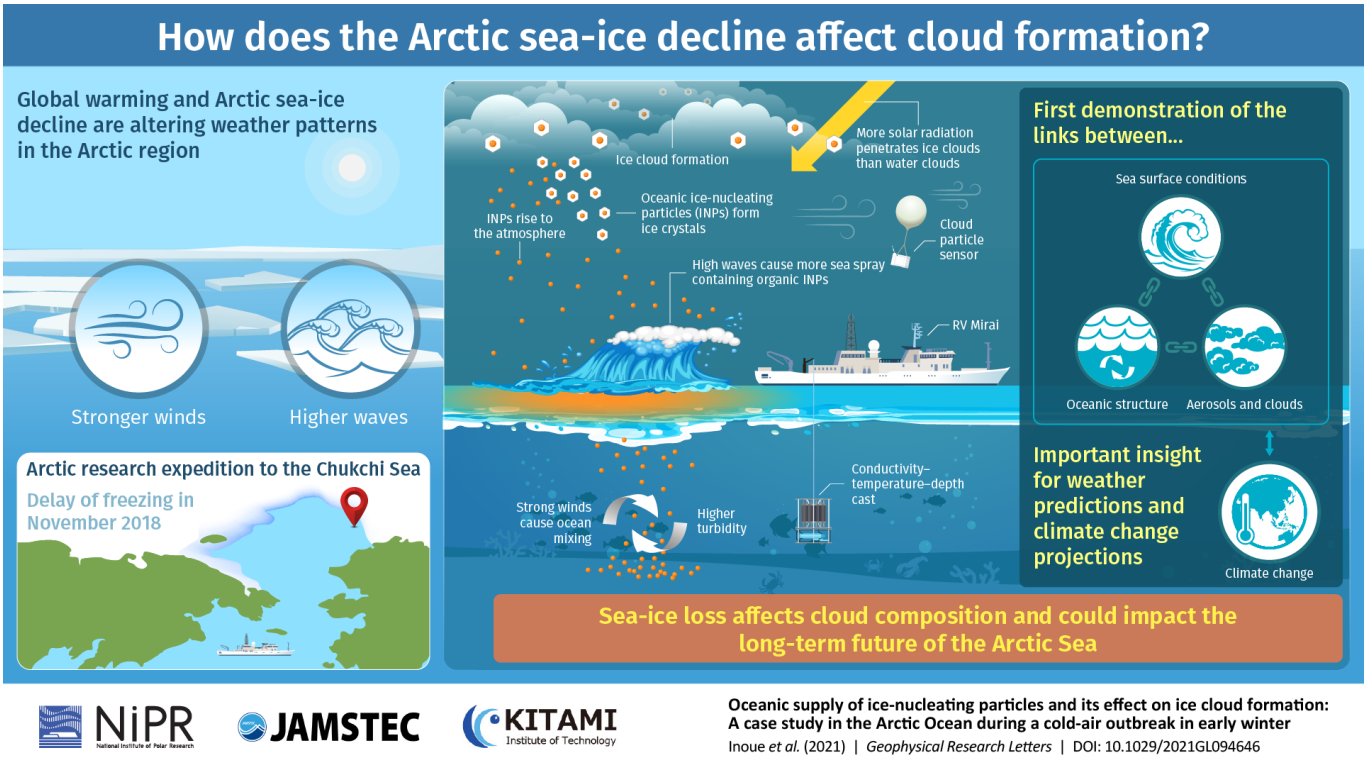

Figure 1. A summary figure

References

Inoue, J., Y. Tobo, F. Taketani and K. Sato (2021), Oceanic supply of ice- nucleating particles and its effect on ice cloud formation: A case study in the Arctic Ocean during a cold-air outbreak in early winter. Geophysical Research Letters, 48, e2021GL094646.

Seasonal change in satellite-retrieved ice cloud fraction in the lower troposphere over the Southern Ocean

Kazutoshi Sato[1] and Jun Inoue[2,3]
[1]*Kitami Institute of Technology*
[2]*National Institute of Polar Research*
[3]*The Graduate University for Advanced Studies*

Cloud in the polar regions plays a major role in the climate system. Various studies related to cloud over the high latitudes in the Southern Hemisphere (SH) have been conducted using numerical climate model and satellite date sets. Although numerical climate models are useful for the study of the atmospheric circulation globally, excess shortwave radiation biases over the SO are major problems in such models. Biases toward higher numbers and larger sizes of ice-nucleating particles (INPs) promote enhanced formation and growth of ice cloud in global numerical climate models, enhancing downward shortwave radiation at the surface over the SO. Therefore, investigation using observational data is required to elucidate the relationship between the fraction of ice cloud and INPs over the SH. This study investigated the temperature and fraction of ice cloud in the troposphere over Antarctica and the Southern Ocean using Cloud-Aerosol Lidar and Infrared Pathfinder Satellite Observation (CALIPSO) satellite data (2006–2015). Although ice cloud usually occurs under very cold conditions (e.g., <−38°C), low-level ice cloud (cloud altitude: <2 km) is observed over the SO under higher temperature conditions because various aerosols influence ice cloud formation during summer and winter. During summer, a local maximum fraction of low-level ice cloud below 2 km is observed under high temperature conditions (>−7.5°C). High fractions of low-level ice cloud under high temperature conditions are observed near coastal Antarctica regions with sea ice, coincident with the highest chlorophyll-*a* concentration. In contrast, the low-level ice cloud has the local maximum fraction under high temperature conditions (>−17.5°C) during winter. The highest fractions of low-level ice cloud under high temperature conditions are over the coastal Antarctic ice-covered area, coincident with considerable heat exchange from the ocean to the air. These satellite and reanalysis datasets suggest that marine aerosols act as INPs for ice cloud formation during summer and winter.

Acknowledgements
This work was supported by a JSPS Overseas Research Fellowship, JSPS KAKENHI (20H04963, 19K14802, 18H05053).

Diffusive CDW flux in the East Antarctic margin

Kaihe Yamazaki[1], Kohei Mizobata[2] and Shigeru Aoki[1]
[1]*Institute of Low Temperature Science, Hokkaido University*
[2]*Tokyo University of Marine Science and Technology*

Circumpolar Deep Water (CDW), the primary source of heat and salt for the Antarctic coasts, is transported across the westward slope current predominantly by transient eddies in the absence of large-scale zonal pressure gradient. In reality, pressure gradient associated with topographic features generates standing eddies, facilitating the meridional water exchange (Mizobata et al., 2020; Yamazaki et al., 2020). Topography-controlled geostrophic flows can transport CDW poleward (e.g., Hirano et al., 2021). However, the steep barotropic potential vorticity (PV) gradient on the upper continental slope (inshore of ~3,000 m isobaths) unlikely allows for the presence of the cross-slope mean flow, and hence eddy diffusion and/or tidal mixing might be essential for the onshore CDW flux near the shelf break (Yamazaki et al., 2020). From an observational standpoint, the present study quests (1) to delineate the controlling factor of the eddy diffusion in the Antarctic margin and (2) to quantify the diffusive CDW flux towards the Antarctic continental shelves. Based on the mixing length framework (Naveira Garabato et al., 2011), eddy diffusivity was derived from hydrography and satellite altimetry synthesis (Figure 1). The isopycnal diffusivity of CDW is relatively high where its intrusion is localized (e.g., 70, 90, 110, 120, 140°E), associated with the gentle slope and the small PV gradient. Applying the diffusivity to the isopycnal thickness field, the onshore CDW/heat transport was quantified in each ocean basin (Figure 2). This estimate suggests that CDW supplies sufficient heat and buoyancy required for the glacial melting (~1 TW) and sea ice formation (~3TW) over the continental shelves.

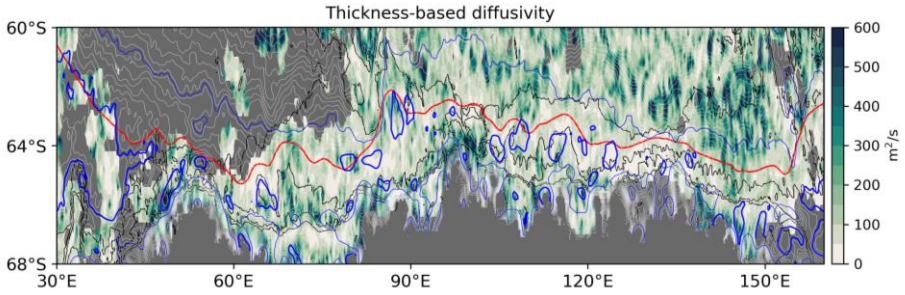

Figure 1. Diffusivity of CDW (color shade) based on layer thickness as a PV-conservative tracer. Red curve is ACC's southern boundary, and thick blue curve is dynamic topography of –1.97 m indicative for recirculating gyres. Black contour is the isobath of 1000 m intervals.

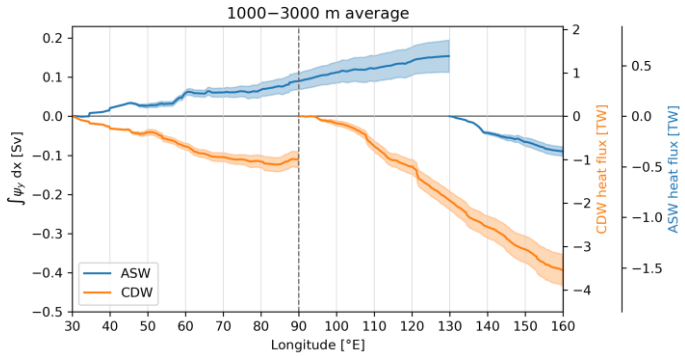

Figure 2. Along-slope integration of meridional volume (Sv = 10^6 m^3/s) and heat (TW) transport. Transports of CDW and Antarctic Surface Water are individually shown. The integration of CDW is divided at 90°E corresponding to the Princess Elizabeth Trough.

References

K. Mizobata, K. Shimada, S. Aoki, Y. Kitade, The Cyclonic Eddy Train in the Indian Ocean Sector of the Southern Ocean as Revealed by Satellite Radar Altimeters and In Situ Measurements. J. Geophys. Res. Ocean. 125 (2020).
K. Yamazaki, S. Aoki, K. Shimada, T. Kobayashi, Y. Kitade, Structure of the Subpolar Gyre in the Australian-Antarctic Basin Derived From Argo Floats. J. Geophys. Res. Ocean. 125 (2020).
D. Hirano, K. Mizobata, H. Sasaki, H. Murase, T. Tamura, S. Aoki, Poleward eddy-induced warm water transport across a shelf break off Totten Ice Shelf, East Antarctica. Commun. Earth Environ. 2 (2021).
A. C. Naveira Garabato, R. Ferrari, K. L. Polzin, Eddy stirring in the Southern Ocean. J. Geophys. Res. Ocean. 116, 1–29 (2011).

Investigation on the interactions between the downslope flow of Antarctic Bottom water and upslope flow of modified Circumpolar Deep Water using a high-resolution model

Vigan Mensah[1], Yoshihiro Nakayama[1], Masakazu Fujii[2], Yoshifumi Nogi[2], Kay I. Ohshima[1]

[1] *Institute of Low Temperature Science, Hokkaido University, Japan*

[2]*National Institute of Polar Research, Tachikawa, Japan*

In the Southern Ocean, the upslope flow of warm modified Circumpolar Deep Water (mCDW) onto the Antarctic shelf is of crucial importance because these warm waters affect ice shelf melting and play a role in maintaining coastal polynyas. The upslope flow of mCDW is favored by the presence of canyons across the continental slope. In a recent study, Morrison et al. (2020) demonstrated that the upslope flow of CDW in canyons is strongly correlated to the downslope flow of Dense Shelf Water (DSW) in dense water formation regions. They also proposed a mechanism explaining the upslope flow by the existence of a cross-canyon pressure gradient and a barotropic geostrophic balance within the canyons.

Here, we develop a high-resolution model (500 m horizontal and 20 m vertical grid spacing) and compare it with Morrison et al. (2020)'s, whose resolution was (O)10^0 km. Our model domain is the Cape Darnley region in East Antarctica, where DSW is formed and flows down the continental slope -via several canyons- to form Cape Darnley Bottom Water. There, very-high resolution bathymetric data were recently acquired by Japanese icebreaker *Shirase* around the Wild Canyon system. The high-resolution bathymetric data and model offer a unique opportunity to further investigate the dynamics affecting the upslope flow as well as interaction with bottom water formation by analyzing data within individual canyons of the Wild Canyon system. We focus on the upslope flow's water masses, properties, and how these change along the slope. We also investigate the existence and relative importance of a baroclinic component within the canyons, and whether mesoscale eddies also play a role in the transfer of water to the shelf break. We also delineate how the various canyons dimensions and presence of sub-canyons affect the upslope flow. We further discuss whether Morrison et al. (2020)'s mechanism may be extended to a whole canyon system, in addition to individual canyons.

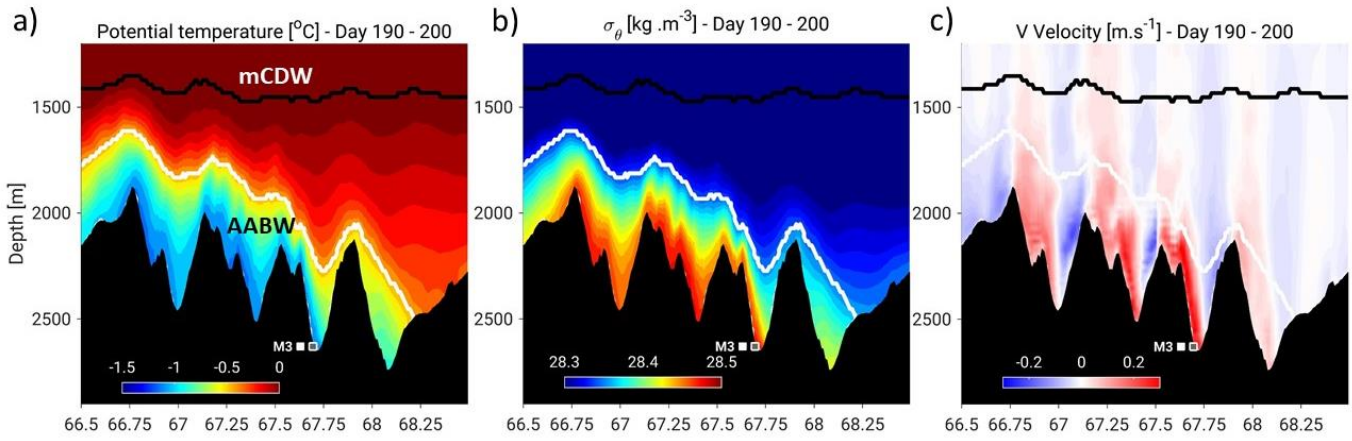

Figure 1. Cross-section of (a) potential temperature, (b) potential density, and (c) meridional velocity across the Wild Canyon system averaged between day 190-200 of our 500-m resolution model in the Cape Darnley region. The black and white solid lines represent the limits of modified Circumpolar Deep Water (mCDW) and Antarctic Bottom Water (AABW), respectively. Opposite-sign velocities in (c) are indicative that downslope flow (warm colors) and upslope flow (cold colors) occur simultaneously within the canyons.

References

Morrison, A.K., Hogg, A.M.C.C., England, M.H., Spence, P., 2020. Warm circumpolar deep water transport toward Antarctica driven by local dense water export in canyons. Sci. Adv. 6 (18), http://dx.doi.org/10.1126/sciadv.aav2516.

Spatiotemporal high-resolution mapping of biological production in the Southern Ocean

Lai XX [1], Pan XL [1], Li BF [2], Makabe R [3], Hirano D [3], Watanabe YW [2]

[1] *Graduate School of Environmental Science, Hokkaido University, Sapporo, Hokkaido, Japan*
[2] *Faculty of Environmental Earth Science, Hokkaido University, Sapporo, Hokkaido, Japan*
[3]*National Institute of Polar Research, Tachikawa, Tokyo, Japan*

The Southern Ocean (SO, south of 30°S) is considered to play an important role in the biogeochemical cycling of carbon and nutrients. During the Last Glacial Maximum (LGM), an increase of biological production in the SO may reduce atmospheric CO2 concentrations and contribute to global cooling. It is still do not know how anthropogenic global warming and climate change are changing biological production in the SO due to the difficulty of observation due to severe weather and ocean conditions. In this study, the new idea of combining autonomous ocean observation robotics and parameterization allowed us to solve this problem. We obtained the detailed spatiotemporal distribution of net community production (NCP) in the SO during the period from 2007 to 2019, indicating annual mean NCP inventory (down export from the surface mixed layer to the ocean interior) of 3.1 Pg-C $year^{-1}$ in the surface mixed layer over the SO, where accounts for 30% of global annual oceanic carbon export even if accounts for 5% of the global oceanic net primary production. Furthermore, the decadal change in the annual NCP inventory from 2013 to 2019 indicated that biological production in the surface mixed layer of the SO was decreasing at a rate of 1% per year.

References

1. Sigman, D. M. & Boyle, E. A. Glacial/Interglacial changes in atmospheric carbon dioxide. Nature 407, 859-869 , 2000.
2. Dunne, J. P., Armstrong, R. A., Gnnadesikan, A. & Sarmiento, J. L. Empirical and mechanistic models for the particle export ratio. Global Biogeochemical Cycles, 19, GB4026, 2005.

Excess silicate removal over the Southern Ocean

Pan XL [1], Lai XX [1], Li BF [2] and Watanabe YW [2]

[1] *Graduate School of Environmental Earth Science, Hokkaido University, Japan*
[2] *Faculty of Environmental Earth Science, Hokkaido University, Japan*

Subantarctic Mode Water (SAMW), which formed in the surface Southern Ocean (SO, south of 30˚S), serves as the major nutrient source (Nitrate: N, Silicate: Si) for marine primary production in low-latitude surface waters. Global ocean model suggested that if we alter SAMW to contain no nutrients, the primary production outside the SO would be reduced to up to a quarter *[Sarmiento et al., 2004; Palter et al., 2010]*. From high-latitude region (~65˚S) to SAMW formation region (~50˚S), the surface water changes from being rich in both Si and N to being N-rich but Si-depleted, indicating that Si is removed in excess from the SO surface water compared to N. This could lead to large-scale Si deficiency in the global surface ocean and limitation of diatom growth. However, there are still few studies that can give us a comprehensive estimation of this excess Si removal over the SO due to the sparseness of detailed observations of nutrients. We recently developed the chemical parameterization technique to achieve the expansion of observational data by combining with sensor-equipped observation instruments (e.g. CTD, Argo float), using only basic hydrographic parameters (temperature, salinity, dissolved oxygen, pressure) *[Li et al., 2019; Pan et al., 2020; Pan et al., submitted]*. In this study, we attempt to quantify the excess Si removal and access the seasonal and annual variation in the SO based on autonomous ocean observation robotics (Argo) data and the parameterization technique. We found that the removal rate of silicate in the mixed layer was ~5 T-mol year^{-1} over the SO as a mean value during 2003-2019, which was 1.3 times that of nitrate. At high-latitude region south of 65˚S, most of the removal of Si occurs, which may be relative to the silicification of diatoms due to iron deficiency. The new findings will help us better understand the SO Si-cycle and its impact on the global ocean.

References

Sarmiento, J., Gruber, N., Brzezinski, M. A., and Dunne, J. P.: High-latitude controls of thermocline nutrients and low latitude biologial productivity, *Nature*, 427, 56–60, 2004.

Palter, J. B., Sarmiento, J. L., Gnanadesikan, A., Simeon, J., and Slater, R. D.: Fueling export production: nutrient return path-ways from the deep ocean and their dependence on the Meridional Overturning Circulation, *Biogeosciences*, 7, 3549–3568, https://doi.org/10.5194/bg-7-3549-2010, 2010.

Li, B. F., Watanabe, Y. W., Hosoda, S., Sato, K. & Nakano, Y. Quasi-Real-Time and High-Resolution Spatiotemporal Distribution of Ocean Anthropogenic CO2. *Geophys. Res. Lett.* 46, 4836-4843, doi:10.1029/2018gl081639, 2019.

Pan, X. L., Li, B. F. & Watanabe, Y. W. The Southern Ocean with the largest uptake of anthropogenic nitrogen into the ocean interior. *Sci. Rep.* **10**, 8838, doi:10.1038/s41598-020-65661-2, 2020.

Pan, X. L., Li, B. F. & Watanabe, Y. W. Intense ocean freshening from melting glacier around the Antarctica during early 21st century. *Submitted*

Antarctic Peninsula warm winters influenced by Tasman Sea temperatures

Kazutoshi Sato[1,2], Jun Inoue[3,4,2], Ian Simmonds[5] and Irina Rudeva[6,5]
[1]*Kitami Institute of Technology*
[2]*Japan Agency for Marine-Earth Science and Technology*
[3]*National Institute of Polar Research*
[4]*The Graduate University for Advanced Studies*
[5]*The University of Melbourne*
[6]*Australian Bureau of Meteorology*

The Antarctic Peninsula of West Antarctica was one of the most rapidly warming regions on the Earth. The enhanced warm advection associated with changes in the atmospheric circulations over the Southern Ocean (e.g., the Amundsen Sea Low [ASL] or the Southern Annular Mode [SAM]) causes the warming over West Antarctica. Previous studies reveal that the El Niño-Southern Oscillation (ENSO) response to tropical sea surface temperature (SST) anomaly modulates the position and strength of the ASL, often called 'tropical-polar teleconnections'. Over the Northern Hemisphere, an atmospheric response to oceanic forcing over the midlatitude accelerated warming of lower troposphere at high latitude. However, the impact of change in SST into the Southern Hemisphere mid-latitudes on Antarctic climate variability remains uncertain. In recent years, warming sea temperature in the Tasman Sea is reported by previous studies. A warming Tasman Sea has strengthened the westerlies between high and mid-latitudes, and thus has influenced cyclone tracks over the Southern Ocean. Therefore, these atmospheric circulation changes related to anomalous SST warming over the Tasman Sea would contribute to recent anomalous warm AP winters. This investigation reveals that warming SST in the Tasman Sea modify Southern Ocean storm tracks in winter. This, in turn, induces warming over the Antarctic Peninsula and sea ice retreats over the Bellingshausen Sea and Drake Passage via planetary waves triggered in the Tasman Sea. We show that atmospheric response to SST warming over the Tasman Sea deepen the ASL, leading to warm advection over the Antarctic Peninsula, even in the absence of anomalous tropical SST forcing.

Acknowledgements
This work was supported by a JSPS Overseas Research Fellowship, JSPS KAKENHI (20H04963, 19K14802, 18H05053).

Reference
Sato, K., Inoue, J., Simmonds, I., & Rudeva, I. (2021). Antarctic Peninsula warm winters influenced by Tasman Sea temperatures. *Nature Communications*, 12.

Seasonal and daily variation in Be-7 concentration of surface air at Syowa Station, Antarctica

Naohiko Hirasawa[1,2], Taku Nakamura[3], Miyoko Miwa[4], Mutsuo Inoue[5], Sakae Shirayama[1], Haruhito Yasuda[3], and Shigeki Tasaka[3]

[1]*National Institute of Polar Research, Research Organization of Information and Systems*

[2]*Department of Polar Science, School of Multidisciplinary Sciences, The Graduate University for Advanced Studies*

[3] *Department of physics, Gifu University*

[4] *Life Science Research Center, Gifu University*

[5] *Low level radioactivity laboratory, Kanazawa University*

Be-7 is a cosmogenic radionuclide produced from nitrogen and oxygen in the lower stratosphere. As soon as Be-7 is generated, it is adsorbed on the nearby aerosol and invades the troposphere with atmospheric exchange between the stratosphere and the troposphere. In the troposphere, it is removed with precipitation. The half-life is about 53 days, and considering the typical time scale of each atmospheric phenomenon, it can be used to elucidate the transport route of the stratospheric atmosphere associated with synoptic-scale disturbance. So far, Be-7 observations of Be-7 in the Antarctic region are not uncommon, but the observation points are limited and the whole picture of the Antarctic region is not given. There is no analysis focusing on atmospheric transport routes. From 2014 to 2017, we analyzed the Be-7 concentration in the atmosphere sampled for one day or half a day at JARE's three summer seasons, "Shirase", Syowa Station, and S17 on the ice sheet. We acquired new data on the spatial distribution over a wide area. As a result, we found concentration fluctuations associated with synoptic-scale atmospheric circulation and diurnal variations (Hirasawa et al. 2021, to be submitted and Hirasawa et al. 2019). Daily observation of Be-7 for the whole year have been started at Syowa Station since 2020, and the analysis for one year was completed in August of this year. In this presentation, we will give an overview of the results obtained from the summer observations from 2014 to 2017, and compare the characteristics of temporal changes that appear in the results of the current year-round observations with the results at Syowa Station of 2005 (Tasaka et al. 2012) and the characteristics of other stations.

References

Hirasawa, N., T. Nakamura, M. Miwa, T. Ojio, K. Yamada, and S. Tasaka (2019): Spatiotemporal variation of surface atmospheric 7Be from Australia to Syowa Station, and S17, The tenth Symposium on Polar Science, Tokyo, December 2019.

Hirasawa, N., T. Nakamura, M. Miwa, T. Ojio, K. Yamada, and S. Tasaka (2021): Spatiotemporal variations of Be-7 concentration in the surface atmosphere in the Antarctic region of the Australian to Indian sector, to be submitted.

Tasaka, S., M. Matsubara, T. Abe and T. Yamanouchi (2012): Mesurement of Be-7 at Syowa Station, The third Symposium on Polar Science, Tokyo, 30 November 2012.

Fractionation of O_2/N_2 and Ar/N_2 in the Antarctic ice sheet from precise gas measurements of the Dome Fuji ice core
-Constraining permeabilities of O_2, N_2 and Ar in the ice sheet with a simple diffusion model-

Ikumi Oyabu[1], Kenji Kawamura1[,2,3], Tsutomu Uchida[4], Shuji Fujita[1,2], Kyotaro Kitamura[1], Motohiro Hirabayashi[1], Shuji Aoki[5], Shinji Morimoto[5], Takakiyo Nakazawa[5], Jeffrey P. Severinghaus[6], Jacob D. Morgan[6]

[1] *National Institute of Polar Research, Japan*

[2] *Department of Polar Science, The Graduate University of Advanced Studies (SOKENDAI), Japan*

[3] *Japan Agency for Marine Science and Technology (JAMSTEC), Japan*

[4] *Division of Applied Physics, Faculty of Engineering, Hokkaido University, Japan*

[5] *Center for Atmospheric and Oceanic Studies, Graduate School of Science, Tohoku University, Japan*

[6] *Scripps Institution of Oceanography, University of California San Diego, USA*

The variations of $\delta O_2/N_2$ and $\delta Ar/N_2$ in the Dome Fuji ice core were measured from 112 m (bubbly ice) to 2001 m (clathrate hydrate ice). Our method, combined with the low storage temperature of the samples (-50 °C), successfully excludes post-coring gas-loss fractionation signals from our data. From the bubbly ice to the middle of the bubble-clathrate transition zone (BCTZ) (112 – 800 m) and below the BCTZ (>1200 m), the $\delta O_2/N_2$ and $\delta Ar/N_2$ data exhibit orbital-scale variations similar to local summer insolation. The data in the lower BCTZ (800 – 1200 m) have large scatters, which may be caused by mm-scale inhomogeneity of air composition combined with finite sample lengths. The insolation signal originally recorded at the bubble close-off remains through the BCTZ, and the insolation signal may be reconstructed by analyzing long ice samples (more than 50 cm for the Dome Fuji core). In the clathrate hydrate zone, the scatters around the orbital-scale variability decrease with depth, indicating diffusive smoothing of $\delta O_2/N_2$ and $\delta Ar/N_2$. A simple gas diffusion model was used to reproduce the smoothing and thus constrain their permeation coefficients. The relationship between $\delta Ar/N_2$ and $\delta O_2/N_2$ is markedly different for the datasets representing bubble close-off (slope ~0.5), bubble-clathrate hydrate transformation (~1), and post-coring gas-loss (~0.2), suggesting that the contribution of the mass-independent and mass-dependent fractionation processes are different for those cases. The method and data presented here may be useful for improving the orbital dating of deep ice cores over the multiple glacial cycles and further studying non-insolation-driven signals (e.g., atmospheric composition) of these gases. In the presentation, we will focus on the diffusion model to constrain the permeabilities of O_2, N_2 and Ar in the ice sheet.

On-shelf warm water circulation toward Totten Ice Shelf, East Antarctica

Daisuke Hirano[1,2], Takeshi Tamura[1,2], Kazuya Kusahara[3], Masakazu Fujii[1,2], Kaihe Yamazaki[4], Yoshihiro Nakayama[4], Kazuya Ono[4], Takuya Itaki[5], Yuichi Aoyama[1,2], Daisuke Simizu[1], Kohei Mizobata[6], Kay I. Ohshima[4], Yoshifumi Nogi[1,2], and Shigeru Aoki[4]

[1]*National Institute of Polar Research*
[2]*The Graduate University for Advanced Studies, SOKENDAI*
[3]*Japan Agency for Marine-Earth Science and Technology*
[4]*Institute of Low Temperature Science, Hokkaido University*
[5]*National Institute of Advanced Industrial Science and Technology*
[6]*Tokyo University of Marine Science and Technology*

Mass loss from the Antarctic Ice Sheet results directly in global sea-level rise. The massive continental ice behind the Totten Ice Shelf (TIS) in East Antarctica, equivalent to 3.5 m of sea-level potential (Greenbaum et al., 2015), might be vulnerable to ocean forcing. Behavior of warm water can hence control the dynamics of TIS and Totten Glacier (Greene et al., 2017; Rintoul et al., 2016). In this talk, we present analyses of comprehensive in-situ observations over the unprecedentedly broad region from the continental slope to TIS. The first multibeam sonar survey reveals details of >1000 m deep glacial troughs connecting the TIS cavity with the outer depression. Hydrographic observations unveil on-shelf circulation of warm modified Circumpolar Deep Water toward TIS via deep topographic passage throughout the shelf break, depression, and glacial troughs, which is also supported by a numerical simulation. The mooring record and multi-year hydrographic profiles at the TIS ice front demonstrate tidal to seasonal and/or interannual variability of temperature near the bottom. This study provides key evidence for identifying environmental settings and variability of the oceanic heat delivery to the TIS, which is indispensable in understanding the response of East Antarctic Ice Sheet.

References

Greenbaum, J. S., et al. (2015), Ocean access to a cavity beneath Totten Glacier in East Antarctica, *Nat Geosci*, 8(4), 294-298, doi:10.1038/Ngeo2388.

Greene, C. A., D. D. Blankenship, D. E. Gwyther, A. Silvano, & E. van Wijk (2017), Wind causes Totten Ice Shelf melt and acceleration, *Sci Adv*, 3(11), e1701681, doi:10.1126/sciadv.1701681.

Rintoul, S. R., et al. (2016), Ocean heat drives rapid basal melt of the Totten Ice Shelf, *Sci Adv*, 2(12), e1601610, doi:10.1126/sciadv.1601610.

Effects of snow and remineralization processes on nutrients distributions in the multi-year land-fast Antarctic sea ice

Reishi Sahashi[1], Daiki Nomura[1, 2, 3], Takenobu Toyota[4], Masato Ito[5], Manami Tozawa[1], Pat Wongpan[6], Kazuya Ono[4], Daisuke Simizu[5], Kazuhiro Naoki[7], Takeshi Tamura[5, 8], Shigeru Aoki[4], Shuki Ushio[5, 8]

[1]Faculty of Fisheries Sciences, Hokkaido University, [2]Field Science Center for Northern Biosphere, Hokkaido University, [3]Arctic Research Center, Hokkaido University, [4]Institute of Low Temperature Science, Hokkaido University, [5]National Institute of Polar Research, [6]Institute for Marine and Antarctic Studies, University of Tasmania, [7]Research and Information Center, Tokai University, [8]Graduate University for Advanced Studies (SOKENDAI)

Multi-year land-fast ice is widely spread around the Syowa Station in Lützow-Holm Bay, East Antarctica,. Fast ice in Lützow-Holm Bay is mostly covered with snow, which facilitates the formation of snow ice and superimposed ice. Both types of ice are snow-based sea ice and are referred to collectively as snow-origin ice in this study. Snow-origin ice formation is expected to affect biogeochemical components through material transport from the atmosphere, seawater intrusion into the snow bottom, and other material cycling processes at the sea ice surface. Nutrient concentrations inside the sea ice is also subject to change during uptake processes and utilization and decomposition processes within the sea ice. Land-fast ice has an important role in biogeochemical cycles and marine ecosystem along the Antarctic coast because it provides habitat conditions such as nutrients, temperature, salinity, and light for stable primary production. Therefore, it is important to know the variability of biogeochemical composition of the land-fast ice because it affect primary production, zooplankton, secondary and higher producers. In this study, we investigated the nutrients dynamics in the land-fast ice near the Syowa Station in Lützow-Holm Bay, and examined the evolution process of biogeochemical components and evaluated the effect of snow cover on the components in the sea ice. We also discussed the factors that cause changes in nutrient concentrations in the sea ice. During the 2015-2019 Japan Antarctic Reserch Expedition (JARE), land-fast ice cores, snow on land-fast ice and under-ice seawater were collected near the Syowa Station, Lützow-Holm Bay, East Antarctica. In the cold room, the ice core was split lengthwise into two halves with an electric band saw. The first half was used for ice texture analysis; the second half was used for measurement of ice bulk salinity, $\delta^{18}O$, chl-a, and nutrient concentrations. The mass fraction of snow in the snow-origin ice was estimated from $\delta^{18}O$ values based on the endmembers of sea ice and snow. The results of salinity, $\delta^{18}O$, and thin section analysis indicate that the upper 2 m of the land-fast ice is composed of snow-origin ice. The snow-origin ice grew year by year, and the fraction of snow in the snow-origin ice up to 2 m above the sea ice gradualy increased from about 88% in 2015 to about 100% by 2018. Nutrient concentrations were low in the upper part of the multi-year ice, which is composed of snow-origin ice. Also, nutrient concentrations were maximum in the lower part of sea ice, which is composed of seawater-origin ice. The determinants of the vertical distribution of nutrient concentrations were discussed. Nutrient concentrations were low in the snow-origin ice because the clean air and precipitation in Antarctica, thereby atmospheric deposition of nutrients is minimal. The high nutrient concentration in the lower part of the sea ice is due to the fact that nutrient regeneration through decomposition of organic matter has been repeated over the years in the sea ice bottom layer where many ice algae is distributed. Furthermore, the concentration ratios of each nutrient indicate that denitrification activity occurred at depths with high organic matter (high chl-a concentrations) in sea ice. The results of this study indicate that snow cover on land-fast ice has the effect of lowering nutrient concentrations in the land-fast ice, and that nutrient regeneration by organic matter decomposition is much more advanced in multi-year ice than in young ice in the lower layers of sea ice.

Distribution and seasonal evolution of supraglacial lakes around Lützow-Holm Bay, East Antarctica

Haruka Itagaki[1]and Masahiro Ishikawa[1]
[1]*Yokohama National University*

Melting of the Antarctic ice sheet is evident on the Antarctic Peninsula and is expected to impact the global sea level significantly. Recent satellite imagery research reveals the development of supraglacial lakes on the margins of the East Antarctic Ice Sheet (Stokes et al., 2019). The development of lakes on the East Antarctic Ice Sheet is not negligible in understanding the water balance in Antarctica. Detailed studies on the seasonal evolution of lakes' distribution in East Antarctica have been limited to some ice shelves and ice glaciers (Arthur et al., 2020; Langley et al., 2016; Moussavi et al., 2020). This study explored the seasonal evolution of supraglacial lakes' distribution on the Shirase Glacier and the Langhovde Glacier in the East Queen Maud Land, East Antarctica(Fig. 1).

Using Landsat 8 and Sentinel-2 satellite images from 2017 to 2020, we applied Normalized Differential Water Index (NDWI) to identify supraglacial lakes around Lützow-Holm Bay, including the Shirase Glacier and the Langhovde Glacier. Next, the geographical distribution of lakes was evaluated using the digital elevation model of Bedmap 2 (Fretwell et al., 2013). In addition, the surface temperature was calculated using satellite images. Supraglacial lakes were identified from November to February, providing the lake area of the Shirase Glacier and the Langhovde Glacier. In addition, the temperature and total solar irradiance were obtained from the data at Showa Station, and the relationship with the seasonal evolution of supraglacial lakes was investigated.

Lakes occurred mainly on the margins of the ice sheet where they developed at low elevations (<100m) and up to 25km inland from the coastline, but they could exist at elevations >700m and 30km inland(Fig.2). The surface temperature of most areas where lakes occurred was from -4.0℃ to -3.0℃. This suggests that lakes can exist even below freezing. In addition, as in other areas reported (Arthur et al., 2020; Langley et al 2016; Moussavi et al., 2020) so far, lakes started to form in late November, expanded in late December, peaked approximately in January, and shrank in late February.

We compared the temperature and total solar irradiance observed at Showa Station with the formation of supraglacial lakes on the Langhovde Glacier. The total area of lakes did not necessarily increase when either the temperature or total solar irradiance was high but tended to increase when both were high. Conversely, the total area of lakes is smaller when both the temperature and total solar irradiance were low(Fig. 3). This suggests that the formation of supraglacial lakes requires temperature and total solar irradiance, and future global warming may lead to the formation of more and more lakes.

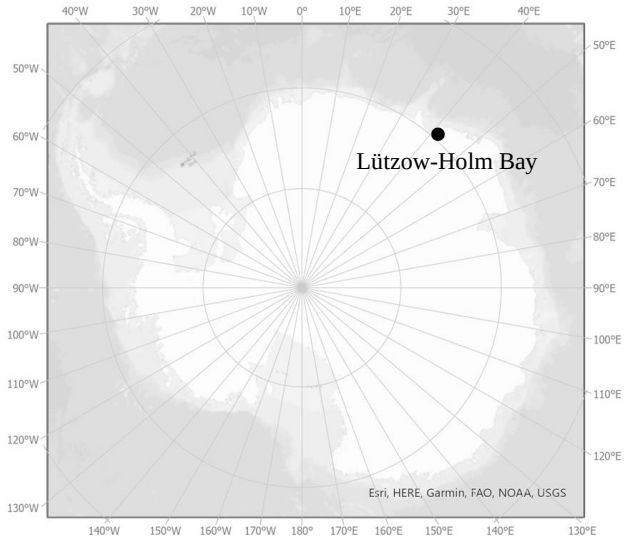

Figure 1. Location of Lützow-Holm Bay.

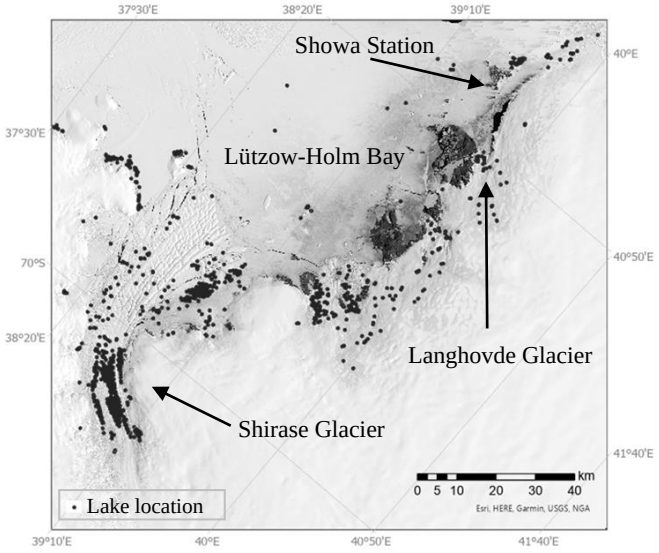

Figure 2. Location of supraglacial lakes on January 14, 2020.

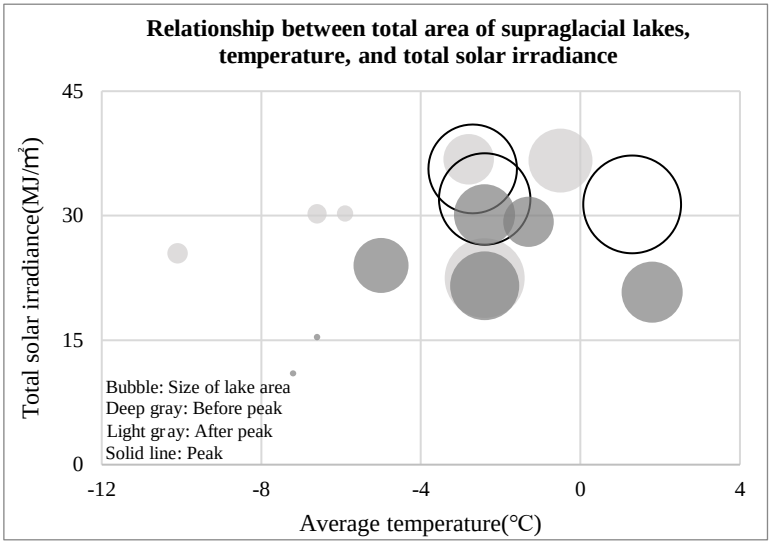

Figure3. Relationship between the area, temperature, and global horizontal irradiation of the lakes of the Langhovde Glacier in 2017/2018, 2018/2019, and 2019/2020.

References

J.F. Arthur et al., Distribution and seasonal evolution of supraglacial lakes on Shackleton Ice Shelf, East Antarctica, The Cryosphere, 14, 4103–4120, 2020.

P. Fretwell et al., Bedmap2: Improved ice bed, surface and thickness datasets for Antarctica, The Cryosphere, 7, 375–393, 2013.

E.S. Langley et al., Seasonal evolution of supraglacial lakes on an East Antarctic outlet glacier, Geophysical Research Letters, 43, Issue16, 8563-8571, 2016.

M. Moussavi et al., Antarctic Supraglacial Lake Detection Using Landsat 8 and Sentinel-2 Imagery: Towards Continental Generation of Lake Volumes, Remote Sens, 12, 134, 2020.

C.R. Stokes et al., Widespread distribution of supraglacial lakes around the margin of the East Antarctic Ice Sheet, Sci Rep, 9, 13823, 2019.

Winter lake snow/ice observation with the IoT time lapse camera and satellite remote sensing

Tatsuru Sato[1]
[1]*National Institute of Technology, Ichinoseki Collage*

IoT and satellite remote sensing are important for monitoring in winter and high latitudes where human activities are limited. They are also advantageous for long-term continuous environmental monitoring. Izunuma and Uchinuma are natural lakes located in the northern part of Miyagi Prefecture. These lakes are located in the northern part of Miyagi Prefecture. This area is registered as a wetland under the Ramsar Convention, an international treaty for the conservation of wetlands. About 100,000 migratory birds come from Siberia and Kamchatka and stay around the lakes for the wintering. The distribution of surface aquatic plants in the lake has changed significantly in recent years (Nakada et al., 2015; Yasuno et al., 2015). It is estimated that the freezing of the lake surface affects lotus and other vegetation. In Izunuma, the surface of the lake freezes in winter and the behavior of birds changes.

In order to analyze the winter environment of Izunuma, we have been analyzing time-lapse images taken at the site, and this time, we conducted the analysis for the winter of 2020. The monitoring camera was also settled by Biodiversity center in Japan, in Japanese Ministry of Environment for its environmental monitoring and preservation activities (Internet nature institute, https://www.sizenken.biodic.go.jp/index_en.php). The camera is located in the Izunuma-Uchinuma Sanctuary Center, Miyagi Prefectual IzunumaUchinuma Environmental Foundation, in Kurihara City. These images were analyzed to monitor the winter environment. The frozen area of the lake was analyzed from the super pixel segmentation of the images and the number of days of freezing of the lake surface over the past 10 years was calculated. The superpixel segmentation was performed using the SLIC method (Achanta et al., 2012). Satellite remote sensing data was analyzed to study the environment of the lake surface over a wide area. The data used were visual images by Landsat. These data were analyzed by using Google earth engine. It is possible to verify the data of the time taken by the satellite and the data of the same time at the site by using the images of the time lapse camera.

The frozen area of the lake was observed from December 2020 to February 2021. The number of frozen days was 48 days. It was the highest in the past five years, exceeding 38 days. In the early 2010s, two freezing days of 40 days or more were measured, confirming that the number of freezing days increases at intervals of several years. The number of freezing days in the winter of 2020 is higher than these values. The number of freezing days in the winter of 2020 is larger than these periods.
The number of frozen days increased significantly from the previous year. The average of freezing days in late 2010 is decreasing from early 2010 though its peak number is not different.

References

Achanta, R., Shaji, A., Smith, K., Lucchi, A., Fua, P., & Süsstrunk, S. SLIC superpixels compared to state-of-the-art superpixel methods. IEEE transactions on pattern analysis and machine intelligence, 34(11), 2274-2282, 2012.

Nakada, S., M. Umeda., T. Shimada., and Y. Fujimoto., Journal of Japan Society of Civil Engineers, Ser. B1 (Hydraulic Engineering), 71, 4, I_757 – I_762, 2015.

Yasuno, N., T. Shimada, J. Ashizawa and M. Hoshi., Influence of hypoxia related to the expansion of lotus vegetation on benthic invertebrate community in Lake Izunuma, Izunuma-Uchinuma Wetland Researches 9: 13-22, 2015.

The 19-year (2002-20) time series of annual sea-ice production in all Antarctic coastal polynyas based on AMSR-E/2 satellite observations

Sohey Nihashi[1], Takeshi Tamura[2], Kay I. Ohshima[3]
[1]*National Institute of Technology (KOSEN) Tomakomai College*
[2]*National Institute of Polar Research*
[3]*Institute of Low Temperature Science, Hokkaido University*

Sea-ice production in Antarctic coastal polynyas has been estimated by a heat flux calculation using thin ice thickness from passive microwave satellite data. The ice thickness is determined from the polarization ratio (*PR*) of the brightness temperature from the *PR*-h_i relationship based on a comparison with the thermal ice thickness (h_i). The thermal ice thickness h_i is estimated from the heat flux calculation using the sea-ice surface temperatures based on infrared satellite images under clear sky conditions. Passive microwave satellite data from SSM/I-SSMIS showed time series of ice production from 1992 (Tamura et al., 2007; 2016). The passive microwave radiometer AMSR-E launched in 2002 and its successor AMSR2 (2012—) has about four times finer spatial resolution in the area (about 6 × 6 km^2) than SSM/I-SSMIS, and they can show the detailed spatial distribution of the ice production (Nihashi and Ohshima, 2015; Nihashi et al., 2017). Previous studies had focused mainly on 13 Antarctic coastal polynyas with large production. This study revealed a time series of ice production in all 110 coastal polynya sites that can be examined by AMSR-E/2 (Fig. 1).

This study applied the following modifications to the previous thin ice thickness estimation and ice production estimation: the AMSR-E/2 *PR*-h_i relationship equations (Nihashi and Ohshima, 2015; Nihashi et al., 2017) were updated for h_i estimation. This is due to the change of meteorological input data to ERA5 from ERA-Interim which will not be updated after September 2019. The ERA5 meteorological data was also used as input data for heat flux calculation for ice production estimation using AMSR-E/2 data. The SSM/I-SSMIS ice production, which is based on Tamura et al. (2007), was also used. This was updated by using ERA5 to estimate the ice production. However, it was not used to derive the *PR*-h_i relationship equation, which remains unchanged. Since the periods of AMSR2 and AMSR-E do not overlap, it is not possible to directly compare their ice production. In this study, we compared the monthly ice production by AMSR-E/2 and SSM/I-SSMIS (Fig. 2) and showed that the amount of ice production from AMSR-E and AMSR2 is consistent; the variation of the ice production from AMSR-E/2 and SSM/I-SSMIS also corresponded well, but the SSM/I-SSMIS production was about 10% smaller. The time series of the total annual production of all 110 coastal polynyas (Fig. 1) is shown in Fig. 3, where the SSM/I-SSMIS ice production was adjusted using the regression line with AMSR-E/2 (Fig. 2). The average annual ice production during AMSR-E (2002-11) and AMSR2 (2012-20) periods were 2948.5 × 10^9 m^3 and 2778.7 × 10^9 m^3, respectively. The trend during the AMSR-E/2 (2002-20) period was -4.8%/decade. The Antarctic sea-ice extent was shown to have declined significantly since 2017 (Parkinson et al., 2019), but the ice production in the coastal polynyas did not show such a distinct change.

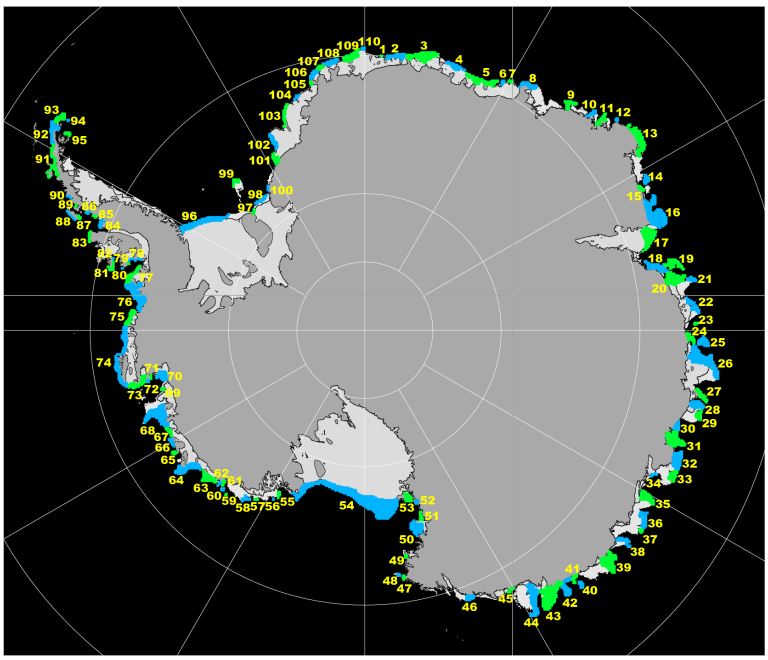

Figure 1. Analysis area of coastal polynyas (110 locations). The area is defined based on the area of >3 m yr^{-1} production from the AMSR-E/2 annual production map for the period 2003-20. Dark gray indicates Antarctica, and light gray indicates ice sheets and fast ice.

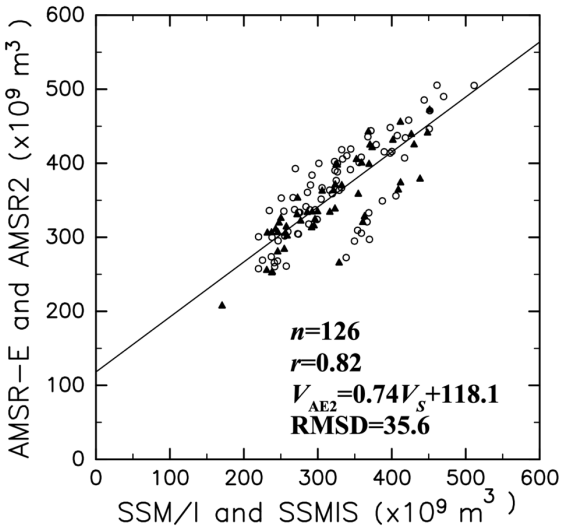

Figure 2. Comparison of monthly sea ice production in all analysis areas (Fig. 1) from SSM/I-SSMIS vs. that by AMSR-E (circles) and AMSR2 (triangles). The solid line indicates the regression line.

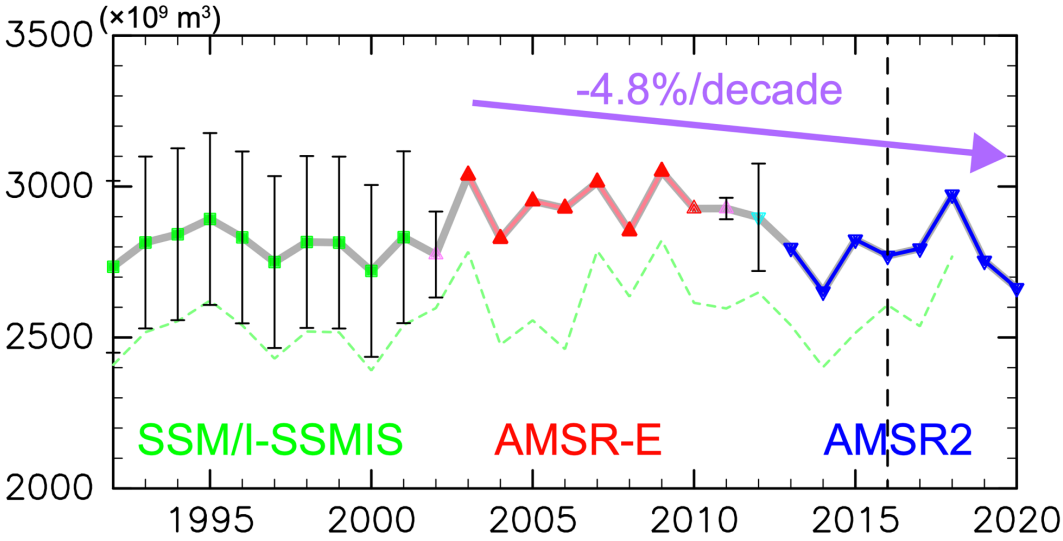

Figure 3. Time series of annual sea ice production in all 110 analysis areas (Fig. 1). The square, triangle, and inverted triangle indicate the annual sea-ice production from SSM/I-SSMIS, AMSR-E, and AMSR2, respectively.

References

Tamura, T., K. I. Ohshima, and S. Nihashi (2008), Mapping of sea ice production for Antarctic coastal polynyas, Geophysical Research Letters, 35, L07606, doi: 10.1029/2007GL032903.

Tamura, T., K. I. Ohshima, A. D. Fraser, and G. D. Williams (2016), Sea ice production variability in Antarctic coastal polynyas, J. Geophys. Res. Oceans, 121, doi:10.1002/ 2015JC011537.

Nihashi, S. and K. I. Ohshima (2015), Circumpolar mapping of Antarctic coastal polynyas and landfast sea ice: relationship and variability, Journal of Climate, 28, 3650–3670, doi: 10.1175/JCLI-D-14-00369.1.

Nihashi, S., K. I. Ohshima, and T. Tamura (2017), Sea-ice production in Antarctic coastal polynyas estimated from AMSR2 data and its validation using AMSR-E and SSM/I-SSMIS data, IEEE Journal of Selected Topics in Applied Earth Observations and Remote Sensing, 10(9), 3912–3922, doi: 10.1109/JSTARS.2017.2731995.

Parkinson, C. (2019), A 40-y record reveals gradual Antarctic sea ice increases followed by decreases at rates far exceeding the rates seen in the Arctic (2019), PNAS, 116(29), 14,414-14,423.

Coupled model for simulating the interaction of waves and ice particles

Zijing Jin
The University of Tokyo

In recent years due to climate change, the ice cover in the polar regions has decreased, and the increase in open water area will allow waves to develop beyond pure wind seas and evolve into swells, which will further accelerate the ice retreat [1]. The effect of waves on ice breakage and movement along the pack ice boundary of the marginal ice zone has become more and more noteworthy. Similarly, the existence of waves also affects the formation of new ice sheets. Under calm sea surface conditions, cooling by the low temperature of the air environment, a relatively flat ice sheet called nilas will be formed. On the turbulent ocean surface, a large number of small ice crystals (called frazil ice) will generate in the supercooled seawater [2]. With further development, there will be ice floes that are approximately round in shape and relatively uniform in thickness, called the pancake ice.

Matsumura and Ohshima [3] represent the development of frazil ice by using their self-developed coupled model. Orzech and Shi [4] simulate wave reflection, diffraction, and transmission as well as ice floe flexure, fracturing, and collision. However, there is no suitable framework for the simulation of the whole process from cooling to ice particle formation and aggregation to form the ice on the ocean surface under the action of waves.

For this reason, in the present study, we introduce a new coupled model framework to simulate ice formation. Starting from the pre-computed velocity and temperature fields, we consider the collision and consolidation of particles, finally reproduce the generation and aggregation of particles under the influence of waves. Through this model, a numerical experiment can be done to show the influence of wave parameters on ice formation. From the ice-wave tank experiment in our laboratory, Fujiwara et al. [5] observed that under the cooling of the environment, due to the waves generated by the wave generator, the resulting ice surface is separated into blocks, resembling the pancake ice. Furthermore, they showed that there seems to be a certain correlation between the size of the ice blocks and the incident wave parameters.

To go beyond the limitations of experimental conditions and try a wide variety of parameters to explore the relationship in more detail, a two-dimensional coupled model is constructed, which includes a dynamic model for calculating wave propagation, a thermodynamic model for cooling, and an ice-particle model to describe ice particle formation, growth, and its motion. For the dynamic model, we chose a two-dimensional Numerical wave tank based on the boundary element method (NWT2D) [6]. Since the cooling process is an unsteady heat conduction problem, the boundary element method is not a common method to deal with. Following the formulation by Wu H.T. [7], a BEM-based program for thermodynamic equations was written for the coupled model. And here we treat each ice particle as an independent element considering buoyancy, water drag, and repelling force due to the collision. In this way, the development and aggregation of ice particles under realistic conditions are simulated as much as possible.

NWT2D is a fully nonlinear time-domain simulation program of free surface waves in a two-dimensional wave tank. BEM is used to solve Laplace's equation of the velocity potential. Through the post-processing of the results, we can obtain the position of the free surface and the velocity potential at any point inside to calculate the velocity.The velocity calculated by the post-processing program is in good agreement with the analytical solution (Airy wave) (Fig.1).

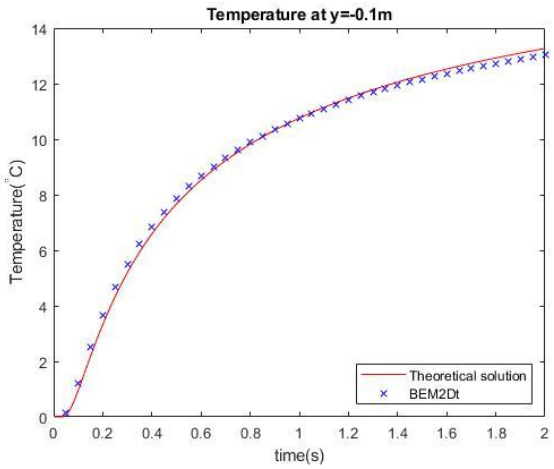

Fig.1 Velocity profiles from NWT2D and Airy wave

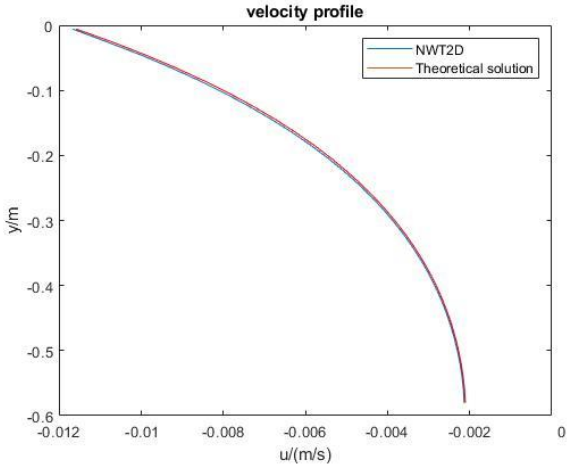

Fig.2 Temperature change and compariso

The formation and development of ice particles are based on changes in the temperature field, so it is necessary to solve the problem of unsteady heat transfer problem. A sample temperature field calculated for a case with surface heating is shown. To verify the accuracy of the program, the vertical temperature profile is compared against the analytical solution (Fig.2). An important point to note is that a static water condition is used here, and the movement of the fluid is completely ignored.

To simulate how ice particles converge on the surface under the influence of waves, a DEM (Discrete Element Model) that can track the position and state of the particles (position, mass, speed, etc.) and the relationship between surrounding particles is necessary. Since this model is based on DEM and deals with imaginary ice particles, we call this model DEMvirtual.

Consider ice particles as a group of disk-shaped grains [8] with variable radiuses. When the temperature of a point in the domain is lower than the freezing point, new particles will be generated and existing particles will grow. This change will also give feedback to the temperature field.

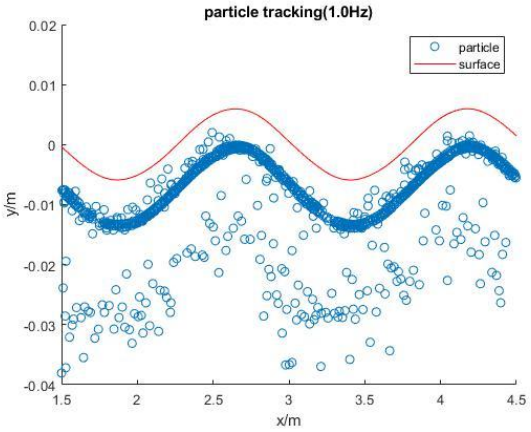

Fig.3 General figure in 1.0Hz wave

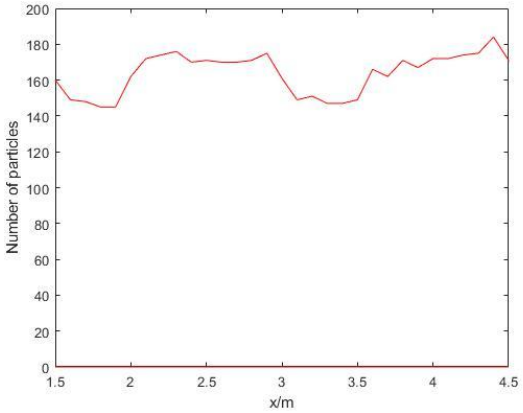

Fig.4 Particle distribution in 1.0Hz wave

After confirming that the coupled model remains stable, the basic parameters are determined, and we have started to use the coupled model to conduct numerical experiments to explore the interaction between ice particles and waves. Here we take the case wave frequency f=1.0 Hz as an example; see the result after 200 steps (2 seconds) of particle locations (Fig.3). However, it is hard to analyze the data directly from the image. By counting the number of particles distributed in the horizontal direction, the particle distribution (Fig.4) can be drawn.

It can be seen from the general figure (Fig.3) that most of the particles will eventually converge on the surface due to the effect of buoyancy, and interestingly, the horizontal distribution shape basically fits the wave itself. From the particle distribution diagrams of 1.0 Hz (Fig.4), the distribution has an apparent periodicity like the incoming waves, and there is an obvious fault before the densely distributed area. But this phenomenon is not obvious in the results of other frequencies, like 0.5 Hz and 1.5 Hz.

The first problem with the existing model is that the virtual heat transfer parameters are used to accelerate the heat transfer process, but it also magnifies the effect of the heat transfer process on the results. Second, due to the limitation of computing resources, unable to perform more complex and long-term simulations. After further optimization, it can be used to test the distribution of ice particles under various waves and temperature conditions and to explore the influence of wave parameters on the formation of the ice floe. After these steps, hopefully some of the mystery is addressed in this study.

References

[1] Thomson J, Rogers W E. Swell and sea in the emerging Arctic Ocean[J]. Geophysical Research Letters, 2014, 41(9).
[2] Martin S . Frazil Ice in Rivers and Oceans[J]. Annual Review of Fluid Mechanics, 1981.
[3] Matsumura Y, Ohshima K I . Lagrangian modelling of frazil ice in the ocean[J]. Annals of Glaciology, 2015, 56(69):373-382.
[4] Orzech MD, Shi F, Veeramony J, et al. A Coupled System for Investigating the Physics of Wave–Ice Interactions[J]. Journal of Atmospheric and Oceanic Technology, 2018, 35(7).
[5] Fujiwara, Y., T. Katsuno, T. Waseda, T. Nose, T. Kodaira, "Laboratory experiments of ice floe formation under wave motions", Japan Geoscience Union meeting 2021, Jun 2021
[6] Tanizawa K . A Nonlinear Simulation Method of 3-D body Motions in Waves[C]// Workshop on Water Waves & Floating Bodies. 1995.
[7] 吴洪潭. 边界元法在传热学中的应用[M]. 国防工业出版社, 2008.
[8] Ushio S, Wakatsuchi M . A laboratory study on supercooling and frazil ice production processes in winter coastal polynyas[J]. Journal of Geophysical Research Oceans, 1993, 98(C11):20321-20328.
[9] Wilson T A . Solid Mechanics[M]. John Wiley & Sons, Inc. 2011.

Near-inertial internal wave generation by mixed layer cooling in the Indian sector of the Southern Ocean

Azevedo M. F.[1] and Kitade Y.[1]
[1]*Tokyo University of Marine Science and Technology, Department of physical oceanography*

The Southern Ocean is peculiar in that its superficial layer loses heat to the atmosphere during most of the year. This causes the the water column to become unstable and convective motion to occur. However, the temporal constrains as well as the dynamic implications of this process are poorly understood, as the challenging conditions in the Southern Ocean have led to sparse spatial and temporal coverage of observations, which increases uncertainty in atmosphere and ocean dynamics and boundary-layer thermodynamic processes (Swart et al., 2019). To bridge this gap in understanding we investigate the importance of the ocean-atmosphere heat flux to the generation of shear, compare its importance relative to the wind contribution, correlate the diurnal forcing of the surface heat flux to the generation of near-inertial period internal waves and characterize the energy distribution on the mixed layer in terms of spectrum.

We compared current, temperature and salinity data from a mooring deployed at 60S 140E during the year of 2012 along with wind and heat flux estimations from the ERA5 reanalysis output. Net heat flux was estimated from the sum $Q_{net} = Q_{SW}(1-\alpha)+Q_{LW} + Q_L+ Q_S$, where the subscripts SW, LW, L, and S are, respectively, the short-wave incoming radiation, long wave outgoing radiation, latent and sensible fluxes and α is the albedo of salt water. ADCP derived current velocity was filtered twice using a 4th order Butterworth filter to separate the signal into noise (period < 4hours), inertial band (period between 8 and 16 hours) and long period (>16 hours). Vertical shear was discretized using an eulerian centered differentiation scheme and wind stress was parametrized as its frictional velocity (V^*, m s^{-1}).

In Fig.1a, the density difference between a layer at a certain depth and the surface can be proxied as the mixed layer depth ($\Delta\rho$ <0.05 Kg $m_{-3,}$ following Montegut et al., 2004), which is seen to increase during the surface cooling period (indicated in Fig.1 in blue) and accompany an increase in inertial velocity at the layers between 66 to 90m (Fig.1b). The maximum shear layer was seen to become shallower during this same period, which offers an exception to the current understanding of the peak shear variance being greater and shallower during summer while being shallower and weaker during winter (Brannigan et al., 2013). The depth of this shear enhancement is calculated to be outside of the mean winter Ekman depth of 47m, which indicates additional factors besides wind are necessary to explain this variability. Peaks of both wind and heat flux generally coincide with an increase in vertically integrated shear (Fig1.c and d), which was also found to be higher during the surface cooling period (Fig. 1d). Reason for this behavior was found to be both the increased shear at the base of the mixed layer and overturning events where shear was observed on the entirety of the mixed layer becoming more common during this time frame. While wind had a good correlation with integrated shear throughout the year, during the surface cooling period it is not sufficient to predict it. When Q_{net} becomes positive (ocean loses heat to the atmosphere) the cross-correlation between shear and Q_{net} increases significantly(Fig.1e). It was also found that shear winter spectrum had a strong but intermittent diurnal component but also had a significative signal in the semi-diurnal band. Energy in both the diurnal and semi-diurnal (inertial) bands are enhanced by this process, which points to a non-linear energy transfer from the diurnal cycle of heating to the semi-diurnal spectrum of inertial motion. Near-inertial internal wave generation was then observed at layers deeper than 100m during these events. Weakly nonlinear theory predicts the transfer of energy from a diurnal mode to a wave pair containing a semidiurnal mode and a diurnal mode of inverse wave number as the resonant triad $\omega_{24}= \omega_{12} - \omega_{24}$. A fully nonlinear study, however, can be examined only through analysis of numerical simulations still in progress.

The significance of these results and the reason they differ from other, northern observations is that we could observe the contribution of surface heat flux to shear in the mixed layer, factor often ignored in the current models. Of paramount importance, we have also verified that the energy generated by this shear is well-structured into inertial-period internal waves capable of propagating both horizontally and into deeper layers, where the energy they transport might enhance turbulent mixing.

Concluding, we analyzed the relation between ocean-atmosphere heat fluxes, wind and shear in the mixed layer. Convection of water in the mixed layer was found to be an important factor for the development of shear and turbulence in this layer and is a possible pathway for the transfer of energy momentum towards deeper ocean layers.

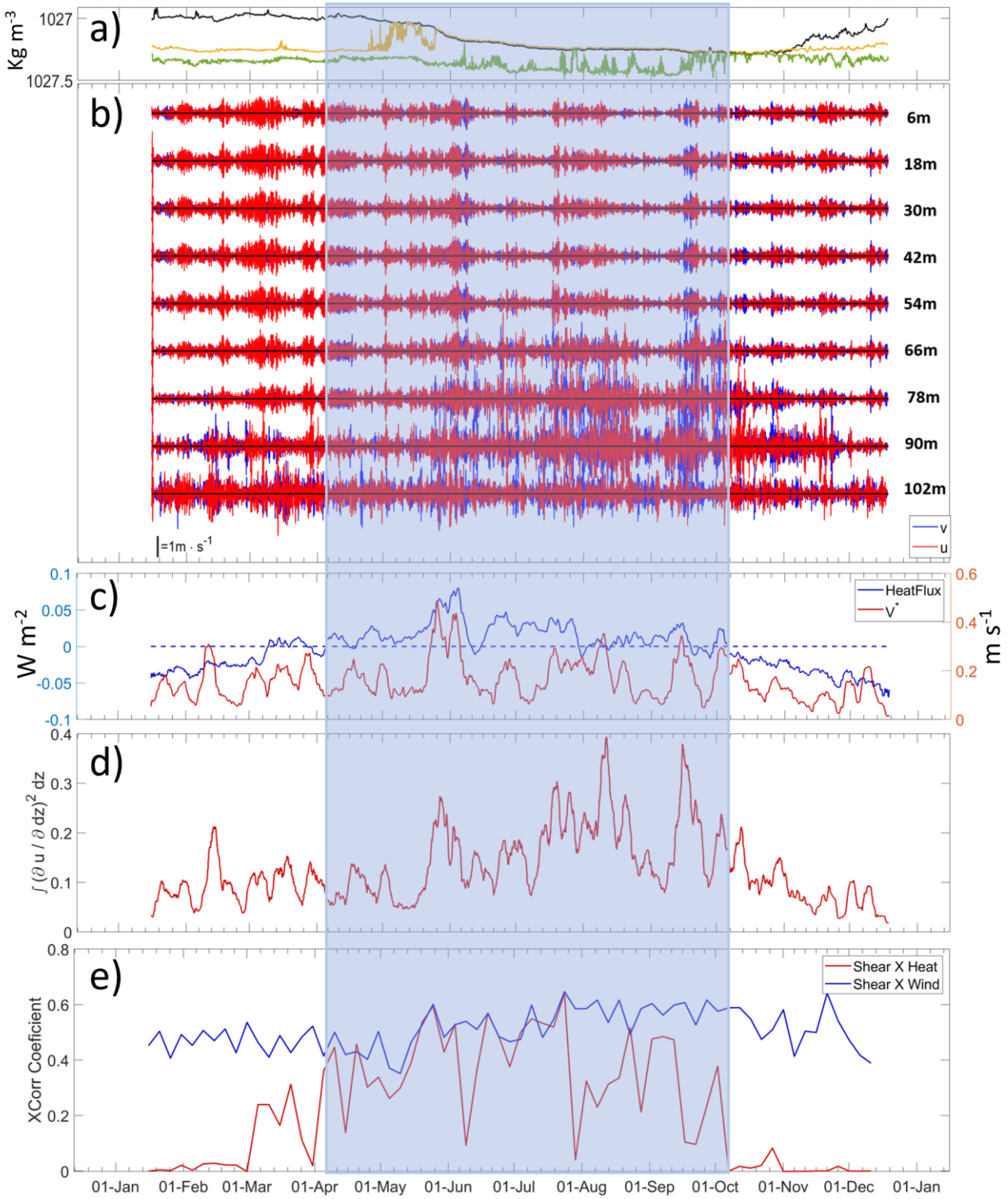

Fig1: Time series of (a) potential density, where the black orange and green lines represent the surface, 100 and 150m respectively, (b) inertial band-passed velocity, (c) V^* and Q_{net}, (d) vertically integrated shear (e) and cross-correlation coefficients between vertically integrated shear and heat. (e, red). Q_{net} is oriented upwards so that positive values mean heat is being transferred from the ocean into the atmosphere.

References

Swart, S., Gille, S., Delille, B., and S Josey. Constraining Southern Ocean Air-Sea-Ice Fluxes Through Enhanced Observations. Frontiers in Marine Science, 6, 421, 2019.

Brannigan, L., Leen, Y., Rippeth, T. P., McDonagh, E., Chereskin, T. K., and J. Sprintall. Shear at the Base of the Oceanic Mixed Layer Generated by Wind Shear Alignment. Journal of Physical Oceanography, 43, 1798-1810, 2013.

Changes in Antarctic Bottom Water formation, deduced from oxygen and CFC-12 in the Indian Ocean sector of the Southern Ocean between 1987 and 2020

Narimi Baba[1], Yoshihiko Ohashi[1], Kenichi Sasaki[2], and Michiyo Yamamoto-Kawai[1]
[1]*Tokyo University of Marine Science and Technology, Japan*
[2]*Japan Agency for Marine-Earth Science and Technology, Japan*

Antarctic Bottom Water (AABW) is formed by the mixing of the newly ventilated dense shelf water and the Circumpolar Deep Water (CDW). The AABW extends into the global abyss and plays major role in driving the deep ocean circulation. In recent years, however, warming and freshening of the AABW have been observed in the Ross Sea and Adélie Land coast, which are the main formation regions of the AABW, suggesting a weakening of the AABW formation.

In this study, we compared temperature, salinity, AOU, and pCFC-12 between observations before 2000 (1987 and 1996) and after 2000 (2013, 2016, 2019, and 2020) in order to understand changes in bottom water ventilation processes in the Indian Ocean sector of the Southern Ocean. Since SF_6 data are also available, the pSF_6 / pCFC-12 method was used to estimate the age of AABW for years after 2000. Assuming that the AABW age (and thus ventilation processes) did not change with time, we can estimate pCFC-12 that AABW should have in each year. The expected pCFC-12 was then compared with the observed pCFC-12 for years before 2000.

Results show an increase in temperature by more than 0.2°C below 500 dbar, and a decrease in salinity by more than 0.002 in the AABW (γ^n > 28.27 kg/m^3). AOU decreased by 3 to 5 μmol/kg east of 70°E. Because a decrease in AOU can be caused by either enhanced ventilation or reduced biological consumption, we compared pCFC-12 in AABW before and after 2000 by the method described above. The observed pCFC-12 before 2000 was lower than the expected pCFC-12 especially at stations east of 70°E. This results, together with the decrease in AOU, suggest an enhanced ventilation of AABW after 2000 in this region.

Silica concentrations of seawater and sea- ice in the coastal regions of the Southern Ocean

Natsumi Nojiro[1], Michiyo Yamamoto-Kawai[1], Ryosuke Makabe[1, 2, 3] and Keigo D. Takahashi[3]
[1]*Tokyo university of Marine Science and Technology, Japan*
[2]*National Institute of Polar Reserch, Japan*
[3]*The Graduate University for Adovanced Studies, SOKENDAI, Japan*

The Southern Ocean plays a major role in the silica cycle of the global ocean, and changes in the silica budget in this ocean may alter biological processes in other oceans. However, silica cycle in the coastal region is not clear, because of the lack of observations. In this study, we investigated dissolved silica (DSi) and biogenic silica (BSi) concentrations in seawater and sea ice collected during the KH20–1 (January–February 2020) and JARE61 (December 2019–March 2020) cruises in the three coastal regions: off Cape Darnley, off Totten Glacier, and in Lützow-Holm Bay.

BSi concentrations in seawater (0–100 m) for each region was 0.1–9.5 μmol/L off Cape Darnley, 0.1–6.5 μmol/L off Totten Glacier, and 0.1–2.9 μmol/L in Lützow-Holm Bay. The highest BSi concentration in seawater (9.5 μmol/L) and the strongest positive correlation between BSi and chl. *a* concentration in seawater was observed in the surface layer (0–100 m) of the Cape Darnley region. This indicates the dominance of diatom in phytoplankton community in this region. Relatively high BSi concentraions were found in the bottom layer along the Wild Canyon, where newely formed Antarctic Bottom Water (AABW) flows, and decreased toward the offshore. This suggests the transport of BSi by AABW from the shelf to the deep ocean.

BSi concentrations in sea ice for each region was 0.4–77.7 μmol/L in Cape Darnley, 0.1–102.7 μmol/L in Totten, and 3.8–75.7μmol/L in Lützow-Holm. The mean concentration of BSi in sea ice was 3–251 times higher than that of surface seawater (0–100 m). In addition, BSi concentration was found to be 6 times higher than DSi concentration in sea ice on average. These results indicate that sea ice transport silica from coastal region to the offshore mainly in the form of BSi. We estimated the amount of BSi transported by sea ice, by multiplying annual sea ice production in coastal polynyas[1] and the mean BSi concentration in sea ice. The annual transport was estimated to be 1.7×10^{-3} T mol in the Cape Darnley polynya and 9.5×10^{-4} T mol in the Dalton polynya, and 3.7×10^{-2} T mol for all Antarctic polynyas.

Reference

[1] Nakata et al. (2021) Mapping of active frazil for Antarctic coastal polynyas, with an estimation of sea-ice production, *Geophys. Res. Lett.*, 48.

Difference of the xCO_2 over two decades (1996 and 2019) in the eastern Indian sector of the Southern Ocean

Manami Tozawa[1], Daiki Nomura[1, 2, 3], Shin-ichiro Nakaoka[4], Masaaki Kiuchi[1], Daisuke Hirano[5], Kaihe Yamazaki[6], Shigeru Aoki[6], Hiroko Sasaki[7], and Hiroto Murase[8]

[1]*Faculty of Fisheries Sciences, Hokkaido University,* [2]*Field Science Center for Northern Biosphere, Hokkaido University,*
[3]*Arctic Research Center, Hokkaido University,* [4]*National Institute for Environmental Studies,*
[5]*National Institute of Polar Research,* [6]*Institute of Low Temperature Science, Hokkaido University,*
[7]*Japan Fisheries Research and Education Agency,* [8]*Tokyo University of Marine Science and Technology*

In order to understand the decadal trend of the CO_2 cycle in the Southern Ocean, we compared the CO_2 concentrations (xCO_2) at the observation in 1996 by the *R/V Aurora-Australis* (BROKE) with that in 2019 by the R/V *Kaiyo–Maru* (KY18) in the east Indian sector of the Southern Ocean. During the 23 years, the mean value of xCO_2 in the sea ($xCO_{2\ sea}$) and in the air ($xCO_{2\ air}$) increased by 25 and 47 ppm, respectively. The sea surface temperature increased by about 1.5℃. The $xCO_{2\ sea}$ estimated from these increases of $xCO_{2\ air}$ and temperature was lower than the observed $xCO_{2\ sea}$ at KY18. The Southern Boundary of Antarctic Circumpolar Current moved southward during the period between the two observations indicates that the upwelling region of Circumpolar Deep Water moved southward. As a result, the maximum concentration of nitrate near the temperature minimum layer (TML) increased, and the difference of nitrate concentrations between the ocean surface and the TML increased. This means that ocean surface nitrate concentrations during the winter were higher in 2019 than in 1996, and more nitrate was consumed by biological production during the summer. Then, strong biological activity offset the effect of the increase of the $xCO_{2\ air}$ and the sea surface temperature.

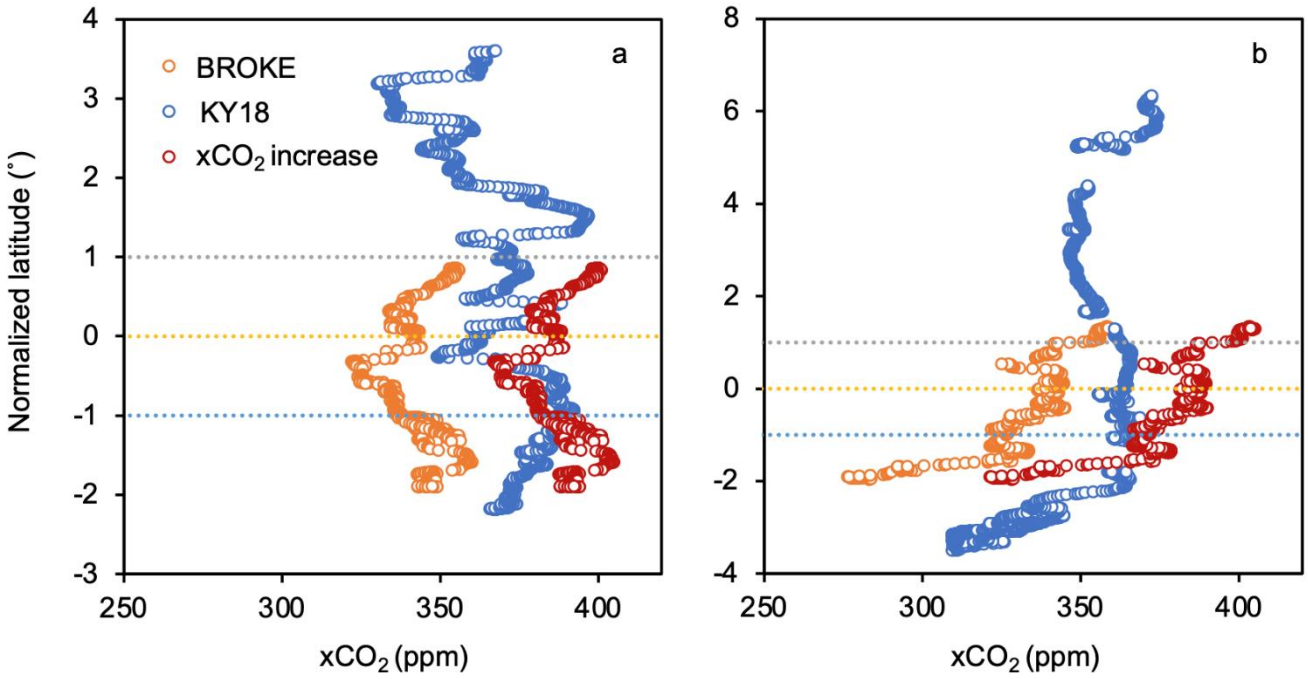

Figure 1. Relationship between normalized latitude and frontal distributions of $xCO_{2\ sea}$ (orange: BROKE, blue: KY18, red: $xCO_{2\ sea}$ increase). The Southern Antarctic Circumpolar Current Front corresponds to 1 on the ordinate; the Southern Boundary to 0, and the Antarctic Slope Front to −1. The $xCO_{2\ sea}$ increase was estimated by adding the difference between $xCO_{2\ air}$ in BROKE and this study (45 ppm) and the $xCO_{2\ sea}$ increase due to the increase of surface water temperature (about 1.5℃) (4% $℃^{-1}$) to the $xCO_{2\ sea}$ in BROKE. (a) 128˚E (b)140˚E

Variations of partial pressure of CO_2 in the surface seawater and air-sea CO_2 fluxes along 110°E in the Southern Ocean

Takayuki Matsuura[1], Shinji Morimoto[1], Gen Hashida[2], Tomomi Takamura[2], Shin-ichiro Nakaoka[3] and Shuji Aoki[1]
[1]*Graduate School of Science, Tohoku University, Japan*
[2]*National Institute of Polar Research, Japan*
[3]*National Institute for Environmental Studies, Japan*

The oceans have played an important role in the global carbon cycle by taking up about 30% of anthropogenic CO_2 released into the atmosphere since the Industrial Revolution. In particular, the Southern Ocean has absorbed about 40% of the anthropogenic CO_2 absorbed by the global oceans. However, in-situ cruise observations of the air-sea CO_2 exchange in the Southern Ocean are limited due to its remoteness from civilization, severe sea conditions and presence of sea ice.

Continuous observations of CO_2 partial pressure in the surface seawater (pCO_2^{sw}) have been conducted on-board R/V "SHIRASE" in the Indian Ocean sector of the Southern Ocean between Australia and ice edge around Syowa Station. pCO_2^{sw} was measured by using an in-situ measuring system with a nondispersive infrared (NDIR) gas analyzer and a flow-through and tandem type gas-liquid equilibrator. In this study, we analyzed temporal and spatial variations of pCO_2^{sw} obtained on-board "SHIRASE" during her ten cruises in the austral summer (December to March) from 2009 to 2019. To investigate long-term variations of pCO_2^{sw}, we focused on the pCO_2^{sw} data along the 110˚E line from 40˚S to 60˚S. Furthermore, the area was divided into three zones of Sub Antarctic Zone (SAZ) , Polar Frontal Zone (PFZ) and Antarctic Zone (AZ) with the average positions of the front as the boundary.

Figure 1 shows mean pCO_2^{sw} obtained from the ten cruises, together with positions of the fronts. pCO_2^{sw} shows the clear latitudinal variation associated with the position of the front, with pCO_2^{sw} in PFZ and AZ being 15 – 20 µatm larger than that in SAZ. The pCO_2^{sw} increase from SAZ to PFZ could be mainly caused by southward increase of dissolved inorganic carbon (nDIC) . From PFZ to AZ, potential of pCO_2^{sw} increase by increasing nDIC is offset by the effect of increasing nTA and decreasing Sea Surface Temperature, resulting in small variations in pCO_2^{sw}. Long-term trend of pCO_2^{sw} for each zone was evaluated by using the observation data for the ten years (Table 1). In the three zones, pCO_2^{sw} increased at a rate of 0.98 – 2.21 µatm/yr. The mean increase rate of the atmospheric pCO_2 (pCO_2^a) was 2.45 µatm/yr for 2009 – 2019, which was larger than the increase rates of pCO_2^{sw} in SAZ and PFZ. On the other hand, the pCO_2^a increase rate was about the same amount as the pCO_2^{sw} in AZ. The component analysis of the pCO_2^{sw} trend showed that the contribution of nDIC increase in the surface ocean was significant. We calculated CO_2 flux between the atmosphere and the surface seawater by using pCO_2^{sw}, pCO_2^a, SST, wind speed and Sea Surface Salinity and the increase rate of the CO_2 flux for each zone. As a result, CO_2 flux (positive represents CO2 uptake by the ocean) increased at a rate of 0.84 and 1.46 gC/m^2/month/yr in SAZ and PFZ. In contrast, there was no increasing trend for the CO_2 flux in AZ. The CO_2 flux increases in SAZ and PFZ were mainly produced by increasing difference in pCO_2 between the atmosphere and surface seawater.

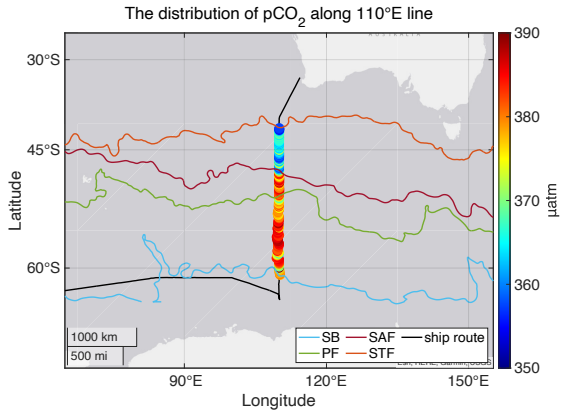

Figure 1. The distribution of pCO_2^{sw} along 110°E line (color circles; color bar on the right). Four color lines represent Sub Tropical Front (STF, orange) , Sub Antarctic Front (SAF, red), Polar Front (PF, green) and Southern Boundary (SB, blue), respectively. Black line represents cruise track of "SHIRASE".

Table 1. Increase rate of partial pressure of CO_2 in the surface seawater (pCO_2^{sw}), in the atmosphere (pCO_2^a) and CO_2 flux for Sub Antarctic Zone (SAZ), Polar Frontal Zone (PFZ) and Antarctic Zone (AZ).

	pCO_2^{sw} [µatm/yr]	CO_2flux [gC/m^2/month/yr]	pCO_2^a [µatm/yr]
SAZ	1.60 ± 0.83	0.84 ± 0.81	2.45 ± 0.06
PFZ	0.98 ± 0.40	1.46 ± 0.44	
AZ	2.21 ± 0.64	0.20 ± 0.64	

Processing of sea ice monitoring videos recorded by surveillance cameras on Icebreaker Shirase

Takeshi Terui[1], Keiko Iino[1], Motomu Oyama[1], Daisuke Simizu[1], and Shuki Ushio[1]
[1]*National Institute of Polar Research*

Observation surveillance cameras were installed on the bridge and starboard side of the icebreaker Shirase for sea ice monitoring. When navigating in the sea ice area, the surveillance camera recorded the outboard state during icebreaking and the movement of shattered ice at 1x speed. The camera installed on the bridge was a top-view camera that recorded the forward direction of the ship. The camera installed on the starboard side was a side-view camera that recorded the ice passing through the ship's starboard side. Both cameras used AXIS surveillance cameras, and Table 1 showed their recording settings. Recordings by this surveillance camera were from JARE53 to JARE61, and the recording period of each JARE was shown in Table 2. Each JARE video had more than 720 hours, and manually checking the 1x speed video would be a big waste of time. Since the video file was divided by 105MB and the number of files is huge, it would take time to search for the target scene file. For these reasons, video processing was required to use of video recorded at 1x speed for research. In this study, video files were concatenated in about 24 hours and processed at 120x speed so that a large number of videos obtained from surveillance cameras could be easily checked. These processes were applied to the recorded videos from JARE53 to JARE61, and the processed videos were published on YouTube. We present these processing procedures and introduce the results of video processing.

Table 1. Recording Preset

	Top-view camera	Side-view camera
Codec	H.264	
Resolution	4CIF 704 x 480	
File extension	ACSM	
Frame rate	5	30
Split size	105 MB	105 MB

Table 2. Recording list for each JARE

		Start date	End date	Number of recording days
JARE 53	Top-view camera	2011-12-17	2012-03-15	90
	Side-view camera	2011-12-17	2012-03-08	83
JARE 54	Top-view camera	2012-12-14	2013-03-13	46
	Side-view camera	2012-12-14	2013-03-13	46
JARE 55	Top-view camera	2013-12-09	2014-03-01	82
	Side-view camera	2013-12-09	2013-12-11	3
JARE 56	Top-view camera	2014-12-13	2015-02-18	56
	Side-view camera	2014-12-13	2015-02-18	56
JARE 57	Top-view camera	-	-	-
	Side-view camera	2015-12-21	2016-02-17	31
JARE 58	Top-view camera	2016-12-19	2017-02-16	60
	Side-view camera	2016-12-19	2017-01-27	60
JARE 59	Top-view camera	2017-12-14	2018-02-16	37
	Side-view camera	2017-12-14	2018-02-16	37
JARE 60	Top-view camera	2018-12-12	2019-03-03	51
	Side-view camera	2018-12-12	2019-03-03	51
JARE 61	Top-view camera	2019-12-03	2020-03-16	105
	Side-view camera	2019-12-28	2020-02-05	40

Characteristics of cloud base height from ceilometer observation onboard R/V *Shirase*

Makoto Kuji[1], Mana Takada[1], Yumi Shimode[1], Sara Hirose[1] and Naohiko Hirasawa[2]
[1]*Nara Women's University*
[2]*National Institute of Polar Research*

Cloud has opposite effects on the earth climate system: warming and cooling. Their magnitudes depend on cloud fraction, height, and so on. They influence the radiation balance on the earth and they are one of the greatest error sources for the climate prediction [IPCC, 2013]. Generally, it is said that high clouds have a warming effect and low clouds have a cooling effect. Nevertheless, it is not easy to make a detailed observation due to their spatial and temporal variability. Furthermore, we do not have enough observation sites over ocean which covers about 70% of the earth surface. It is, therefore, important to elucidate their behavior. Thus, we make a periodical shipboard observation to investigate maritime cloud base height using ceilometer observations onboard R/V *Shirase* between Japan and Antarctica.

Shipboard observations were carried out onboard R/V *Shirase* (AGB-5003) [Kuji et al., 2016]. The ceilometer is an instrument to determine cloud base height by measuring the return time of laser beam (Vaisala CL51). The observation interval is 36 s. We have 312,961 profiles from 27 November 2013 to 6 April 2014 (JARE 55), 197,286 profiles from 11 November 2014 to 9 February 2015 (JARE 56), 321,681 profiles from 16 November 2015 to 12 April 2016 (JARE 57), 193,585 profiles from 11 November 2016 to 22 March 2017 (JARE 58), 321,358 profiles from 29 November 2017 to 12 April 2018 (JARE 59), 362,399 profiles from 10 November 2018 to 9 April 2019 (JARE 60), and 350,401 profiles from 12 November 2019 to 5 April 2020 (JARE 61). We can obtain up to three cloud base heights with the software built in the system.

As a result of the preliminary analysis, examining the cloud base height of the first layer, it is found that there are many cases where the cloud base height is 1 km or less throughout the 7 cruises between Japan and Antarctica. Moreover, there was a difference in the distribution of cloud base height around 50° S. We are going to examine the characteristics of the cloud base height estimated from the ceilometer along the ship tracks. Furthermore, we will make a validation study comparing the cloud base height from R/V *Shirase* as well as satellite observations.

Acknowledgments

The shipborne observation was conducted in cooperation with NationalInstitute of Polar Research. The authors are grateful to those who related to the observations onboard R/V Shirase during JARE 55, 56, 57, 58, 59, 60 and 61.

References

Intergovernmental Panel on Climate Change (IPCC2013), Climate Change 2013.

Kuji M., R. Fujimoto, M. Miyagawa, R. Funada, M. Hori, H. Kobayashi, S. Koga, J. Matsushita, and M. Shiobara, Cloud fractions estimated from shipboard whole-sky camera and ceilometer observations, Transactions of the Japan Society for Aeronautical and Space Sciences, Aerospace Technology Japan, Vol. 14 (2016) No. ists30, 7-13.

Characteristics of cloud fraction from whole-sky camera observation onboard R/V *Shirase* from 2013 to 2020

Sara Hirose[1], Mana Takada[1], Makoto Kuji[1] and Masahiro Hori[2]
[1]*Graduate School of Humanities and Sciences, Nara Women's University*
[2]*School of Sustainable Design, University of Toyama*

Cloud has opposite effects on the earth climate system: warming and cooling. Their magnitudes depend on cloud fraction, height, and so on. They influence the radiation balance on the earth and cloud is one of the greatest error sources for the climate prediction [IPCC, 2013]. Nevertheless, it is not easy to make a detailed observation due to their spatial and temporal variability. Furthermore, we do not have enough observation sites over ocean which covers approximately 70% of the earth surface. It is, therefore, important to elucidate their behavior. Particularly, the analysis of clouds in the Southern Ocean is important in terms of climate model improvement and clouds of feedback studies, because many climate models do not adequately represent Antarctic Ocean clouds [Trenberth and Fasullo, 2010]. Thus, we make a periodical shipboard observation to investigate maritime cloud with whole-sky camera observation onboard R/V *Shirase* (AGB-5003) between Japan and Antarctica, including over the Southern Ocean [Kuji et al., 2016]. We investigated cloud fraction for a total of seven years from JARE 55 to JARE 61, i.e., from 2013 to 2020. The whole-sky camera system mainly consists of a digital camera (Nikon D7000, Nikon Corporation) and a circular fisheye lens (4.5 mm F2.8 EX DC Circular Fisheye HSM, SIGMA Corporation) to take a photo of a whole sky. The observation interval is 5 min. We investigated the distribution of clouds over ocean by estimating cloud fraction from whole-sky camera images based on a cloud detection method [Yoshimura and Yamashita, 2013]. However, we analyzed the whole-sky images over sea ice region for each cruise as a function of solar height because sea surface albedo over sea ice regions is very different from that over open ocean [Kuji et al., 2018]. As a result, the daily-average cloud fraction was generally more than 55% in all seven cruises over the Southern Ocean. Furthermore, we examined the cloud fraction in three areas: sea ice, outward and return open water areas. It is found that the average cloud fraction was more than 70% only in the open water areas. These results suggest that cloud fraction tends to be particularly large in the open waters over the Southern Ocean from December to March of each observation year.

Acknowledgments
The shipborne observation was conducted in cooperation with Japan Aerospace Exploration Agency (JAXA) and National Institute of Polar Research. The authors are grateful to those who related to observations onboard R/V Shirase during JARE 55-61.

References

Intergovernmental Panel on Climate Change (IPCC2013), Climate Change 2013.

Kuji M., R. Fujimoto, M. Miyagawa, R. Funada, M. Hori, H. Kobayashi, S. Koga, J. Matsushita, and M. Shiobara, Cloud fractions estimated from shipboard whole-sky camera and ceilometer observations, *Trans. JSASS Aerospace Tech. Japan*, **14**, 7-13, 2016.

Kuji, M., A. Murasaki, M. Hori, M. Shiobara, 2018: Cloud Fractions Estimated from Shipboard Whole-Sky Camera and Ceilometer Observations between East Asia and Antarctica. *J. Meteor. Soc. Japan*, **96**, 201-214.

Trenberth, K. E., and J. T. Fasullo, 2010: Simulation of present-day and twenty-first-century energy budgets of the southern oceans. *J. Climate*, **23**, 440-454.

Yoshimura M. and M. Yamashita, Contribution of Ground-Based Cloud Observation to Satellite-Based Cloud Discrimination, *J. Environ. Sci. Eng. A*, **2**, 379-382, 2013.

Characteristics of cloud fraction and shortwave downward radiation at Ny-Ålesund and Syowa station

Makoto Kuji[1], Yumi Shimode[1], Mana Takada[1], Sara Hirose[1] and Masanori Yabuki[2]
[1]*Graduate School of Humanities and Sciences, Nara Women's University*
[2]*Research Institute for Sustainable Humanosphere, Kyoto University*

Cloud has opposite effects on the Earth's climate: a greenhouse effect that absorbs earth radiation and a cooling effect that reflects solar radiation. The effects depends on shape, height, and amount of clouds. However, it is not easy to observe clouds in detail because of their large spatiotemporal variability and wide variety of shapes and distributions. Cloud is one of the major sources of error in radiative forcing and temperature estimation in future [IPCC 2013]. In addition, polar regions have an important influence on the global climate because of the sea ice or ice sheet. Therefore, it is predicted that the rise of temperature was most significant in the latter half of the 21th century in the Arctic in particular.

In this study, we investigate the characteristics of clouds and shortwave downward radiation at Ny-Ålesund in the Arctic and Syowa Station, Antarctica. We estimated the cloud fraction from Micro Pulse LIDAR (MPL) and visual observations at Ny-Ålesund and Syowa from 2005 to 2018. Cloud is detected by MPL that emits micro-pulse laser beams into the atmosphere and receives the light scattered back by cloud base heights. Since MPL can detect the presence of clouds, cloud fraction is estimated as the occurrence frequency. On the other hand, the visual cloud amount were obtained from the Norwegian Meteorological Agency for Ny-Ålesund and the Baseline Surface Radiation Network (BSRN) for Syowa, respectively. The observations are conducted every 6 h at Ny-Ålesund and every 3 h at Syowa, respectively. The shortwave downward radiation data were obtained from BSRN. It is observed by a pyranometer and the data are available every 1 min.

We also estimated the trends of monthly-mean cloud fraction from MPL and visual observations and shortwave downward radiation from January 2005 to December 2018. As a result, no trend was found for cloud fractions from MPL and visual observations as well as for shortwave downward radiation at Ny-Ålesund. At the Syowa, on the other hand, there was a positive trend for the MPL cloud fraction, but no trend was found in the visual cloud fraction and shortwave downward radiation. We will also discuss the results in terms of correlation between cloud fractions and shortwave downward radiation in detail.

Acknowledgments
The authors are grateful to those who devoted themselves to the observations. Cloud fraction with Eye observation at Ny-Ålesund was provided from the Norwegian Meteorological Institute (http://sharki.oslo.dnmi.no). Cloud fraction with Eye observation at Syowa Station and Shortwave downward radiation at Ny-Ålesund and Syowa Station were provided from Baseline Surface Radiation Network (http://www.bsrn.awi.de/en/).

Dating and solid particle analysis of a shallow ice core obtained from EGRIP, Greenland

Yuki Komuro[1], Fumio Nakazawa[1,2], Kumiko Goto-Azuma[1,2], Naoko Nagatsuka[1], Motohiro Hirabayashi[1], Jun Ogata[1], Kaori Fukuda[1], Naoyuki Kurita[3], Kyotaro Kitamura[1], Ayaka Yonekura[2], Trevor J. Popp[4], Dorthe Dahl-Jensen[4]

[1]*National Institute of Polar Research*

[2]*The Graduate University for Advanced Studies, SOKENDAI*

[3]*Nagoya University*

[4]*University of Copenhagen*

Temporal variations in concentration and size distribution of mineral dust on the Greenland ice sheet are related to temporal variations in ground surface conditions on their source areas. For example, decreases of snow- and ice-covered areas on the Greenland coast due to global warming can increase soil areas and mineral dust emissions on the coast, thus increase mineral dust fluxes and concentrations on the Greenland ice sheet. Also, mineral dust transported from remote source areas (e.g., Asian desert) is dominated by small particles, while that from the Greenland coastal areas contains coarse particles (e.g., Simonsen et al., 2019). Thus, the size distribution of mineral dust on the ice sheet can be used to evaluate their source areas. We analyzed a shallow ice core drilled by the East Greenland Ice Core Project (EGRIP) to estimate past temporal variations in ground surface conditions of the source areas of mineral dust. In this study, we will report the results of the dating and solid particle analysis of the ice core.

The shallow ice core was analyzed using a continuous-flow analysis (CFA) system at NIPR. Stable water isotope ratios ($\delta^{18}O$ and δD), solid particle concentrations (1.2–10.5 μm), and elemental concentrations (Na, Mg, Al, Si, S, K, Ca, and Fe) were measured by a water isotope analyzer (Piccaro, L2130-i), a laser particle counter (Klotz, Abakus), and an ICP-MS (Agilent technologies, 7700), respectively. For accurate analyses of solid particles, a portion of meltwater was collected using a fraction collector at a depth interval of 0.12 m. The solid particle concentrations and size distributions (0.6–18 μm) in the collected samples were measured by a coulter counter (Beckman Coulter, Multisizer 4e). Additionally, for tritium measurements, ice core samples at depths of 13–15 m were cut and melted. Tritium measurements of the samples were conducted using a scintillation counter (ParkinElmer, Quantulus 1220).

Depth profiles of $\delta^{18}O$ and δD did not show seasonal variations at depths deeper than 7 m. This result is consistent with a previous ice core study at EGRIP (Vallelonga et al., 2014). Na, Ca, and solid particle concentrations showed clear seasonal variations at all depths. Therefore, we dated this ice core by annual layer counting. A tritium peak due to nuclear bomb testing was found at a depth of 14.1 m, thus we regarded this depth as 1963. In the depth profile of S, high peaks were found at depths of 23.3 m, 39.8 m, 44.7 m, 83.7 m, and 105.5 m. We assumed those peaks to be the signatures of Katmai (1912), Tambora (1815), Laki (1783), Kuwae (1458), and Samalas (1257) eruptions. Based on those results, we estimated that the ice core covers about the past 1000 years. Solid particle analyses showed that coarse particle concentrations after around 1600 were higher than in earlier periods. This suggests that snow and ice areas on the Greenland coast have decreased since around 1600.

References

Simonsen et al., East Greenland ice core dust record reveals timing of Greenland ice sheet advance and retreat, Nature Communications, 10 (4494), 2019.

Vallelong et al., Initial results from geophysical surveys and shallow coring of the Northeast Greenland Ice Stream (NEGIS), The Cryosphere, 8, 1275-1287, 2014.

Variations in mineralogy of dust in ice cores obtained from Greenland over the past 100 years

Naoko Nagatsuka[1], Kumiko Goto-Azuma[1,2], Akane Tsushima[3], Koji Fujita[4], Sumito Matoba[5], Yukihiko Onuma[6], Remi Dallmayr[7], Motohiro Hirabayashi[1], Jun Ogata[1], Yoshimi Ogawa-Tsukagawa[1], Kyotaro Kitamura[1], Masahiro Minowa[5], Yuki Komuro[1], Hideaki Motoyama[1,2], Teruo Aoki[1,2], Fumio Nakazawa[1], Trevor James Popp[8], Dorthe Dahl-Jensen[8]

[1]*National Institute of Polar Research, Japan*
[2]*SOKENDAI (The Graduate University for Advanced Studies), Japan*
[3] *Chiba University, Japan*
[4] *Nagoya University, Japan*
[5] *Hokkaido University, Japan*
[6] *University of Tokyo, Japan*
[7] *Alfred Wegner Institute for Polar and Marine Research, Germany*
[7] *University of Copenhagen, Denmark*

Snow and ice on glaciers and ice sheets contain aeolian mineral dust that provides key information about global and local climate change. Dust deposited on ice sheets in the past can be obtained by ice core drilling, and the variations in its sources and transportation processes can be reconstructed by particle analysis of ice cores. However, there is limited information about possible sources of mineral dust in interglacial periods during which dust concentrations are low. In this study, we analyzed the morphology and mineralogical composition of mineral dust from ice cores drilled in Northwest Greenland with a Scanning Electron Microscope (SEM, QUANTA FEG 450) and an Energy Dispersive X-ray Spectrometer (EDS).

The ice core was drilled at the SIGMA-D site (N77°64', W59°12') of 2100 m a.s.l. in 2014 (Matoba et al., 2015). The ice core samples were collected every five years in plastic bottles and freeze dried on a polycarbonate filter to concentrate micro-particles. Here we report the temporal variations in size distributions and compositions of the minerals during the past 100 years (A.D 1915-2013).

The SEM observation revealed that the mean size of mineral dust in the SIGMA-D ice core ranged from 1-3μm, which is similar to that of the other Greenland ice core dust that seems to be derived from distant areas. This suggests that the ice core contained mainly long–range transported wind-blown mineral dust. The EDS analysis revealed the ice core dust consisted mainly of silicate minerals and that the composition varied substantially on multi-decadal and inter-decadal scales, suggesting that the ice core minerals originated from different geological sources in different periods during the past 100 years. The multi-decadal variation trend differed among mineral types. Kaolinite, which generally formed in warm and humid climatic zones, were abundant in colder periods (1950–2004), whereas mica, chlorite, feldspars, mafic minerals, and quartzes, which formed in arid, high-latitude, and local areas were abundant in warmer periods (1915–1949 and 2005–2013). Comparison to Greenland surface temperature records indicates that multi-decadal variation in the relative abundance of these minerals was likely affected by local temperature changes in Greenland. Trajectory analysis shows that the minerals were transported mainly from the western coast of Greenland in the two warming periods, which was likely due to an increase of dust sourced from local ice-free areas as a result of shorter snow/ice cover duration in the Greenland coastal region during the melt season caused by recent warming. Meanwhile, ancient deposits in northern Canada, which were formed in past warmer climates, seem to be best candidate during the colder period (1950–2004). Our results suggest that SEM-EDS analysis can detect variations in ice core dust sources during recent periods of low dust concentration (Nagatsuka et al., 2021).

To reveal spatial variations in the mineral composition on the Greenland Ice Sheet, we have applied this SEM-EDS analysis to an ice core obtained from East Greenland (EGRIP) and identified temporal variations in the mineral dust composition during the past 100 years. We have also compared the results to those of the SIGMA-D ice core. Detailed results will be shown in our presentation.

References

Matoba, S et al., Glaciological and meteorological observations at the SIGMA-D site, northwestern Greenland Ice Sheet. Bull. Glaciol. Res., 33, 7-10, DOI:10.5331/bgr.33.7 2015.

Nagatsuka, N., Goto-Azuma, K., Tsushima, A., Fujita, K., Matoba, S., Onuma, Y., et al : Variations in mineralogy of dust in an ice core obtained from northwestern Greenland over the past 100 years, Clim. Past, 17, 1341–1362, 2021.

Effects of the glacial meltwater supply on carbonate chemistry in Bowdoin Fjord, northwestern Greenland

Takahito Horikawa[1], Daiki Nomura[1,2,3]*, Shin Sugiyama[3,5], Yasushi Fukamachi[3], Naoya Kanna[4]

[1] Faculty of Fisheries Sciences, Hokkaido University, [2] Field Science Center for Northern Biosphere, Hokkaido University, [3] Arctic Research Center, Hokkaido University, [4] Atmosphere and Ocean Research Institute, The University of Tokyo, [5] Institute of Low Temperature Science, Hokkaido University

To understand the effects of the glacial meltwater supply on carbonate chemistry and the air–sea CO2 flux within the fjord, water samples were collected in Bowdoin Fjord in northwestern Greenland in the summers of 2016 and 2017. The samples were analyzed for dissolved inorganic carbon (DIC) concentration, total alkalinity (TA), oxygen isotopic ratio (δ18O), and chlorophyll a concentration.The partial pressure of CO_2 (pCO_2) in surface water, calculated from DIC and TA, was less than 200 μatm, and was significantly lower than that in the atmosphere (399 ± 3 μatm). Therefore, surface water of the fjord acts as strong sink for CO_2 in the atmosphere (–4.9 ± 0.7 mmol m^{-2} d^{-1}). To evaluate the effect of dilution by glacial meltwater on pCO_2 in the fjord, we calculated the changes in salinity and carbonate chemistry that would result from the mixing of seawater with freshwater and their effect on pCO_2 ($pCO_{2\,mix}$). With the distance from the glacier, pCO_2 obs decreased and fell below the value of pCO_2 mix, suggesting that dilution is not a single control on pCO_2 in the fjoldExamination of the relationship between salinity-normalized DIC and TA showed that $pCO_{2\,obs}$ was reduced by increased biological productivity as well as by the dilution effect.

Development of an ice-sheet model IcIES-1 and IcIES-2: benchmark simulation on idealized and realistic ice-sheet configuration

SAITO Fuyuki[1], Ayako ABE-OUCHI[2], Takashi OBASE[2] and Ryouta O'ISHI[2]
[1]*Japan Agency for Marine-Earth Science and Technology*
[2]*Atmosphere and Ocean Research Institute, Univ. of Tokyo*

Ice sheet model for Integrated Earth-system Studies (IcIES) is a three-dimensional numerical ice-sheet model, which has been developed under collaboration between Atmosphere and Ocean Research Institute, Univ. of Tokyo (AORI) and Japan Agency for Marine-Earth Science and Technology (JAMSTEC). The model is based on the Shallow-Ice Approximation that is a typical framework for large-scale and long-term ice-sheet modeling. It has been utilized for Antarctic ice-sheet simulation (e.g., Saito and Abe-Ouchi 2010), Greenland ice-sheet simulation (e.g., Saito et al. 2016), and past Northern Hemisphere ice-sheet simulation (Abe-Ouchi et al. 2013).

Recently a new ice-sheet model called IcIES-2 has been developed from a scratch, which partially inherits the policy and design of the original IcIES (IcIES-1). IcIES-2 has (will have) the following features in comparison with IcIES-1:

- Open-source
- Fully parallelized using MPI library
- Inclusion of ice-shelf processes using the Shallow-Shelf Approximation
- Inclusion of grounding-line parameterization (such as Schoof 2007 scheme)
- Inclusion of enthalpy scheme for polythermal ice-sheet (based on Blatter and Greve 2015)
- Higher-order advection/transport scheme (such as RCIP scheme)

In this study, recent status of both IcIES-1 and IcIES-2 will be presented. In particular, the effect of inclusion of a higher-order advection scheme on thermodynamics will be reported. In addition, a series of Greenland ice-sheet simulation using a new bedrock topography data (based on BedMachine v4, Morlighem et al. 2021) will be presented.

Greenhouse gases flux through the land surface at the terminus of Glaciers in Alaskan Range

Keiko Konya[1], Tetsuo Sueyoshi[2], Go Iwahana[3], Tomoaki Morishita[4] and Jun Uetake[5]
[1]*JAMSETC,* [2]*NIPR,* [3]*UAF,* [4]*FFPRI,* [5]*Hokkaido Univ.*

1. Introduction

Carbon dioxide is the most influential greenhouse gas. Methane, which has a global warming potential of 28, has attracted attention as a gas with a high greenhouse effect, even though its amount is small, and its balance on a global scale. On a global scale, methane is considered to be mainly emitted from land areas at low and mid-latitudes, and in the Arctic region, methane emission from frozen ground is attracting attention, although it is not well observed. On the other hand, large amounts of methane have been observed at glacier termini in Greenland and Iceland due to the outflow of meltwater saturated with methane (Burns et al., 2018; Lamarche-Gagnon et al., 2019). If the same amount of methane is released from glacier termini in other regions, the impact on atmospheric methane concentrations will be larger than previously thought. In this study, we conducted observations to determine whether similar methane emissions are observed in small mountain glaciers in Alaska, and what their origin is.

2. Study site

We observed methane emissions from the surface and collected water and sediment samples at the terminus of Gulkana and Canwell glacier in the Alaska Range in July 2021. The Alaska Range is a mountainous region where there are many glaciers of various sizes. The Gulkana Glacier is a small glacier that has been observed to shrink in recent years. The location of the outflowing river varied from year to year, and in 2019 it was flowing from the left bank. In 2019, the outflow was observed from the left side of the glacier. The observation sites were selected where glacial sediments and meltwater were accumulated, among the sites considered to be the ground surface exposed after the recent glacier retreat. However, the surrounding area is littered with debris-covered ice, and the subsurface conditions are unknown because no geological survey was conducted.

3. Method

Methane emissions were measured using the chamber method by Morishita et al. (2015) and portable gas analyzer (Picarro G4301). Gas samples collected in the chamber were brought back to FFPRI and analyzed for the analysis of methane and carbon dioxide concentrations by gas chromatography.

Water samples were collected from runoff streams and surface water pools. Water samples were collected from the outflowing rivers and surface water pools, and temperature and water quality measurements (water temperature, pH, and conductivity) were taken. Water samples were analyzed for stable isotope ratios at the Japan Agency for Marine-Earth Science and Technology. Sediments were analyzed by RNA sequencing and compared with previous studies for methanogen community.

4. Results

Gas samples collected from seven locations in wet sediments and ponds at the terminus of the Gulkana Glacier showed slight methane generation of up to 10 μg C /m/hr in 2019. However, in 2021, the observed concentrations at several glacier terminus were almost the same as that in the atmosphere. Therefore, it is considered that the methane emission could not be detected in the observation in 2021.

References

Burns, R., Wynn, P. M., Barker, P., McNamara, N., Oakley, S., Ostle, N., A. W. Stott, H. Tuffen, Z. Zhou, F. S. Tweed, A. Chesler, and M Stuart, 2018: Direct isotopic evidence of biogenic methane production and efflux from beneath a temperate glacier, Scientific reports, 8(1), 1-8.

Lamarche-Gagnon, G., J. L. Wadham, B. Sherwood Lollar, S. Arndt, P. Fietzek, Beaton, A. J. Tedstone, J. Teling, E. A. Bagshaw, J. R. Hawkings, T. J. Kohler, J. D. Zarsky, M. C. Mowlem, A. M. Anesio, and M. Stibal, 2019: Greenland melt drives continuous export of methane from the ice-sheet bed, Nature, 565, 73-77.

Morishita, T., K. Noguchi, Y. Kim and Y. Matsuura, 2015: CO2, CH4 and N2O fluxes of upland black spruce (Picea mariana) forest soils after forest fires of different intensity in interior Alaska, Soil Science and Plant Nutrition, 61(1), 98-105.

acknowledgements

This is study has been conducted as a part of ArCSII project. Methane isotope analysis was conducted by Dr. S. Kawaguchi (JAMSTEC).

Extreme Wildland Fire in Sakha in 2021

Hiroshi Hayasaka
Arctic Research Center, Hokkaido University

Large-scale wildland fire occurred in Sakha in 2021. Fire activities and fire weather in Sakha were analyzed using daily hotspot data (until September 9) and various weather maps. Main part of Sakha (57.5–72.5° N, 110–140° E, roughly about 74% of Sakha) in **Figure 1** was divided into 36 areas to grasp fire distribution like shown n **Figure 1**. **Figure 2** shows fire history in Sakha since 2002. The total number of hotspots in 2021 exceeded 267,000. This is about 5.8 times the average number of fires over the last 19 years from 2002. **Figure 3** shows number of daily hotspots (HSs) in Sakha and highest fire density area (HFA, 62.5–65° N, 125–130° E). Fire weather analysis was conducted with reference to the results of our papers on wildland fire in Siberia and Alaska[1-4]. The largest number of daily hotspots in Sakha was 16,226 detected on August 2. Active fire in August occurred under stagnant high-pressure systems over Sakha created by the large meandering of westerlies caused by the stagnation of low-pressure systems in the southern part of the Barents Sea. Warm air masses (cTe: continental temperate) from south also was stagnant over Sakha. High-pressure systems at lower air level in the Arctic Sea supplied strong wind into Sakha from around July 27. On August 7, about half of daily hotspots (52.6%=8,175/15,537x100) were detected in HFA near Yakutsk. Wind conditions during the active fire-period on August were shown in **Figure 4**. Large number of HSs (8,175) was detected on August 7 under the strong southeasterly wind (wind velocity about 12 m/s (43 km/h) in **Figure 4**). Strong wind conditions in HFA on August 7 were made by high-pressure systems at lower air level in the Arctic Ocean (H_{930}, 78° N, 155° E) shown in **Figure 5**. Locations of hotspots in HFA coincided with strong wind areas on the v-wind map shown in **Figure 6**. The very active fire occurrence in 2021 will be classified one of extreme phenomena (evidences) related to rapid climate change.

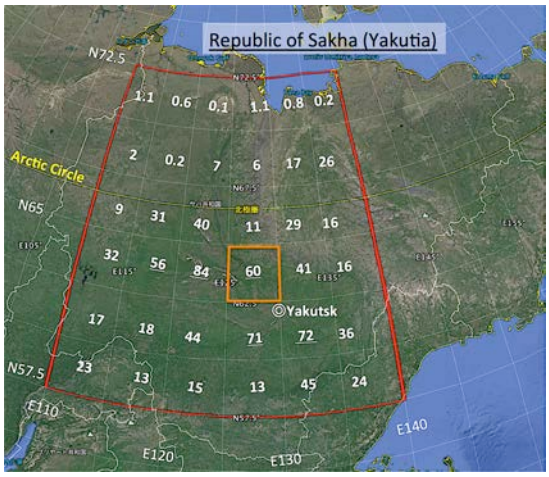

Figure 1. Study region in Sakha. Numbers in 36 areas such as "84" are total number of hotspots (x 10^3) from 2002 to 2020.

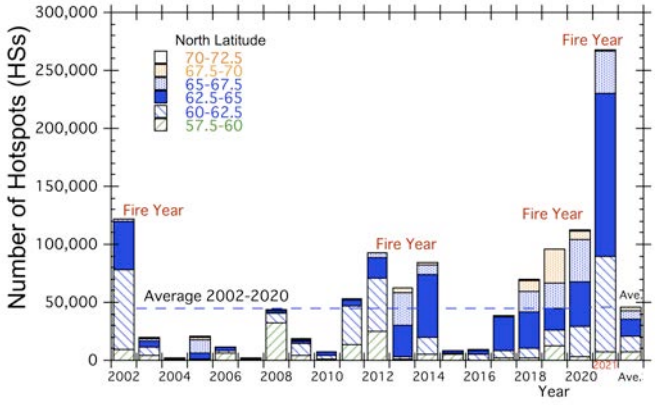

Figure 2. Fire history in Sakha since 2002.

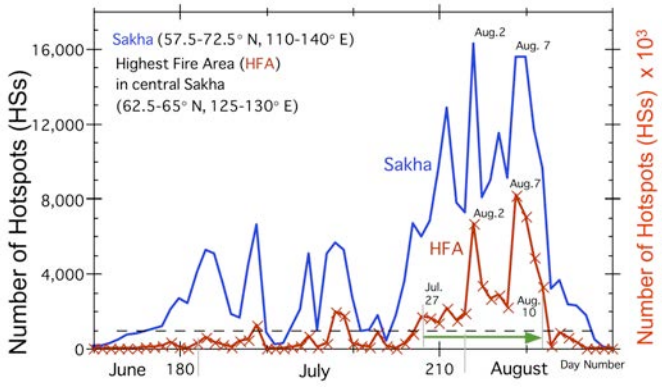

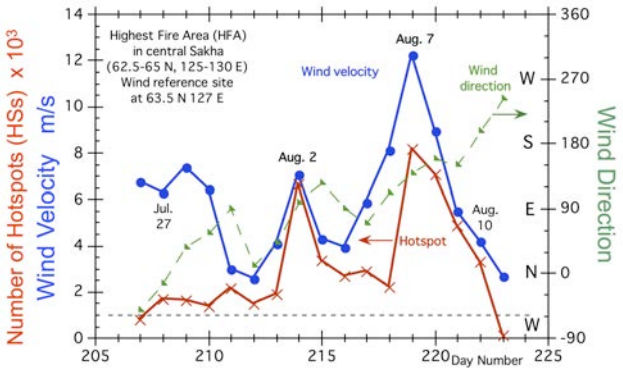

Figure 3. Number of daily hotspots (HSs) in 2021.

Figure 4. Wind conditions during the active fire (HS) period.

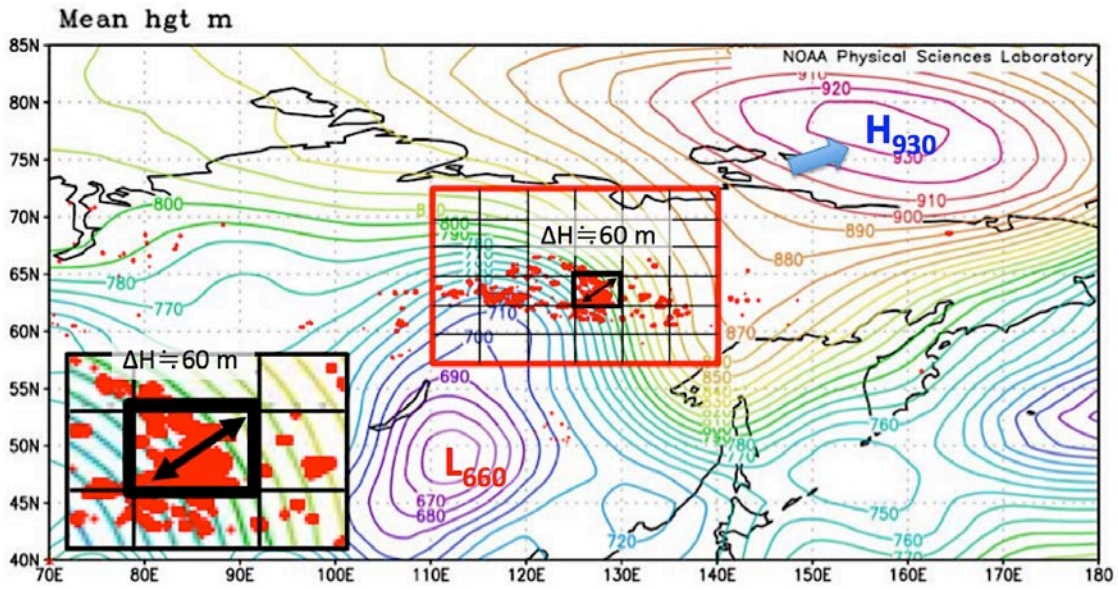

Figure 5. Weather map at lower air level on August 7.

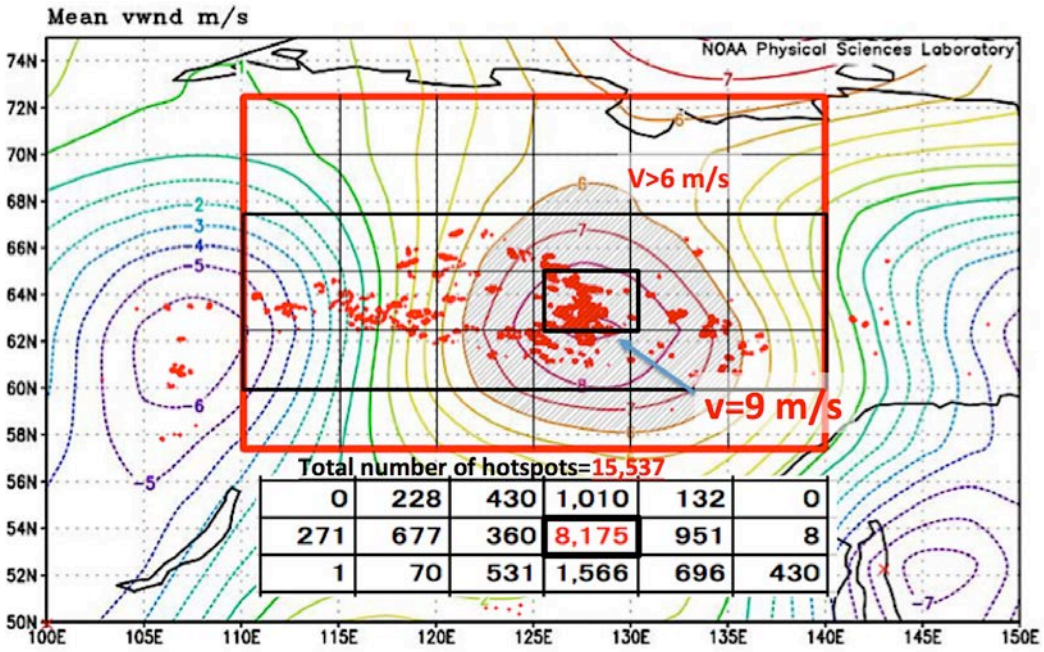

Figure 6. V-wind map on August 7. The symbol "+" means southerly wind.

References

1. Hayasaka, H.; Tanaka, H.L.; Bieniek,P.A. Synoptic-scale fire weather conditions in Alaska, Volume 10, Issue 3, Polar Science, pp. 217-226, 2016. http://dx.doi.org/10.1016/j.polar.2016.05.001

2. Hayasaka, H.; Yamazaki, K.; Naito, D. Weather conditions and warm air masses in southern Sakha during active wildfire pe-riods. 2019 J. Disaster Res. 14–4, 641–648. https://doi.org/10.20965/jdr.2019.p0641

3. Hayasaka, H.; Yamazaki, K.; Naito, D. Weather Conditions and Warm Air Masses during Active Fire-periods in Boreal For-ests, 2019 Vol. 22, pp.1-8, Article 100472, Polar Science. https://doi.org/10.1016/j.polar.2019.07.002

4. Hayasaka, H.; Sokolova, G.V.; Ostroukhov, A.; Naito, D. Classification of Active Fires and Weather Conditions in the Lower Amur River Basin, Remote Sens. 2020, 12(19), 3204; https://doi.org/10.3390/rs12193204

Forecasting sea-ice distribution during the summer season in the arctic with statistical method

Motomu Oyama [1], Hajime Yamaguchi [1] and Noriaki Kimura [2]

[1] *Arctic Sea Ice Information Center, National Institute of Polar Research*

[2]*Atmosphere and Ocean Reseaerch Institute, The University of Tokyo*

The Arctic Sea Ice Information Center, established at the National Institute of Polar Research from the FY2021, released sea ice forecasts for the period from July to the end of September in May, June and July.

The method of our ice prediction is based on a correlation between the spring ice thickness and summer ice concentration. Although there are various factors that may cause the change in thickness, this analysis focused on the redistribution (divergence/convergence) of sea ice during winter, and sea ice age. The sea ice predictions are obtained from a linear single regression or a linear multiple regression model of the particle density distribution or the sea ice age distribution at the end of April, May and June and the sea ice concentration on a given day from July to September. The particle density distribution is obtained by the tracking of particles placed at intervals of 20 × 20 km to cover the sea ice distribution in December, using the daily sea ice drift vectors (Kimura et al., 2013) until the end of April, May and June. Sea ice age is estimated by backward tracking of particles placed over the ice cover, using daily sea ice drift vectors. We define the sea ice age as the period of time until the sea ice concentration at the location of the particle becomes less than 15%. The particle density distribution is considered to be an indicator of year to year changes in ice thickness due to the redistribution of sea ice during winter, while the sea ice age distribution is considered to be an indicator of long-term changes in sea ice thickness.

Predicted ice area on September 10 released in May and June are shown in Fig 1 left and middle, respectively. These results are obtained by single regression analysis of deviation from the linear trend of sea ice concentration and particle density. There was no significant difference in the results; sea ice would retreat significantly from the Russian and Canadian coasts. Same ice area released in July is shown Fig 1 right. It is obtained by multiple regression analysis of deviation from the linear trend of sea ice concentration, sea ice age distribution (Fig 2), and particle density. We can find the unmelted sea ice due to the old ice in the Beaufort Sea. In the presentation, these results will be compared and discussed with the actual sea ice distribution.

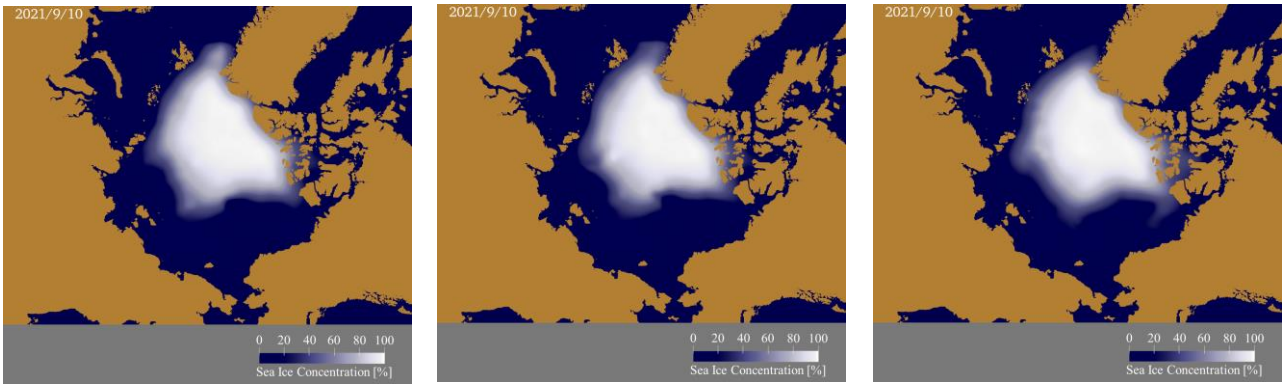

Fig 1: The results of the September 10, 2021 prediction conducted in May (Left), June (Middle) and July (Right).

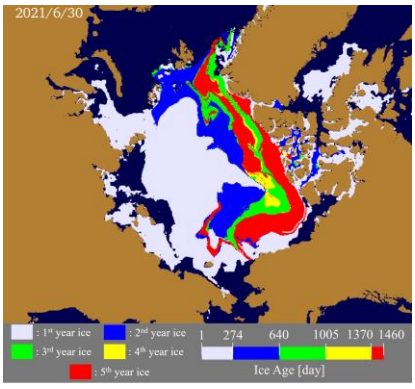

Fig 2: Sea ice age distribution at the end of June, 2021.
1st, 2nd, 3rd, 4th and 5th year ice are light blue, blue, green, yellow and red, respectively.

References

N. Kimura, A. Nishimura, Y. Tanaka and H. Yamaguchi, Influence of winter sea ice motion on summer ice cover in the Arctic, Polar Research, 32, 20193, 2013.

Validation of AMSR2 sea ice motion vector product

Eri Yoshizawa[1], Rigen Shimada[1], Misako Kachi[1], Noriaki Kimura[2], and Koji Shimada[3]
[1] *Earth Observation Research Center, Japan Aerospace Exploration Agency*
[2]*Atmosphere and Ocean Research Institute, The University of Tokyo*
[3] *Department of Ocean Sciences, Tokyo University of Marine Science and Technology*

Sea ice motion vector is a key parameter to understand mechanical air-ice-ocean interactions affecting polar climate system. Despite such an importance, in situ observations are very limited in time and space, and thus tracking techniques of sea ice motion based on remote sensing have been developed. This especially relies on passive microwave radiometer observations that are capable of monitoring across the Arctic/Antarctic Ocean on daily basis without severe could contaminations. To date, JAXA has conducted the observations since 2002 by operating Advanced Microwave Scanning Radiometer-EOS/2 (AMSR-E/2). Moreover, AMSR3 is planned to be launched subsequently. These sequential observations have an advantage to monitor decadal sea ice variability.

By finding correlation peaks between two temporally separate imageries of passive microwave brightness temperatures, sea ice displacements are detected and converted into motion vectors. Currently, based on this methodology, two algorithms are proposed for AMSR2 research products. In this study, we present validation results of outputs from these algorithms applied for the Arctic Ocean. For validations, we here use the following two in situ data: ice drifting buoy and ocean mooring data. The former data has been historically utilized for validations of satellited-derived products, however, its observations are limited to multiyear ice. Since multiyear ice has been substantially replaced by seasonal ice in the Arctic Ocean during the last few decades, there is of increasing importance of data quality of seasonal ice motions. Therefore, the latter data, which captures motions of not only multiyear ice but also seasonal ice, is also employed for validations. In the presentation, we will also introduce detailed validation results and quality controls.

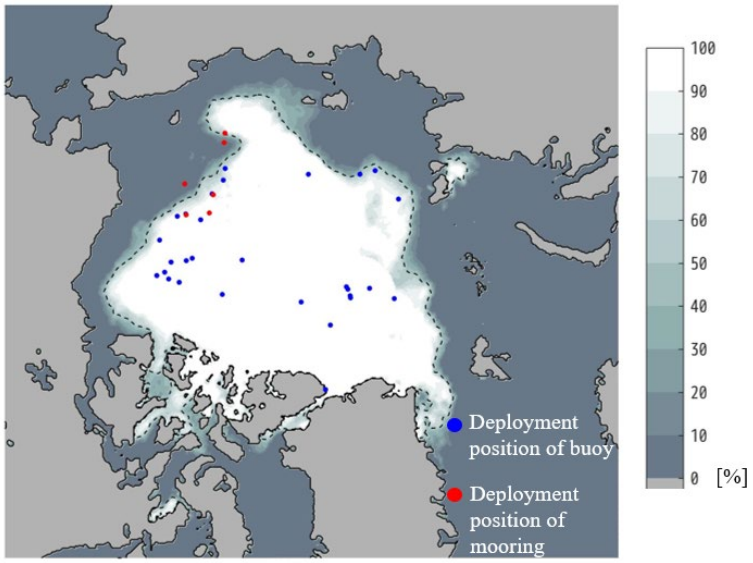

Figure 1 In situ data distributions in 2013/2014 winter with AMSR2 sea ice concentrations averaged for September 2013.

Experimental study on the ice – wave interaction in the small ice floes and regular wave - Relationship between ice concentration and ice vertical motion -

Junji Sawamura
Department of Naval Architecture and Ocean Engineering, Osaka University

Reduction of sea ice coverage in the Arctic Ocean has increased vessel operations in marginal ice zones (MIZ), where ice cover consists of individual broken ice floes. Vessels operating in MIZ are affected by small ice floes and waves. The estimation of the ice force for ships advancing into the wave–ice interaction is vital for the safe and effective operations of ice-going vessels. In order to estimate the ice resistant of ship in wave–ice interaction, the ice floe's motion in wave has to be understood correctly [1]. This research investigated the relation between the ice floe's motions and ice concentration in the regular wave experimentally. The experiment was conducted in the 2D wave tank in Osaka University, Japan. Disk–shaped polypropylene (PP) plate were used as an ice floe. The vertical amplitude was measured by the laser range finder. The ice concentration and the ship motions (trajectory, velocity and acceleration) of ice floes were obtained by the video camera and image processing. Figure 1 shows the experimental setup. Figure 2 shows the time history of the amplitude of the inlet regular wave (CHW01 in Figure 1) and the ice floe (CHI03 in Figure 1) in the regular wave. The ice concentration in Figure 2 was approximately 70 %. There is no significant differences of the amplitude between the inlet regular wave and ice floes. Figure 3 shows the relationship between the ice concentration and ice floe's vertical displacement in regular wave. The vertical axis of the Figure 3 shows the wave attenuation in the ice floes (Ice amplitude / inlet wave amplitude). The horizontal axis is the ice concentration. The left figure in Figure 3 shows the case in the wave steepness (wave height / wave length) = 0.03 and 0.04. The right figure shows the case in 0.02. The wave amplitude in the case of the wave steepness = 0.03 and 0.04 rapidly decreases from over the 80 % ice concentration, but in the case of the 0.02 decrease from 75 %. From those results, the relationship between the ice floe's vertical motion (wave attenuation in the ice floes) and the ice concentration might be explained by the wave steepness.

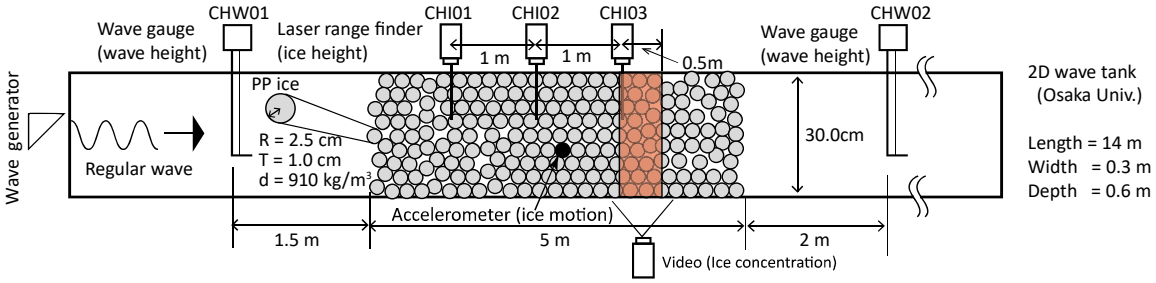

Figure 1 Experimental setup (measurement system of ice height and ice concentration in 2D regular wave).

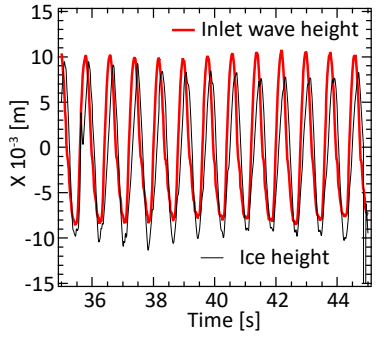

Figure 2 Time history of inlet wave and ice height. (Inlet wave amplitude = 2.0 cm, length = 1.0m)

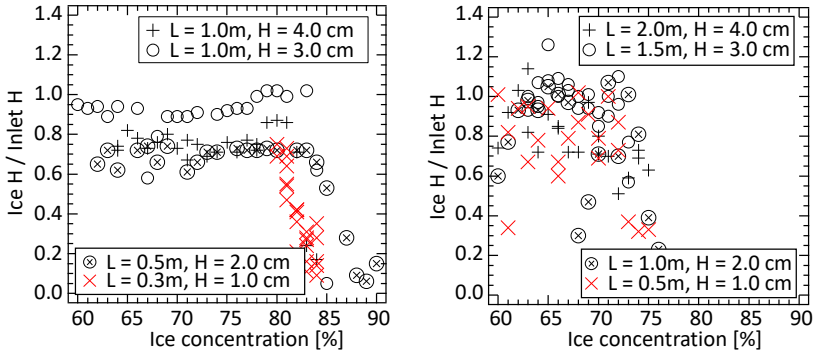

Figure 3. Relationship between ice concentration and ice height in regular wave (Left: Inlet H / Inlet L = 0.03 and 0.04, Right: Inlet H / Inlet L = 0.02).

References

[1] Junji Sawamura, Kensuke Imaki, Takaya Shiraishi and Hidetaka Senga, Ice resistance test using synthetic ice of a ship in small pack ice floes and wave interaction, The proceeding of 28th International Offshore and Polar Engineering Conference, pp.1586-1590, 2018.

Observation of Total Ice Thickness Using UAV-SfM in the Saroma-ko Lagoon

Kohei Sato[1], Kazutaka Tateyama[2], Tatsuya Watanabe[2] and Tomonori Tanikawa[3]
[1]*Graduate School of Engineering, Kitami Institute of Technology*
[2]*School of Earth, and Environmental Engineering Kitami Institute of Technology*
[3]*Meteorological Research Institute, Japan Meteorological Agency*

Measurement of sea ice thickness is important for understanding climate change, and providing useful information of economical activity in ice covered sea area. Sea ice thickness is measured by observations from drilling, electromagnetic induction device (EM) measurements and submarine monted sonar. Although an unmanned aerial vehicle (UAV) would be useful tool for sea ice thickness mesurement, the UAV operation under very cold condition remains challengnging. In this study, we aims to develop a system that measurs a wide range of sea ice thickness distribution using a fixed-wing UAV. An UAV with structure from motion (UAV-SfM) survey used in geomorphology, was applied for sea ice thickness measurement. We conducted various obsrvations over the Saroma-ko Lagoon in the East Hokkaido. In this observation, we used the fixed-wing UAV and ground control points with water level gauge. Figure1 shows the location and the observation area of the Saroma-ko Lagoon. The result of UAV-SfM survey shows the distribution of lake ice surface height as a degital surface model (DSM). It is possible to estimate the lake ice thikness from freeboard by DSM. The total thickness of lake ice and snow (H_T) was estimated by two different methods from the total freeboard of lake ice and snow (h_F) obtained by UAV-SfM survey. First, total ice thickness was obtained from the regression analysis results of H_T and h_F. Second, it was obtained using the hydrostatic equilibrium. This method is the same as ICESat ice thickness product. Ice density, snow density, and seawater density required for the calculation were determined by the data of snow pit work and ice core analysis. We estimated the snow depth and the freeboard accuracy of 0.03 m in absolute error. The error between dorill measurement and UAV-SfM measurement was about 6 % to the average of total ice thickness and mean absolute errorwas about 0.037 m. Figure2 shows the spatial distribution of total ice thickness estimated by the UAV-SfM survey. The total ice thickness was 0.4 m-0.8 m. The snow surface roughness and the trace of the snowmobile were confirmed in the image.

In this presentation, we will compare total ice thickness from the UAV-SfM with the EM data to discuss the accuracy of total ice thickness measurement by the UAV-SfM.

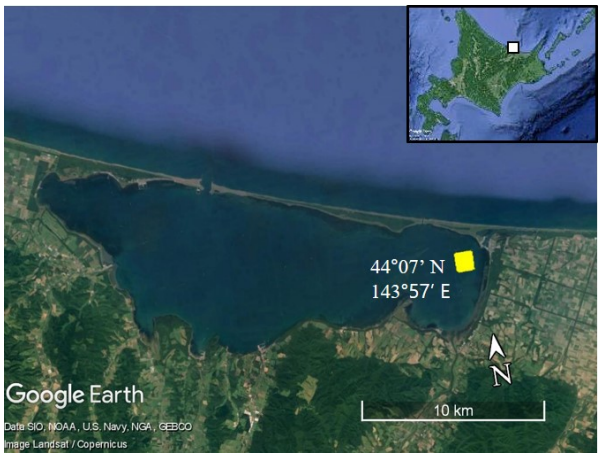

Figure 1. The location and observation area of Saroma-ko Lagoon

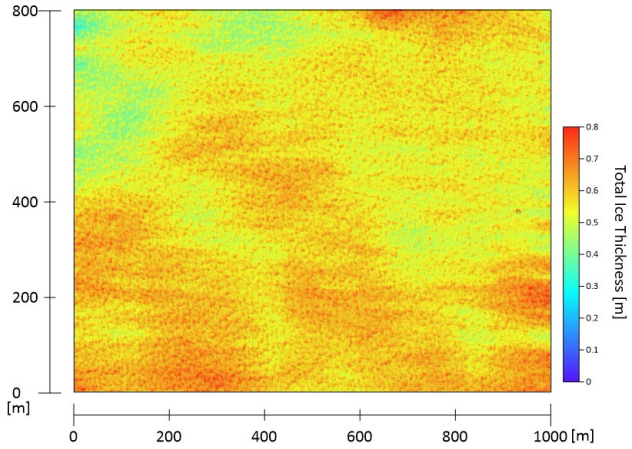

Figure 2. Spatial distribution of total ice thickness over the area of yellow in Fig.1.

Seasonal cycle and inter-annual variation of atmospheric freshwater input into the Sea of Okhotsk and associated large-scale atmospheric circulation

Kazuhiro Oshima[1], Yoshihiro Tachibana[2] and Kensuke K. Komatsu[3]
[1]*Aomori University, Aomori, Japan.*
[2]*Mie University, Tsu, Japan*
[3]*The University of Tokyo, Kashiwa, Japan*

The Sea of Okhotsk is the southern limit of sea ice in the Northern Hemisphere and the low salinity surface layer plays an important role in the sea ice formation. The low salinity layer is affected by freshwater inputs into the Sea of Okhotsk: river discharge from surrounding land areas, precipitation over the sea, and seawater exchanges between the surrounding ocean. Previous studies pointed out that the major source of freshwater input is river discharge from the Amur River, however, the quantitative freshwater budget is still unclear. Here we re-examined the freshwater input from the atmosphere and further investigated the cause of the variability. While our previous study investigated the water budget in the watershed of Amur River (Tachibana et al. 2008), we apply almost the same analysis method.

We estimated moisture flux convergence over the Sea of Okhotsk based on atmospheric reanalysis data (JRA-55). We used vertically integrated moisture flux data from 1979 to 2020 and calculated area-averaged flux convergence over the sea area where is defined as 45°-60° latitude and 140°-155° longitude. Figure 1 shows the climatological seasonal cycle of moisture flux convergence (hereafter, MFC) over the Sea of Okhotsk. As expected, the MFC shows large values from May to August during the summer season. It is noteworthy that the MFC has two peaks in May and August, and a minimum value in June. This suggests that summertime atmospheric circulation over this region affects this local minimum. We further compared the inter-annual variation of MFC and large-scale circulation. The correlation between the MFC and 850hPa geopotential height (z850) in each month indicated that negative values from May to August. This implies that the high-pressure system of summertime atmospheric circulation pattern, i.e. Okhotsk High, reduces the precipitation in the summer season.

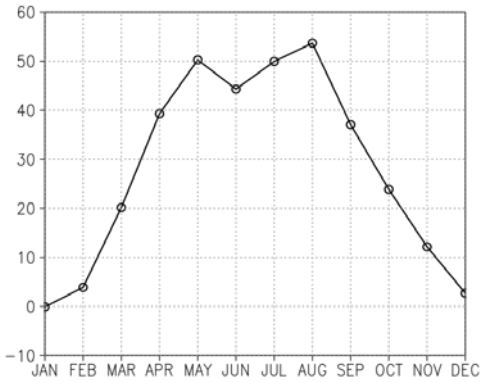

Figure 1. Climatological seasonal cycle of moisture flux convergence (MFC) over the Sea of Okhotsk. Unit is mm/month.

References

Tachibana, Y., K. Oshima, and M. Ogi, 2008, Seasonal and interannual variations of Amur River discharge and their relationships to large-scale atmospheric patterns and moisture fluxes, Journal of Geophysical Research, 113, D16102, doi:10.1029/2007JD009555.

Interannual variation of Warm Arctic – Cold Eurasia pattern investigated by using large ensemble experiment

Xiling Zhou[1], Tomonori Sato[2], Tetsu Nakamura[2], and Shixue Li[1]
[1]*Graduate School of Environmental Science, Hokkaido University*
[2]*Faculty of Environmental Earth Science, Hokkaido University*

Despite the rapid Arctic warming represented by the drastic sea ice loss, severe winters (such as winter 2009/10 2011/12) occurred frequently in Eurasia during recent decades. The second mode of winter surface air temperature (SAT) anomalies over Eurasia is referred to as the warm Arctic-cold Eurasia (WACE) pattern, which is influenced by sea ice decline over the Barents-Kara Seas (e.g., Mori et al. 2014).A historical simulation dataset obtained from 100-member ensemble experiment was analyzed in this study to better understand the mechanism of WACE pattern, in particular the interannual variation of WACE pattern over the past decades and the key factors responsible for the variation. The empirical orthogonal function (EOF) was conducted on 5900 snapshots of DJF-averaged SAT anomalies over 40°N -90°N, 0°E -150°E during 1951/52-2009/10. The second leading mode indicates the WACE pattern, with positive SAT anomalies over the Arctic, especially over the Barents-Kara Seas, and negative SAT anomalies over central Eurasia (Figure 1a). Ensemble averaged PC2 shows an increasing trend caused by the increasing SAT over the Barents-Kara Seas accompanied by large internal variability in each member, which indicates external forcing could strengthen WACE pattern in recent decades (Figure 1b). Next, we chose 10 best and 10 worst members with respect to the correlation coefficients of interannual variation of PC2 against that obtained from the reanalysis data (High CC Group and Low CC Group, respectively) (Figure 1b). Through a comparison of these groups, we found that colder surface temperature over the Central East Pacific and less sea ice over the Arctic marginal seas from autumn to winter in High CC Group, which indicates La Nina condition and sea ice decline are important for the development of WACE pattern (Figure 2a and 2b).

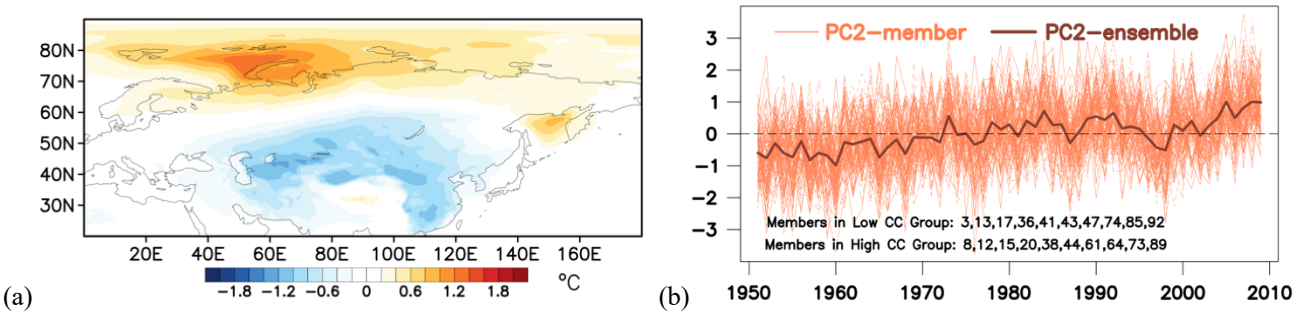

Figure 1. (a) Regression pattern of DJF-averaged SAT anomalies on the normalized PC2, (b) Interannual variations of the normalized PC2 for each member (thin lines) and ensemble mean (thick line).

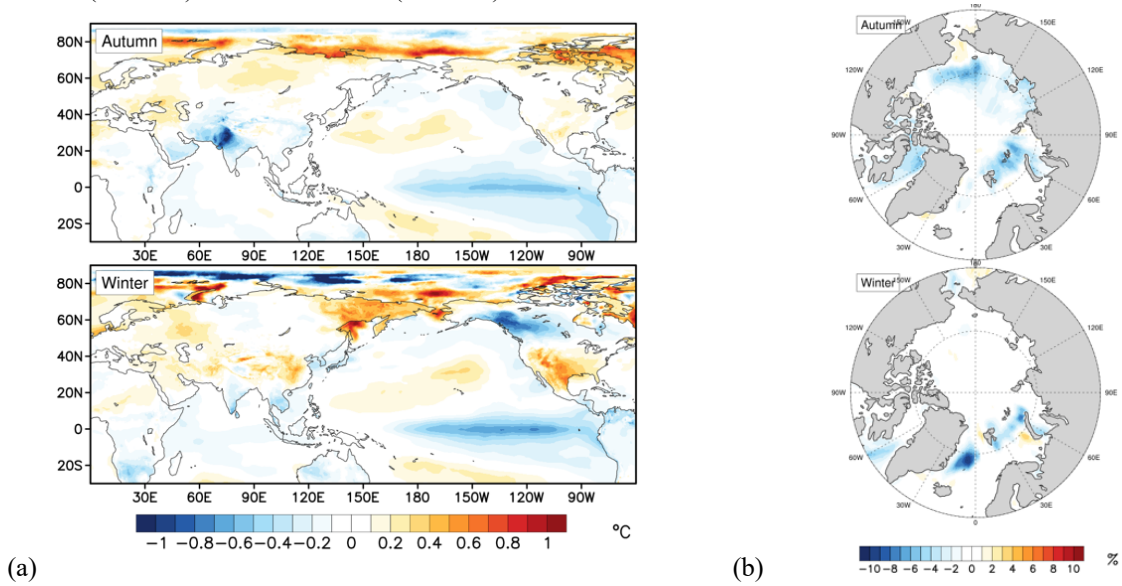

Figure 2. (a) The difference between regressed anomalies of autumn and winter surface temperature onto the PC2 between High CC Group and Low CC Group during 1951-2009, (b) is same with (a), but for sea ice concentration.

References

Mori, M., Watanabe, M., Shiogama, H., Inoue, J. and Kimoto, M. Robust Arctic sea-ice influence on the frequent Eurasian cold winters in past decades, Nature geoscience, **7**, 869-873, 2014.

An assessment of dominant patterns of lower tropospheric temperature advection contributing to the Arctic Amplication using a large-scale ensemble model experiment.

Masatake E. Hori[1] and Masakazu Yoshimori[1]

[1]*Atmosphere and Ocean Research Institute, The University of Tokyo, Kashiwa, Japan*

Using an AGCM large scale ensemble experiment, we investigate the role of lower tropospheric temperature advection in the intraseasonal timescale towards polar amplification. The dataset we use is the "database for policy decision making for future climate change" (d4pdf) which consists of a 60-year historical and non-warming simulation with 100 members each. The dataset also includes a 60-year simulation of the climate 4K and 2K warmer than the pre-industrial climate with 90 and 54 members each. Using the non- warming simulation (HPB_NAT) as a reference, we conduct an EOF analysis on the wintertime (DJF) daily 2m temperature eld over the Arctic circle (60˚-90˚N) to discern the dominant mode of temperature variability. Four patterns of temperature variability are isolated where EOF1 is the basin-wide warming in the central Arctic, EOF2 is associated with the warm advection along the Eurasian continent, EOF3 is associated with the intrusion of mid-latitude airflow from the Greenland and the Canadian Arctic Archipelago, and EOF4 is associated with warm air intrusion from east Siberia and the Bering strait. We further investigate the role of each of these patterns by comparing the probability of each EOFs occurring under different SST and sea-ice boundary condition of the historical simulation (HPB) and the 2K/4K simulation. Preliminary analysis of the warm advection shows that the difference in basic state of the lower tropospheric temperature leads to substantial increase in warm advection in the Eurasian continent. Heat budget analysis shows that such changes are driven by the climatological mean state difference and the dynamical term of EOF1 and EOF2 in which the climatological 850hPa temperature field is advected by the anomalous wind field. Further results regarding the change in circulation pattern sustaining these temperature advection pattern and their contribution towards the simulated Arctic amplification pattern is discussed in the presentation.